Co-delivery of Growth Factor-Loaded Microspheres and Adipose-Derived Stem Cells In A Gel Matrix for Cartilage Repair

By

ABBY SUKARTO

Thesis submitted to the Department of Chemical Engineering

in conformity with the requirement for

the degree of Doctor of Philosophy

Queen's University

Kingston, Ontario, Canada

June, 2011

ABSTRACT

Co-delivery of the embedded growth factor-loaded microspheres and adult stem cells in a hydrogel matrix was studied for its potential as a cell-based therapeutic strategy for cartilage regeneration in partial thickness chondral defects. A photopolymerizable *N*-methacrylate glycol chitosan (MGC) was employed to form an *in situ* gel that was embedded with two formulations of growth factor-loaded microspheres and human adipose-derived stem cells (ASC). The polymeric microspheres were used as a delivery vehicle for the controlled release of growth factors to stimulate differentiation of the ASC towards the chondrocyte lineage. The microspheres were made of amphiphilic low molecular weight (M_n < 10,000 Da) poly(1,3-trimethylene carbonate-*co*-ε-caprolactone)-*b*-poly(ethylene glycol)-*b*-poly(1,3-trimethylene carbonate-co-ε-caprolactone) (P(TMC-CL)$_2$-PEG)). This triblock copolymer is solid below 10^0C, but liquid with a low degree of crystallinity at physiological temperature and degrades slowly, and so acidic degradation products do not accumulate locally. Bone morphogenetic protein-6 (BMP-6) and transforming growth factor-β3 (TGF-β3) were delivered at 5 ng/day with initial bursts of 14.3 and 23.6%, respectively. Both growth factors were highly bioactive when released, retaining greater than 95% bioactivity for 33 days as measured by cell-based assays. To improve ASC viability within the MGC vehicle, an RGD-containing ligand was grafted to the MGC backbone. Prior to chondrogenic induction within the MGC gel, ASC viability was assessed and greater than 90% of ASC were viable in the gel grafted with cell-adhesive RGD peptides as compared to that in non-RGD grafted gels. For ASC chondrogenesis induced by the sustained release of BMP-6 and TGF-β3 in MGC gels, the ASC cellularity and glycosaminosglycan production were similar for 28 days. The ratio of collagen type II to I per cell (normalized to deoxyribonucleic acid content) in the microsphere delivery group was significantly higher than that of non-induced ASC or with

soluble growth factor administration in the culture media, and increased with time. Thus, the co-delivery of growth factor-loaded microspheres and ASC in MGC gels successfully induced ASC chondrogenesis and is a promising strategy for cartilage repair.

ACKNOWLEDGEMENTS

First I would like to acknowledge my supervisor, Dr. Brian Amsden, for his research guidance and direction throughout my PhD study in Queen's University. I have learnt valuable lessons from him of how to be good researcher, gained knowledge from him as well as comprehended his strive for science in research. Thus, I am grateful to be trained under his supervision.

I would also like thank Dr. Lauren Flynn for taking time to train me on isolation procedures of adipose stem cells (ASC), providing the access to obtain fat tissues from patients in Kingston General Hospital and her input in ASC chondrogensis subject. Dr. Francois Sauriol has also given me a great help in the suggesting the best running conditions for my NMR samples.

My shared experience and thought with my friends during my PhD study: Aasma Khan, Denver Surrao, Oladunni Babasola, Yulia Uvarova, Yimu Zhao, Rafi Chapanian, Bo Qi, Ariel Chan and Elizabeth Srokowski, are greatly valued and remain in me.

Last but not least is my gratitude towards my family (Tjokro Sukarto, Alice Sarman, Nany Sukarto Cardella, Banda Sukarto and Angela Sukarto Lam) that has supported me throughout, regardless of my decision, as well as loved me unconditionally.

TABLE OF CONTENTS

LIST OF FIGURES

LIST OF TABLES

LIST OF ABBREVIATIONS

Sol	sol content
$m_{dry,ini}$	mass of the dried gel before swelling
$m_{dry,fin}$	mass of the dried gel after swelling
m_{wet}	mass of wet gel
p	indenting force
ω	indenting depth
a	radius of a given indenter
κ	a correction factor that accounts for the finite layer effect
E	Young's modulus
h	height of gel
v	Poisson ratio
I	integration peak
T_f	melting point of the copolymer
T_f^o	melting point of the crystallizable homopolymer in its pure state
R	gas constant
X_B	mole fraction of noncrystallizable comonomer
ΔH_f	heat of fusion
T_g	glass transition temperature
ΔH_m	enthalpy of melting
X	degree of crystallinity
M_n	number average molecular weight
η	viscosity
Ac-G*C*GYG**RGD**SPG-NH_2	RGD peptide sequence

ACI	articular cartilage implantation
ASC	adipose-derived stem cells
BMSC	bone marrow-derived stem cells
BMP-2, 4, 6 and 7	bone morphogenetic protein-2, 4, 6 and 7
BSA	bovine serum albumin
C2C12	mouse myoblast cell line
COL1A1	collagen type I gene
COL2A1	collagen type II gene
COL10A1	collagen type X gene
c[RGDfK (Ac-SCH_2CO)]	cyclic RGD peptide
DMSO	dimethyl sulfoxide
DNA	deoxyribonucleic acid
DOS	number of grafted *N*-methacrylate groups per 100 residues
ECM	extracellular matrix
EDC	carbodiimide
EWC	equilibrium water content
FGF-a	fibroblast growth factor-acidic
FGF-b	fibroblast growth factor-basic
GAGs	glycosaminoglycans
HT-2	mouse spleen T lymphocytes
IGF-1	insulin-like growth factor-1
IL-1β	interleukin-1β
Irgacure 2959/ I2959	2-hydroxy-4′-(2-hydroxyethoxy)-2-methylpropiophenone
LCST	lower critical solution temperature
MAGC	*N*-methacrylate, *N*-acrylamide glycol chitosan
MGC	*N*-methacrylate glycol chitosan

MMP-1, 3, 8 and 13	matrix metalloproteinases-1, 3, 8 and 13
mRNA	messenger ribonucleic acid
MSC	mesenchymal stem cells
NHS	*N*-hydroxysuccinimide
NO	nitric oxide
OA	osteoarthritis
Oct-P(TMC-CL)	octanol initiated poly(1,3-trimethylene carbonate-*co*-ε-caprolactone)
OPF	oligo(poly(ethylene glycol) fumarate)
PCL	poly (ε-caprolactone)
PDI	polydispersity
PDLA	$_{D}$-PLA
PDLLA	$_{D,L}$-PLA
PEG	polyethylene glycol
PGA	poly(glycolic acid)
pI	isoelectic point
PLA	poly(lactic acid)
PLGA	copolymer poly($_{D,L}$-lactic-co-glycolic acid)
PLLA	$_{L}$-PLA
POC	poly(1,8-octanediol citrate)
PTHrP	parathyroid hormone-related peptide
PTMC	poly (1,3-trimethylene carbonate)
P(TMC-CL)$_2$-PEG	poly(1,3-trimethylene carbonate-*co*-ε-caprolactone)-*b*-poly(ethylene glycol)-*b*-poly(1,3-trimethylene carbonate-co-ε-caprolactone)
PUR	poly(urethane)
RT-PCR	reverse transciption polymerase chain reaction

SOX-9	SRY (sex determining region Y)-box9
SPDP	*N*-succinimidyl 3-(2-pyridyldithio)-propionate
sulfo SANPAH	sulfosuccinimidyl-6-(4'-azido-2'-nitrophenylamino) hexanoate
TGF-β	transforming growth factor-β
TNF-α	tumor necrosis factor-α

CHAPTER 1

INTRODUCTION AND LITERATURE REVIEW

1.1. Introduction

Joint pain is a major cause of disability in the middle-aged and older populations as well as athletes. The pain is usually caused by the degeneration of articular cartilage due to osteoarthritis or injury, leading to loss of cartilage and intra-articular bleeding. Cartilage has very little tendency to self-repair and this leads to further degeneration [2].

In cases where virtually the whole articular layer has degenerated, joint arthroplasty is necessary. Joint arthroplasty is a total replacement of both joint surfaces by metal and high density polymer. Approximately 488,000 people underwent total knee arthroplasties annually in the United States at an estimated cost of $6.3 billion in 2004 [3]. However, total joint arthroplasties do not reproduce normal joint function and have a limited life span. Tremendous efforts have been made in developing surgical interventions to effectively repair damaged articular cartilage, but they have achieved little success and only temporarily relieve the joint pain. This lack of success has led to the examination of tissue engineering approaches to develop replacements for damaged articular cartilage. Tissue engineering uses a combination of scaffolds, cells and suitable biochemical and physio-chemical factors to manufacture a functional, engineered tissue construct mimicking native tissue [4].

This project focuses on producing a hydrogel scaffold incorporated with stem cells and bioactive signals to regenerate articular cartilage tissue, by rationally selecting the potential scaffold materials for cell and bioactive macromolecule delivery vehicles.

1.2. Articular cartilage

There are three different types of cartilage: the elastic, the fibrous and the hyaline cartilage, with predominant fibers of elastin, collagen type I and type II, respectively. Elastic cartilage is found in the pinna of ear, the walls of the Eustachian tubes and the epiglottis (a thin valve-like flap that covers the entrance of larynx to prevent food entrance during swallowing). Fibrous cartilage is mainly found in annulus fibrosus of intervertebral discs, meniscus, and temporomandibular joint. Hyaline cartilage is located mainly in the ventral ends of the ribs, larynx, trachea, bronchi and on the articular surface of bones, and has better biomechanical properties. [5]

Articular cartilage is an avascular tissue capable of withstanding repeated load bearing activities and distributing load to the subchondral bone. It has a high resistance to wear due to its low friction coefficient. Cartilage is comprised primarily of extracellular matrix (ECM) and 2% by volume of a single type of cells called chondrocytes. The matrix components include tissue fluid/ water (75 to 80% wet wt.), collagens (50 to 73% dry wt.), proteoglycans (15 to 30% dry wt.) and other minor components, all of which are synthesized and maintained by the chondrocytes [1].

1.2.1. Extracellular Matrix Components

1.2.1.1. Collagen

The types of collagen in articular cartilage are II, V, VI, IX, X and XI. However, collagen type II is the most abundant and provides 90% of the total collagen content and 50% of the dry weight of cartilage [6-8]. Type IX and XI collagen have roles in stabilizing and strengthening the meshwork as inter- and intrafibrillar crosslinking agents to collagen type II

fibrils, which provides tensile strength and physical entrapment of macromolecules [6, 7, 9, 10]. Type VI collagen helps the attachment of the chrondocytes to the ECM meshwork [11, 12] and type X has role in mineralization on the calcified, thin layer of cartilage tissue next to the subchondral bone. [1, 13]

1.2.1.2. Proteoglycans

Proteoglycans are macromolecules composed of 95% sulfated subunits of polysaccharides (glycosaminoglycans) and 5% protein. The glycosaminoglycans (GAGs), such as chondroitin sulfate, dermatan sulfate and keratan sulfate, are bound to a protein core. Multiple protein cores containing GAGs are linked to hyaluronic acid forming the proteoglycan aggregates aggrecan and versican (Figure 1.1) that fill most of the interfibrillar space of the ECM [14-17]. In addition, the aggregation prevents diffusion of proteoglycan out of the matrix during joint loading. Since GAGs are negatively charged due to sulfate and carboxylate groups, they attract positively charged ions (Na^+), resulting in an increase in osmolarity and hydrophilicity, and repel one another, keeping the macromolecules distended. Hence, aggrecans are assumed to be responsible for stress distribution in articular cartilage. The expansion force of proteoglycans is counter-acted by the interconnected collagen fibrils to maintain the structural integrity of the matrix and the arrangement contributes to the compressive stiffness of hyaline cartilage. Other proteoglycans present in hyaline cartilage tissue include decorin, biglycan, perlican, and fibromodulin. [1, 18]

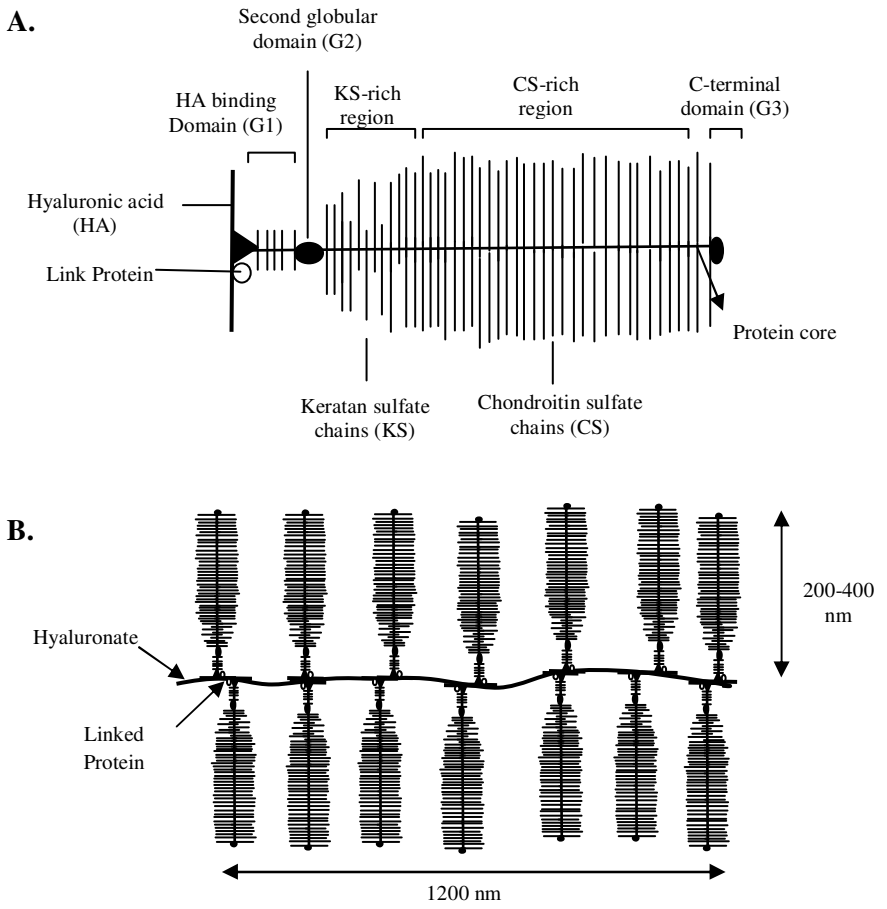

Figure 1. 1. Structures of (A) proteoglycans and (B) proteoglycan aggregates (adapted from [1])

1.2.1.3. Noncollageneous ECM composition

Minor components of cartilage include nonspecific lipids, non-collagenous protein (link protein, fibronectin and tenascin), glycoproteins (anchorin CII and cartilage oligomeric protein) and growth factors [19-22]. Glycoproteins, which consist of a small amount of oligosaccharides bound to a protein core, help to stabilize the ECM, anchor chondrocytes to the surrounding matrix, and promote chondrocyte-matrix interactions [18]. Fibronectin and tenascin are considered to serve a similar function as that of glycoproteins. [1, 13]

1.2.1.4. Tissue fluid

Tissue fluid contains water, gases, metabolites and a large amount of mobile cations to balance the negatively charged GAGs. The exchange of tissue and synovial fluid supplies nutrients and oxygen to the avascular cartilage and removes metabolic waste from the tissue. Tissue fluid interaction with ECM components also allows cartilage to resist compression and return to its normal shape after deformation. [18]

1.2.2. Zones of articular cartilage

The morphology, physiology and matrix arrangement of articular cartilage varies with the depth of the tissue. Cartilage consists of four morphological layers: the superficial, middle or transitional, deep or radial, and calcified zones. The zonal arrangement of articular cartilage is described in the next section and shown in Figure 1.2. [1, 18]

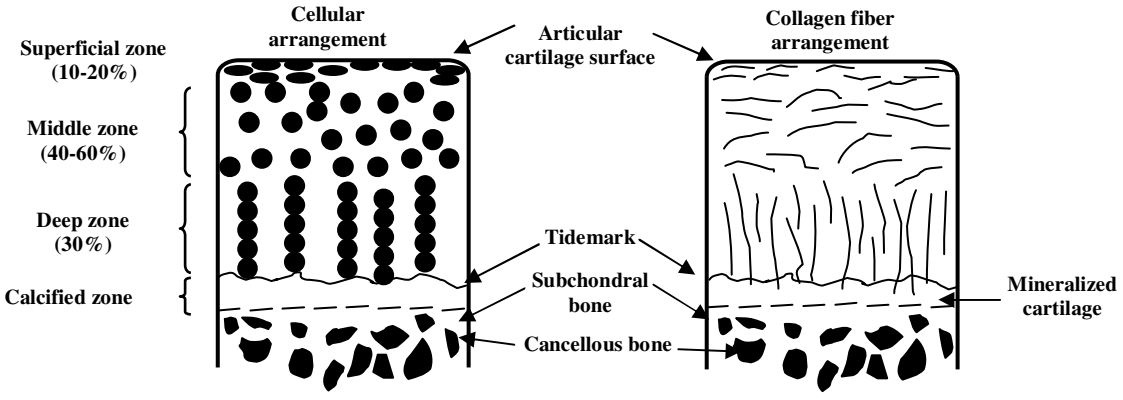

Figure 1. 2. Cellular and collagen arrangement of zonal articular cartilage (adapted from [1])

The superficial zone is the top layer of articular cartilage, occupying 10 to 20% of the total volume and is comprised of two distinct layers: an acellular sheet consisting of collagen fibers, and a deeper layer containing flattened chondrocytes. This zone contains a low concentration of proteoglycans, a high concentration of horizontally arranged collagen and a large amount of fibronectin and water. It provides compressive strength and resistance to shear stresses [23-25], and possibly isolates cartilage from the immune system. [1, 13, 18]

The middle zone, taking up 40 to 60% of the volume of the tissue, retains a high concentration of proteoglycans, a low concentration of larger-diameter collagen and water, and spherical chondrocytes. The collagen fibrils are oriented randomly in a non-parallel fashion. These spherical chondrocytes possess synthetic organelles such as endoplasmic reticulum, Golgi bodies and mitochondria. [1, 13, 18]

The deep zone, occupying 30% of the total volume of cartilage, contains column-arranged spheroidal chondrocytes, the largest diameter of collagen fibers that are parallelly aligned and oriented perpendicular to the subchondral bone, and the least amount of water. The chondrocytes in this zone show synthetic activities of approximately ten times that of the superficial zone. The collagen fibers extend into the tidemark that indicates the beginning of the calcified zone. [1, 13, 18]

Finally, the calcified zone maintains very small numbers of chondrocytes that have a low level of metabolic activity. The chondrocytes in this region are smaller and have no endoplasmic reticulum. This zone is rich in type X collagen and functions as a fixation between cartilage and the underlying subchondral bone. Significant shear stresses are produced in this zone due to the load transfer from the hyaline cartilage to the stiff underlying subchondral bone. [1, 13, 18]

1.2.3. Physiology of articular cartilage

Cartilage tissue behaves in a hydraulic fashion. The interstitial fluid flows out of the matrix during compression and returns into the matrix after load removal. The low permeability of the superficial layer prevents a large amount of fluid from flowing out of the matrix rapidly. This protects the solid phase of the underlying subchondral bone from strong, sudden compressions, and maintains the compressive force for hundreds to thousands of seconds before the fluid flows out of the matrix and reaches equilibrium. Moreover, movement of the joint, leading to compressive forces on the cartilage, results in synovial and tissue fluid movement into and away from the tissue. This fluid shift serves a metabolic function for chondrocytes, in that the synovial fluid supplies nutrients, while the tissue fluid removes wastes from the tissue [1].

1.3. Cartilage damage

Cartilage damage is mainly caused by osteoarthritis and trauma. Osteoarthritis (OA) is a progressive joint disease associated with the aging process and is commonly experienced by older individuals. On the other hand, some traumatic injuries are caused by excessive mechanical stresses in the joint, and eventually lead to osteoarthritis development.

OA is characterized by an imbalance between the anabolic (synthesis) and catabolic (resorption) activities of chondrocytes. The process of degeneration is initiated by proteoglycan loss, followed by disruption of the collagen fibril network resulting in chondrocyte apoptosis and eventually functional cartilage damage. The factors leading to OA are interconnected and include senescence (chondrocyte aging), apoptosis (programmed cell death), local inflammatory processes, and excessive mechanical stress [1].

1.3.1. Senescence

Senescence-related changes in cartilage tissue are one of the major leading factors in the development of OA. Chondrocyte changes associated with aging result in the decline of cellular activities that reduces the synthesis of proteoglycans and collagens. As a consequence, the structural and biochemical matrix become re-organized, collagen linking is increased, and tensile strength and stiffness are decreased. The characteristics of chondrocyte aging are specifically identified by their decreased metabolic activities, slower proliferation rates, the production of smaller and irregular aggrecans due to decreased proteoglycan synthesis, increased β-galactosidase (cell senescence marker) expression in chondrocytes, telomere erosion and decreased response to numerous growth factors. In addition, it has been demonstrated that the proteins (stromelysin-1, interstitial collagenases and chitinase-like protein) secreted by the chondrocytes from normal, senior (68.8 ± 4.2 years) patients were similar to those of chondrocytes from OA patients [26]. [27]

1.3.2. Apoptosis

Programmed cell death, or apoptosis, is an essential part of homeostasis for all tissues. Studies have shown that chondrocyte apoptosis occurs after injury from impact, resulting in cytokine and nitric oxide (NO) release and chondrocyte aging. In contrast, some studies have shown that apoptosis was linked to proteoglycan depletion within the ECM [28, 29] and others indicated that apoptosis only occurred in the calcified layer [30]. Regardless of the different findings in the role of apoptosis, it leads to the development of OA [27].

1.3.3. Local inflammatory response

Local inflammatory responses within the damaged cartilage have been shown to contribute to OA development. They are usually accompanied by cytokine activities initiated by interleukin-1β (IL-1β) and tumor necrosis factor-α (TNF-α). Cytokines, soluble molecules mediating cell-cell interactions, have low activities in normal cartilage. IL-1, a prototypical pro-inflammatory cytokine, stimulates the production of matrix metalloproteinases (MMP) such as MMP-1, 3, 8 and 13. MMPs are a family of enzymes that degrade collagen, elastins and other ECM components. These enzymes co-localize with other pro-inflammatory catabolic enzymes to degrade cartilage. Both IL-1 and TNF-α also enhance cartilage damage, inhibit proteoglycan synthesis and increase nitrous oxide (NO) synthesis. NO radicals down-regulate matrix synthesis, up-regulate matrix degradation via MMPs and induce chondrocyte apoptosis. Other cytokines responsible for cartilage degradation in OA are the chemoattractive cytokines (chemokines), such as CC chemokine (i.e. CCL2) and CXC chemokine (i.e. CXCL1 and CXCL8). The engagement of these chemokines to their corresponding receptors induces the release of degrading enzymes (e.g. MMP-1, 3, 13 and N-acetyl-β-D-glucosaminidase). [27]

1.3.4. Mechanical stresses

Mechanical factors leading to cartilage damage are compromised joint protection and excessive load. The former might be caused by mal-alignment, muscle weakness, genetic predisposition or aging, while the latter may be due to obesity, certain physical activities and acute trauma. The results of these mechanical stresses are ECM degradation, an increase in the production of matrix degradation enzyme MMP-3, and increased cell death and proteoglycan loss. [27]

1.4. Repair process and interventions of articular cartilage

The ability of cartilage to repair itself is extremely limited because cartilage tissue is not surrounded by blood vessels that engage in blood transport and thus there is an absence of blood cells (i.e. leukocytes) that mediate and promote the healing process [31]. As a result, the healing response to cartilage injury largely depends on the depth of the lesions formed. These lesions are classified as partial and full-thickness injuries.

1.4.1. Partial thickness injury

Partial thickness injuries are superficial lesions on cartilage tissue without damaging the subchondral bone. Despite a brief period of chondrocyte proliferation and matrix synthesis after injury, the new matrix does not fill the lesion, resulting in no healing progress. The healing disruption in partial thickness injuries might be caused by the relatively low metabolic activities and slow proliferation rates of mature chondrocytes. In addition, the ECM and proteoglycans impede chondrocyte migration and prevent cell adhesion in filling the defect. [1, 18]

The interventions of partial thickness defect include lavage and arthroscopy, shaving, debridement and laser abrasion/ laser chondroplasty. The approaches involve removing diseased chondral tissues or free bodies from the joint by thorough rinsing, shaving and mechanical cutting. Nonetheless, fibrocartilaginous tissue is formed rather than hyaline tissue. [31]

The first attempt at cartilage repair using a cell-based therapy in a clinical setting was an articular cartilage implantation (ACI) [32]. This approach involves the isolation of healthy chondrocytes from a biopsy of less-load bearing cartilage during an arthroscopic procedure followed by an *in vitro* expansion. The expanded chondrocytes in suspension were injected into a defect, covered with a periosteal flap harvested from the tibia and sutured or glued with fibrin to

the edges of the cartilage lesions. The ACI procedure for cartilage regeneration resulted in a high degree of success; 84 to 90% with a 2 to 10 year follow-up [33]. To reduce the number of surgical sites during the ACI procedure, the periosteum was replaced with a collagen membrane, which had a significant improvement on clinical/ functional results [34]. The ACI technique was further improved using cells grown on a carrier membrane (i.e. matrix-induced autologous chondrocyte implantation, MACI) [35] and hyaluronic scaffold [36, 37]. Both of the implanted scaffolds resulted in hyaline-like cartilage tissue.

1.4.2. Full thickness injury

Full-thickness injuries arise from damaging the entire cartilage thickness, with the damage penetrating the subchondral bone. Blood exposure to the defect triggers the healing response. Initially, the injury site is filled with a fibrin clot and undifferentiated mesenchymal stem cells from the bone marrow after three days. These stem cells mediate the healing process and form cancellous bone at the base of the defect after two weeks, with complete bone regeneration after 12 weeks. Meanwhile, the chondrogenic mesenchymal stem cells start to produce ECM in the cartilage defect that was initially filled with irregular connective tissue. However, this newly formed tissue does not possess the morphological and biochemical composition of native cartilage, resulting in no integration to the surrounding tissues, but extensive tissue degeneration. The degenerative process is identified by superficial cartilage fibrillation, hypocellularity and a decrease in proteoglycan content. [1]

The therapeutic interventions for full thickness defect are abrasion chondroplasty, Pridie drilling, microfracture and spongialization, osteochondral transplantation (mosaicplasty) and allogenic osteochondral grafting. The first three methodologies involve surgical access into the underlying subchondral bone to allow blood flow from the bone marrow to stimulate a

spontaneous tissue healing response. Nonetheless, fibrocartilaginous tissue is formed rather than hyaline tissue [31]. The last two therapies involve transplantation of biological tissues into the defect. Mosaicplasty is a translocation of autologous osteochondral tissue from low load bearing sites to high load bearing ones with the insertion of several small cylindrical tissues into the defect site after drilling a bone hole. Mosaicplasty is currently the most established surgical technique in the treatment of large osteochondral defects, but this technique results in tissue degeneration in the new location because of a lack of lateral mechanical support. Moreover, it suffers from donor site morbidity. Allogenic osteochondral grafts of healthy articular cartilage from cadavers have also been employed with reasonable success. Nevertheless, donor shortage, cryopreservation problems, and the risk of disease transmission limit the continuity of the approach [31].

1.5. Cartilage Tissue Engineering

Most of the interventions for cartilage repair result only in temporary relief instead of hyaline cartilage regeneration, except for the ACI procedure that has had a high success in clinics. Randomized studies comparing cartilage repair interventions of ACI and mosaicplasty also showed that ACI resulted in better clinical outcome [38]. Thus, it is imperative to prevent a cartilage injury to deteriorate to a full thickness cartilage defect. The replacement of chondrocytes through injection of cells seeded on scaffolds has stimulated the field of tissue engineering in orthopedic research. Tissue engineering utilizes a biomaterial scaffold, cells and bioactive factors to engineer a functional tissue and allows properties of the graft to be customized *in vitro* before implantation to achieve structural, biological and biomechanical signals that mimic native tissue [4]. However, there are also several limitations in engineering an *ex vivo* cartilage tissue replacement. These limitations are elaborated in the next section.

1.5.1. Challenges in chondral tissue scaffold design

Several challenging issues in producing chondral tissue constructs still remain. Tremendous efforts have been spent to reduce and eventually eliminate these obstacles. The primary concerns are as follows:

1. Cell source

It is generally accepted that a homogeneous cell population capable of producing hyaline cartilage is necessary in the articular scaffold region [31]. Human chondrocyte expansion without loss of phenotype can be carried out in a three-dimensional culture, such as microcarriers [39]. However, it has been demonstrated that autologous tissue transplantation within porous scaffolds and hydrogels produced fibrous tissue interface with the host tissue [40-42]. The choice of cells for this region has been directed towards adult stem cells from human. Adult stem cells should be a more appropriate cell choice since the potency of chondrogenic stem cells in cellular signaling and communication with the host tissue is higher [43, 44].

2. Mechanical Properties

The mechanical properties of the scaffolds determine the overall success in producing functional articular cartilage tissue for cartilage repair and have been the most challenging issue to solve. The Young's modulus of adult knee articular cartilage for humans ranges between 2.1 to 11.8 MPa [45, 46]. Many of the *in vitro* studies for cartilage tissue repair were analyzed based on gene expression measured using real-time polymerase chain reaction (RT-PCR), histology and immunohistochemistry staining and GAG quantification. However, the mechanical properties of the scaffold containing newly synthesized ECM were not measured.

3. Tissue maturation and integration with host tissue

Although human adult stem cells seeded within the scaffold might stimulate tissue integration better than autologous chondrocytes, rapid and stable differentiation of the stem cells throughout the scaffolds is important to reduce healing time. Therefore, incorporation of growth factors into the constructs may be necessary to differentiate stem cells to chondrocytes [47]. Also, *in vitro* culture time should be minimized to obtain good tissue integration. Obradovic et al. showed that bovine chondrocytes cultured on a polyglycolic acid scaffold for 5 days had better integration with a cartilage grown on the same scaffold for 5 weeks prior to implantation in the explant [48]. This result was considered to be due to the presence of proliferating cells migrating into the adjacent tissue. Chondrocytes grown for longer time periods tended to secrete matrix components into the acellular interface, leading to poor integration with the apposed tissue.

1.5.2. Cell Source

Cell source is an important parameter that determines the success of a functional tissue scaffold. In articular cartilage repair, cell sources include chondrocytes from normal and osteoarthritic (OA) tissues and adult stem cells derived from various tissues of the patients. Chondrocytes can be obtained from load- or non-load- bearing cartilage, while adult stem cells can be isolated from the bone marrow, periosteum, synovial membrane and adipose tissues.

Utilizing human chondrocytes as a cell source has numerous drawbacks. Autologous chondrocytes have demonstrated fibrous tissue formation at the junction of the tissue scaffold and host tissue [40]. In addition, mature chondrocytes tend to synthesize the ECM rather than to proliferate; thus, an acellular interface is formed and an integration with the host tissue is absent [48]. Besides, chondrocyte isolation requires invasive surgery and only a small number of cells

are obtained so that further expansion is required before enough cells can be seeded into a scaffold. Chondrocytes are also prone to phenotypic de-differentiation into fibroblasts in two-dimensional culture, lose re-differentiation after expansion [49-51], and replicate slowly [47]. Thus, chondrocyte expansion is not favorable.

Because of the difficulties in isolating and expanding chondrocytes, adult stem cells are an alternative source for obtaining chondrocytes. Adult stem cells are highly replicative cells, have multilineage differentiation capacity, and are accessible from many tissues. Due to their proliferation rates, adult stem cells can be rapidly expanded. In addition, chondrogenic adult stem cells have higher metabolic activities in proliferation and greater matrix synthesis that leads to better integration between the engineered and host tissue [52-54].

The most popular location for obtaining adult stem cells is the bone marrow. Human bone marrow-derived stem cells (BMSC) are the most extensively studied adult stem cell for their chondrogenic potential. However, bone marrow aspirates are associated with high morbidity from wound infection, potential sepsis complications, pain and low cell yields [55]. Adult stem cells derived from the periochondrium layer containing cartilage progenitor cells have also been studied for their use in cartilage repair. Nevertheless, the need for two surgical interventions, highly variable results in experimental studies so far and long-term instability of the repair tissue formed have prevented this cell source from entering clinical practice to date [31, 56, 57].

Furthermore, human synovial-derived stem cells also have a chondrogenic potential that was demonstrated to be higher than BMSC, periosteum- and adipose-derived stem cells from the same patients [58-60]. However, the low availability of synovial membrane and thus isolated stem cells has limited their use in experimental studies for cartilage tissue engineering. On the other hand, human adipose-derived stem cells (ASC) have gained a lot of attention in experimental studies of cartilage repair over the last decade. Adipose tissue as a source to obtain

adult stem cells has advantages because it is readily accessible, available in large quantities with minimal donor site-morbidity and patient discomfort and yields a large quantity of harvested multipotent cells [61]. Hence, human ASC are the focus of the cell source in this study. The appropriate growth factors required for chondrogenesis induction of ASC are to be discussed in the next section.

1.6. Scaffold materials for cartilage repair

As mentioned above, partial and full thickness lesions do not elicit a healing response. Prior to cartilage degeneration from partial to ultimately full thickness lesions, the chondral defect must be immediately restored using a tissue engineering approach. Many studies of engineered chondral tissues have been carried out using various biomaterials. Several biocompatible and biodegradable biomaterials have been applied to the fabrication of a tissue scaffold for cartilage repair and include natural and synthetic polymers (Table 1.1) [62].

Table 1. 1. Natural and synthetic polymers used in cartilage

Source	Materials
Natural	Collagen
	Agarose
	Gelatin
	Alginate
	Fibrin
	Hyaluronic acid
	Chitosan
Synthetic	Polyethylene glycol
	Oligo(poly(ethylene glycol) fumarate)
	Poly (α-hydroxy esters)
	Poly(1,8-octanediol citrate)
	Poly(urethane)

Ideally, scaffold material and design should mimic the native tissue as closely as possible. The scaffold property requirements for cartilage regeneration are to be biodegradable, to prevent an inflammatory and immune response, to promote cell adhesion, to have a degradation rate that matches the newly synthesized ECM, to produce non-cytotoxic degradation products and to have a compressive strength and elasticity or structural stability similar to that of native articular cartilage [63, 64]. This set of criteria implies that a hydrogel would be a preferred matrix, due to their high water content and three-dimensional organization. However, the mechanical properties of hydrogels are not close to native articular cartilage tissue and so porous scaffolds have also been used. Porous scaffolds are non-covalently linked polymer networks that form dry constructs with certain pore size and porosity. They are usually prepared from synthetic polymers that dissolve in organic solvents and the pores are formed using various techniques following organic solvent removal. Nevertheless, a scaffold with all the required properties has not been achieved so far. Thus, scaffold material and design that have some of these features are being developed.

1.6.1. Hydrogels

Cartilage tissue is highly hydrated and is comprised of a large number of proteins and polysaccharides. Such scaffold designs that mimic cartilage tissue structure and provides three-dimensional organization are hydrogels. Hydrogels have high water content surrounded by insoluble polymer networks that are physically or chemically crosslinked and can be prepared in aqueous solution at ambient temperature. Hydrogels allow efficient solute transport (i.e. nutrients, metabolic products, oxygen and macromolecular drugs) within the gels and to the surrounding environment [65, 66]. In addition, crosslinking density, degree of swelling and

degradation rate of the gels can be tailored to the desired release kinetic of macromolecules [67-69]. For these reasons, hydrogels have been employed for cell and drug encapsulation.

Hydrogel networks can be formed via physical and chemical crosslinking. These crosslinking methods are applied to achieve the desired hydrogel properties for the intended applications. Physically crosslinked hydrogels can be obtained by hydrogen bonding, hydrophobic and electrostatic interactions of the polymer chains. Hydrophobic interactions occur in hydrogels that are sensitive to temperature. When the bulk temperature of the polymer in solution is higher than its lower critical solution temperature (LCST), the dissolved polymer loses its bound-water and interacts through its hydrophobic chains, leading to a de-swollen gel. An example of such a gel is poly(*N*-isopropyl acrylamide), which has a LCST of 32^0C and solidifies upon injection into human body at 37^0C [70]. Electrostatic interactions between polymer molecules can also form hydrogel networks. These types of gels contain ionizable groups and are sensitive to solution pH. For example, alginate consists of guluronic and manuronic acid residues that possess a pK_a of 3.2 and 4, respectively [71]. When immersed in a solution of a pH higher than the pK_a of the residues, alginate is deprotonated and thus crosslinked in calcium chloride solution due to the presence of calcium ions. This mechanism is also applied for cationic hydrogels that protonate and swell when the external pH is lower than the pK_b of the ionizable groups. Chemically crosslinked hydrogels are formed by covalent crosslinking of the polymer molecules. These types of gels can be fabricated via photocrosslinking (a free radical photopolymerization approach) and are more desirable as they are mechanically stable and do not require external stimuli (i.e. temperature, pH or ionic solution). [72]

Hydrogels can be prepared from natural polymers as well as some synthetic polymers. Natural polymers utilized in cartilage tissue engineering consist of protein-based polymers (collagen, gelatin and fibrin) and carbohydrate-based polymers (alginate, agarose, hyaluronan and

chitosan). The most common synthetic polymers are poly(ethylene glycol)-based polymers and oligo(poly(ethylene glycol) fumarate).

1.6.1.1. Collagen

Type I collagen from bovine or porcine has received the most attention initially as a tissue scaffold. Collagen can be gelled physically (ultraviolet or heat) and chemically (using chemicals such as glutaraldehyde, formaldehyde or carbodiimides). Collagen gels seeded with human mesenchymal stem cells (MSC) from various tissues (i.e. bone marrow, umbilical cord blood and synovium) have been reported to promote chondrogenesis [73-76]. However, the gel prevents cell migration within the matrix and thus reduces cartilage repair [32]. In addition, collagen sterility, fabrication and availability have been challenging issues due to a low assurance of pathogen transmission [18, 77, 78]. Besides, the degradability of collagen is poorly controlled and it rapidly loses its mechanical properties [79].

1.6.1.2. Gelatin

Gelatin is a thermally denatured collagen and cell-adhesive protein. It is also soluble in water at physiological conditions. Gelatin has been used as a scaffolding structure in cartilage tissue engineering and reported to support chondrogenesis of adult stem cells derived from human bone marrow and adipose tissues [80, 81]. Nevertheless, gelatin elicits a significant inflammatory response and foreign body giant cell reaction when exposed to vascularized tissues [31].

1.6.1.3. Fibrin

Fibrin is the polymerized form of fibrinogen in the presence of thrombin. It has been used as a cartilage tissue scaffold because of its role in spontaneous wound clotting that facilitates tissue healing activities within the extravascular space [31]. It is pro-inflammatory, induces its own degradation followed by cellular component substitution, and produces non-toxic degradation products [31]. Fibrin has been employed as a stand-alone scaffold and a delivery vehicle for human MSC and growth factors [31, 82]. However, fibrin has poor mechanical properties and exogenous fibrin may evoke an immune response [31, 83, 84].

1.6.1.4. Alginate

Alginate is a linear polysaccharide containing (1→4)-linked β-$_D$- mannuronic acid (M) and α-$_L$-guluronic acid (G) monomers isolated from brown seaweed and bacteria. It can be used as an injected liquid for defect stabilization in the presence of calcium ions. It is also utilized as a crosslinked gel in slab or bead form to encapsulate cells. Human MSC seeded in alginate beads can differentiate into chondrocytes both *in vitro* and *in vivo* if presented with appropriate chemical and mechanical signals [85-90]. Nevertheless, alginate inhibited spontaneous cartilage repair when implanted alone and articular cartilage engineered from it *in vitro* induced severe foreign body giant cell and immunological reactions, when implanted in full thickness defects in animals [31]. In addition, alginate is not degradable *in vivo* and can only be eliminated from the body when its molecular weight is less than 20 kDa [91].

1.6.1.5. Agarose

Agarose is a polysaccharide containing repeating $_{L}$- and $_{D}$- galactose monomers isolated from Asian seaweeds. Use of agarose allows uniform distribution of chondrocytes throughout the scaffolds and it has been used to study the behavior of chondrocytes *in vitro* [31]. Agarose has also been utilized as a cell carrier for examining the chondrogenesis of human MSC [80, 92, 93]. Nevertheless, agarose is poorly degraded *in vivo* due to the absence of appropriate enzymes in mammalian tissues, and has been shown to inhibit spontaneous repair in an osteochondral defect in rabbits, due to foreign body giant cell reactions [31].

1.6.1.6. Hyaluronan

Hyaluronan is a high molecular weight polysaccharide containing repeating disaccharides of (1→3) and (1→4)-linked β-D-glucuronic acid and *N*-acetyl-β-glucosamine. Hyaluronan would be an ideal tissue scaffold material because it is a physiological component in articular cartilage and it is biodegradable. Moreover, a hyaluronan tissue scaffold was able to downregulate the expression of catabolic factors, decreased the level of matrix metalloproteinases (MMPs) and cell apoptosis, and inhibited the production of molecules involved in cartilage degenerative diseases [27, 31]. However, the usefulness of hyaluronan as a long-term biomaterial implant is hindered by its rapid enzymatic degradation in the body. For instance, hyaluronan is degraded at a rate 5 g/day, of the normal 15 g in human body [94]. To slow down and control the degradation rate, hyaluronan has been modified through an esterification crosslinking and synthetic polymer conjugation. The gelation of modified hyaluronan can be prepared via photocrosslinking [95-99], Michael addition reaction [100-102] and carbodiimide coupling [103].

Additionally, hyaluronan degradation products (oligosaccharides with residue less than 6) may lead to chondrolysis and proteoglycan depletion in human articular cartilage [104].

1.6.1.7. Chitosan

Chitosan is a deacetylated form of the polysaccharide chitin, which is extracted from crustacean shells. It contains a linear chain of (1→4)-linked D-glucosamine and *N*-acetyl-β-glucosamine units. The degree of *N*-deacetylation varies from 50% to 90%. Chitosan is only soluble in aqueous solution below pH ~5 due to amine protonation. Chitosan can be crosslinked with polyanion chondroitin sulfate to form a hydrogel [105, 106]. Chitosan shares some molecular characteristics of GAGs found in articular cartilage, such as *N*-acetyl glucosamine, and so it has been widely applied as a tissue scaffold in cartilage defects [31]. Chitosan was able to maintain the round morphology of chondrocytes, which produced cell-specific ECM, and, with GAG incorporation, exhibited improved mechanical properties and collagen stability [107, 108]. A thermosensitive chitosan gel was also reported to support chondrogenesis of human bone marrow-derived MSC from the posterior iliac crest [109]. Moreover, it is non-cytotoxic, biodegradable and promotes wound healing [110].

1.6.1.8. Polyethylene glycol

Polyethylene glycol (PEG) hydrogels have been extensively used in drug delivery devices due to their biocompatibility and non-immunogenicity. They have been recently examined for cartilage tissue engineering. Unmodified PEG hydrogels, produced by γ-irradiation or electron beam irradiation, are not biodegradable. On the other hand, chemically modified PEG hydrogels, containing terminal ester linkages, are biodegradable via hydrolysis. They can be

prepared via photocrosslinking [111-113] and Michael addition reaction [114, 115]. In addition, PEG gels have been utilized for chondrogenesis of encapsulated human bone marrow-derived MSC [116-120]. It was found in recent studies that PEG hydrogel degradation controlled the ECM deposition by rat chondrocytes [121]. The major limitation of PEG is its lack cell adhesion sites [122, 123].

1.6.1.9. Oligo(poly(ethylene glycol) fumarate)

Oligo(poly(ethylene glycol) fumarate) (OPF) is a PEG-based macromer with unsaturated double bonds along the macromolecular backbone. OPF hydrogels can be prepared using redox radical initiators (i.e. ammonium persulfate) and reducing agents. The radical initiator affects cell viability in a concentration-dependent manner. They have been used to encapsulate bovine chondrocyte and rabbit MSC for cartilage regeneration. Nevertheless, chondrogenesis of human MSC has not been studied with these polymers to date. [124]

1.6.2. Porous scaffolds

Porous scaffolds also are employed in cartilage tissue engineering. They can provide mechanical properties close to native cartilage and necessary to obtain functional engineered tissue. However, the scaffold structure is far from cartilage tissue and thus increases the difficulties in obtaining the desired cell differentiation state. Porous scaffolds can be prepared from synthetic polymers that are available in unlimited supply and are easily processed into the desired properties (physical, chemical and degradation). Synthetic polymers have lower risk of toxicity and immunogenicity than natural polymers. However, they lack biological cues that can promote desirable cell response and cell-material interaction [125].

Several methods have been developed to fabricate porous scaffolds. These include solvent casting combined with particulate leaching, freeze drying, super-critical fluid technology, fiber meshes and bonding, phase separation, melt molding and combination of these techniques [126]. The processing technique must produce an accurate geometry of a 3D scaffold that fits the implant site, lead to interconnected and dense porosity with uniform size and distribution, and have a good reproducibility [127]. Synthetic polymers used for cartilage tissue engineering application include poly(α-hydroxy esters), poly(1,8-octanediol citrate) and poly(urethane).

1.6.2.1. Poly(α-hydroxy esters)

Poly(α-hydroxy esters) are commonly used synthetic polymers in tissue engineering because of their biodegradability and use in FDA approved devices. They include poly(glycolic acid) (PGA), poly(lactic acid) (PLA) and the copolymer poly($_{D,L}$-lactic-co-glycolic acid) (PLGA). PLA exists in three forms: $_{L}$-PLA (PLLA), $_{D}$-PLA (PDLA) and $_{D,L}$-PLA (PDLLA). These polyesters are degraded by hydrolysis to form monomeric acid which is subsequently metabolized to carbon dioxide and water. The degradation products also autocatalyze the hydrolysis reaction. Limitations of these materials include possible cytotoxicity from the acidic degradation products, and the induction of a foreign body giant cell reaction [128, 129]. PLLA and PDLA are more hydrophobic, less crystalline and toxic, and degrade at a slower rate than PGA. PLGA polymer and PDLLA are utilized to control the degradation rate because they have amorphous structures and thus degrade faster than PGA, PLLA and PDLA. Another family member of polyesters is poly(ε-caprolactone) (PCL), which has slower degradation kinetics. Another major drawback of poly(α-hydroxy esters) and PCL is their hydrophobicity, which leads to poor wetting and cellular attachment and interaction. [18, 83, 125, 130]

1.6.2.2. Poly(1,8-octanediol citrate)

Poly(1,8-octanediol citrate) (POC) is a biodegradable polyester elastomer that can sustain repeating compression and tensile with recovery ratio greater than 90% [131]. It is degraded by hydrolysis to form citric acid, 1,8-octanediol and oligomers that can be cleared by the kidney *in vivo* [131]. A POC elastomer has been demonstrated to support cartilaginous matrix synthesis in bovine chondrocytes [132]. However, it has not been studied for chondrogenesis of human MSC or ASC so far. In addition, one of the breakdown products of citric acid is acetic acid, a pH-lowering acid [133].

1.6.2.3. Poly(urethane)

Biodegradable poly(urethane)-based scaffolds have gained increasing attention in the tissue engineering as they possess a broad range of mechanical and physical properties. Scaffolds from these polymers can be prepared from casting. They consist of hard and soft segments along the backbone of the polymer. The hard segment is a linear diisocyanate used to avoid toxic or carcinogenic degradation products, while the soft segment is typically represented by a degradable polyester (i.e. PLA, PGA or PCL) [126]. Poly(urethane)-based scaffolds can sustain physiological forces at the implant site and thus establish contact with native tissue favoring cell proliferation [134]. Poly(urethane) foam has been demonstrated to provide a conducive environment for chondrogenesis of human MSC loaded into the scaffold using a fibrin gel [135]. However, the acidic degradation products from hydrolysis of the polyester segment may cause *in vivo* inflammation [136]. In addition, prolonged culture has resulted in de-differentiation of chondrocytes [137].

In this project, glycol chitosan was chosen as the basis for preparing an *in situ* setting hydrogel. As mentioned in section 1.6.1.7, chitosan shares some molecular characteristics as the GAG found in articular cartilage, and has been widely employed as a tissue scaffold for articular cartilage. An advantage of glycol chitosan is its aqueous solubility over a wide range of pH, which allows molecule grafting onto glycol chitosan backbone under mild conditions and cell encapsulation at room temperature.

1.7. Growth factors

Chondrocyte proliferation, differentiation and homeostasis are regulated by ECM-bound mediators and ECM interaction with soluble mediators, such as dexamethasone, ascorbic acid, and growth factors. The ECM provides signals to chondrocytes through binding to cell transmembrane receptors (integrins). Integrins, which are composed of α and β subunits, transmit signals in two directions: 'inside-out' to allow binding to their ligands and 'outside-in' to regulate cellular activation [138]. For example, chondrocyte integrin binding to an ECM molecule (i.e. fibronectin) also links the integrin to the intracellular actin cytoskeleton, resulting in focal adhesion formation. This linkage triggers several signaling pathways related to anchorage-dependent survival and growth of cells. In addition, some signaling must be shared with growth factors for cellular activation. For example, the interaction between collagen type II and transforming growth factor-β (TGF-β) increases chondrocyte proliferation and proteoglycan synthesis [139, 140]. Similarly, binding of bone morphogenetic protein-2 (BMP-2) to collagen type IIA triggers chondrogenic pathways, resulting in stem cell differentiation to chondrocytes [141]. Cellular activities triggered by growth factor binding to cell membrane receptors depend on the number of receptors being activated. Hence, growth factor effects are concentration- and time-dependent [142]. In addition, the activated growth factor degrades rapidly and the

biological half-life of most growth factors is short (in the range of minutes) [143, 144]. Therefore, to successfully develop a functional tissue scaffold, growth factor incorporation is crucial to allow adequate signals being transmitted to the embedded cells within a scaffold, but the growth factors must be administered in a controlled manner to enhance their efficacy [138]. The growth factors known to have important roles in normal cartilage function are TGF-βs, insulin-like growth factor-1 (IGF-1) and BMPs [145-147].

1.7.1. TGF-βs

TGF-β1 is a 25-kDa homodimeric protein with each subunit containing 112 amino acids, linked by a single disulfide bond [148]. Most cells can secrete TGF-β1 and express TGF-β1 receptors and thus TGF-β1 plays a key role in cellular activities for proliferation and differentiation [149]. The half-life of TGF-β1 in the body is less than 30 min [150], due to rapid binding to the ECM components that activates, inhibits or neutralize its activities [144]. In addition, TGF-β1 was the first growth factor used to successfully induce chondrogenesis of *in-vitro* 3D rabbit MSC in the presence of dexamethasone [151]. Thus, it is the most extensively studied growth factor for chondrogenesis. Later, the combination of TGF-β1 and dexamethasone was used for inducing chondrogenesis of human BMSC [152-154] and ASC [61, 155, 156] in pellet cultures. The effective dose response of TGF-β1 on ASC was 5 ng/mL/day to obtain the greatest sulfated proteoglycan and aggrecan expression in pellet culture for a 14-day culture period [157]. Nevertheless, TGF-β1 also induced undesirable effects, such as inflammatory responses and osteophyte formation in articular cartilage following a prolonged period of exposure in knee joints [158].

TGFβ-2 and TGF-β3 are homologous isoforms of TGF-β1 (70-80% sequence homology), but they are less abundant in the human body [149, 159]. TGF-β2 induced chondrogenic differentiation of ASC in pellet culture *in vitro* and embedded in alginate gel *in vivo* (nude mice) with the evidence of the expression of the mature chondrocyte markers collagen type II and aggrecan [146]. However, the extent of collagen type I production *in vivo* was not examined to determine the extent of formation of hyaline cartilage tissue from the ratio of collagen type II to I. TGF-β3 in the presence of dexamethasone was superior in collagen type II (COL2A1) gene expression and GAG synthesis in the chondrogenic induction of ASC and BMSC, in comparison to TGF-β1 and TGFβ-2 [145, 153]. Nevertheless, the concentrations of 5 to 25 ng/mL/day TGF-β3 in the presence of dexamethasone for a culture period of 42 days was not sufficient to induce chondrogenic gene expression of ASC similar to the level of BMSC under the same conditions [160].

1.7.2. IGF-1

IGF-1 is a globular protein containing 70 amino acids and is structurally related to insulin [161]. It is synthesized in the liver under growth hormone regulation and plays a role in chondrocyte proliferation and synthesis of the ECM (proteoglycan and collagen type II) [162, 163]. The half-life of IGF-1 is 10 to 20 min in the body [164]. IGF-1 can be associated with IGF-1 binding protein as a reservoir to provide long-term stability [161]. Administration of IGF-1 alone at 5 ng/mL/day for 42 days did not induce ASC chondrogenesis in pellet culture, based on COL2A1 gene expression and collagen type II immunohistochemical staining [160].

1.7.3. BMPs

BMPs are a subfamily of the superfamily of TGF-β that has homologous amino acid sequences to TGF-β. BMPs were originally known as protein regulators of bone and cartilage formation by initiating chondrogenesis that subsequently serves as a template for bone morphogenesis. Nowadays, BMPs have been shown to play roles in growth, differentiation, chemotaxis and apoptosis of several cell types, such as mesenchymal, epithelial, neuronal and hematopoietic cells [165]. In comparison to all BMP types, BMP-6 is the most studied growth factor for ASC chondrogenesis. BMP-6 is a 26.2-kDa homodimer glycoprotein consisting of two 117 amino acid subunits. ASC encapsulated in alginate and induced with 250 ng/mL/day BMP-6 for 7 days demonstrated a very significant increase in aggrecan and collagen type II gene levels, while not inducing significant collagen type I gene expression [145]. *In vitro* and *in vivo* studies of ASC chondrogenesis in pellet culture using BMP-2 showed an increase COL2A1 gene expression after 28 days, but COL1A1 gene expression was not evaluated [147].

1.7.4. Use of combinations of growth factors

IGF-1 combined with TGF-β3 at a concentration of 5 ng/mL/day was fed to human ASC pellet culture for 42 days. The growth factor cocktail was only able to induce the expression of the COL2A1 gene from cells from 2 donors out of 3 after 42 days [160]. In addition, ASC encapsulated in alginate beads and induced with 50 ng/mL/day IGF-1 and 5 ng/mL/day TGF-β3 expressed lower COL2A1 gene and an increase of collagen type X (COL10A1), in comparison to ASC induced with aforementioned growth factors combined with 250 ng/mL/day BMP-6 after 7-day induction [145]. Im et al. also showed that 50 ng/mL/day IGF-1 combined with 2.5 ng/mL/day TGF-β2 did not induce chondrogenesis of ASC in pellet culture and fibrin scaffolds to

the same level as that of BMSC from the histology and collagen II immunohistochemical staining after 28 days [166]. However, with a high dose (250 ng/mL/day IGF-1 and 12.5 ng/mL/day TGF-β2 for 28 days), the gene expression of COL2A1 messenger ribonucleic acid (mRNA) was obtained to be the same level as those in BMSC induced with 2.5 ng/mL/day TGF-β2 [167].

The concentrations of 50 ng/mL/day BMP-2, -6 and -7 in addition to 2.5 ng/mL/day TGF-β2 has also been analyzed for the ability to induce chondrogenesis of ASC in pellet culture for 28 days [168]. The best growth factor combination was found to be BMP-7 and TGF-β2 as mRNA gene expression of COL2A1 was increased with stabilized collagen type X (COL10A1) gene expression. Nevertheless, COL1A1 was also increased. A similar dose of this growth factor combination in the presence of parathyroid hormone-related peptide (PTHrP) resulted in an increase of COL2A1 and SOX-9 (SRY (sex determining region Y)-box9) gene expressions without lowering COL1A1 for 14 days [169].

A wide range of chondrogenic growth factors, such as BMPs (-2, -4, -6, -7), fibroblast growth factor acidic (FGFa), FGF basic (FGFb), IGF-1 and PTHrP, alone or in combination with TGF-β3, was studied for their effectiveness in inducing human ASC chondrogenesis in pellet culture [160]. The concentration of each growth factor was 5 ng/mL/day administered for 42 days. BMP-6 combined with TGF-β3 resulted in the most positive results on both COL2A1 gene expression (all donors, 6/6) and collagen type II immunohistochemistry staining (7 out of 9 donors), in comparison to other growth factors, alone or in combination with TGF-β3. In addition, ASC chondrogenesis induced with this growth factor combination achieved the same chondrogenic potential as BMSC induced with TGF-β3 alone. The authors showed that the endogenous TGF-β receptor I protein was expressed on ASC in the presence of BMP-6 and thus the ASC sensitivity to TGF-β3 was enhanced. Another study demonstrated that higher mRNA gene expression of chondrocyte protein markers (COL2A1 and aggrecans) and similar collagen

type I (COL1A1) gene expression were obtained using this growth factor cocktail (5 ng/mL/day each for 14 days) for ASC encapsulated in alginate beads, in comparison to those of ASC induced with TGF-β3 (5 ng/mL/day) or BMP-6 (250 ng/mL/day) alone [86]. In addition, chondrogenic progenitor cells harvested from late stage osteoarthritis patients was demonstrated to have increasing chondrogenesis marker gene expression using this growth factor combination at the concentrations of 1.25 ng/mL/day TGF-β3 and 20 ng/mL/day BMP-6 for 42 days [170]. Thus, to date, it appears that BMP-6 and TGF-β3 are the most effective growth factor combinations for ASC chondrogenesis. Nevertheless, this combination also increased collagen type X, which remained negative in normal articular cartilage, except at the osteochondral tidemark.

The review on chondrogenic growth factors has shown that the use of growth factor combinations is more effective in ASC chondrogenic induction. The combined administration of BMP-6 and TGF-β3 was able to induce chondrogenesis of ASC in alginate beads at a low dose (5 ng/mL/day) for a short period of time (14 days) [171]. In addition, this low-dose growth factor cocktail was able to induce ASC chondrogenesis to the same level as BMSC in pellet culture [160]. Thus, this growth factor cocktail will be used in this study and incorporated into the selected delivery vehicle.

1.8. Controlled Release of Growth Factors

Due to the short half-life of growth factors and potential side effects of high doses if applied with direct injection (e.g. fibrosis in kidney, liver and injection site [144]), a sustained delivery growth factor is necessary with the use of a delivery vehicle. The important parameters for controlled release of growth factors are obtaining a release rate, dose, and duration that provide optimal chondrogenic induction while avoiding side effects, and the released growth

factors are still bioactive. With these considerations, the desired properties of the delivery vehicle are to be biodegradable, provide a slow release rate with low burst effect and require a straightforward manufacturing process. Moreover, growth factor activity must be retained once released from the delivery vehicle. Protein denaturation is elicited by exposure to high temperature and pressure, organic solvent, ultraviolet light, surface tension and adsorption, all of which lead to changes in protein conformation [172].

Various approaches for sustained growth factor delivery in cartilage tissue engineering include growth factor loaded microspheres or liposomes incorporated in hydrogels or prefabricated scaffolds [173-176], polymer coating applied on a compression molding scaffold [177] and scaffolds soaked with growth factor [178-180]. Growth factor adsorption on scaffolds by soaking seems to be the easiest. Nevertheless, this method does not provide a controlled release of the growth factors from the scaffold and adsorption resulted in protein denaturation [181]. Furthermore, a drawback of using a scaffold as the combined growth factor and cell delivery is the need for fitting a pre-shaped scaffold into a defect site. Thus, growth factor loaded microspheres incorporated into a hydrogel was considered the most desirable approach as it allows cell and microsphere encapsulation within a gel matrix in a non-invasive injection, prior to implantation [173, 182].

Growth factor incorporation within microspheres or hydrogels has been achieved using various strategies. For example, an affinity-based approach used heparin as a preferential binding site for growth factor, by conjugating heparin to PLGA nanospheres [183, 184] and incorporating heparin within a thermoreversible hydrogel [184]. The commonly used microsphere materials for chondrogenic growth factor delivery are PLGA, gelatin and chitosan. Different strategies have been employed to incorporate dual growth factors in microspheres. The strategies include homogeneous encapsulation of both growth factors in microparticles [176, 182, 185], mixing 2

populations of growth factor loaded microspheres in the gel matrix, or adsorbing one growth factor within a gel that was incorporated with microspheres loaded with another growth factor [186], microspheres loaded with dual growth factor bound together with dichloromethane (DCM) vapor [187] and growth factors coated onto the microsphere surface [188, 189]. The release profile of the growth factors depends on the properties of the growth factors and the design of the growth factors incorporated in the microspheres to generate similar or sequential release. In addition, the initial burst of growth factor also depends on the design of the growth factor incorporation within the microspheres.

1.9. Release mechanisms

Sustained release of water-soluble drug particles distributed throughout solid polymers is governed by various mechanisms. These mechanisms include dissolution of interconnected particles that form pores in the polymer and allow the dissolved drug to diffuse to the surface [190, 191], degradation of the polymer that generates a porous network [192] and osmotic pressure that forms microcracks within the polymer due to water drawn into polymer-surrounded particle capsules [193-195]. The dissolution mechanism of interconnected particles requires high particle loading (20-30%) to allow continuous pore formation from the dissolved drug and thus release from a solid polymer [196]. On the other hand, for degradation-driven release mechanism, the polymer employed for releasing water-soluble drug must be tailored to have a degradation rate that matches the desired release kinetics [191]. In addition, the diffusional mechanism generates a monotically decreasing release rate with time, which results in non-zero release kinetics [197]. On the other hand, osmotically driven release mechanism is characterized by a nearly zero order release rate that provides consistent release within the time frame to optimally induce chondrogenesis of stem cells [197].

PLGA microspheres have been mainly employed to deliver growth factors for the chondrogenesis of human MSC [187, 198-204]. The release mechanism is governed by degradation, primarily by hydrolysis, generating acidic degradation products that decrease the pH within the vicinity of the scaffold [205-207] and around the implant [129, 208, 209]. These degradation products can lead to adverse effects, such as inflammatory reaction [210], foreign body reaction [128, 211] and denaturation of protein within the matrix [212-214]. Acidity as low as pH 3.8 within the cartilage milieu would be detrimental to chondrocytes [215]. Moreover, PLGA is brittle at body temperature, and so free PLGA microspheres may induce mechanical irritation in the synovial space.

Gelatin and chitosan microparticles have also attracted great interest for growth factor delivery. The release of TGF-β1 from gelatin microparticles has been demonstrated to maintain chondrocyte phenotype [176] and increase cartilaginous matrix synthesis from rabbit MSC [186]. Similarly, TGF-β1 released from chitosan microspheres induced the proliferation and GAG production of chondrocytes [185]. However, the growth factor release from these microparticles was too fast, with complete release by 7 days. This release profile would not be suitable for chondrogenesis of adult stem cells since cartilaginous matrix would not have been produced within this time frame. Cartilaginous tissue requires at least 14 days to be produced [216]. In addition, matrix production is highly dependent on the source of stem cells, the types of growth factors and their doses, scaffold types and biomechanical stimulation. Another study used a hybrid of gelatin-chitosan to form microparticles to release growth factors to induce chondrogenesis of rabbit ASC [217]. The release was also fast, with 70% cumulative mass released on day 7. In addition, growth factors were loaded into the gelatin microparticles by mean of absorption, which is inefficient.

The approach of heparin binding as a preferential site for growth factor loaded in gel matrix has been reported for its potential *in vivo* use [184, 201, 202, 218, 219]. Many growth factors, such bFGF, BMPs and TGF-β, have an affinity binding site for heparin via its highly negative charge and binding may prevent protein denaturation [220-223]. Heparin can be conjugated with the prepolymer of the gels or nanospheres loaded in the gel. However, the loading efficiency and the dose of the growth factors were not mentioned in the studies. In addition, the release was too fast, 70% cumulative release on day 4 and 11 [184, 218], and was initiated with a high burst (> 40%) [201].

1.10. Proposed Approach

The approach used for cartilage repair in this study was to use a photocrosslinkable chitosan derivative, *N*-methacrylate glycol chitosan (MGC), as an injectable cell delivery vehicle, incorporated with human ASC and growth factor loaded microspheres to direct ASC differentiation to the chondrocyte lineage. A schematic diagram of the proposed delivery system for cartilage repair in *in vitro* study is illustrated in Figure 1.3. As discussed above, adipose tissue can be obtained readily in a minimally invasive manner, and yields a large quantity of stem cells [224]. Moreover, adipose-derived stem cells (ASC) remain undifferentiated during *in vitro* expansion, and can be differentiated towards the chondrocyte lineage [61].

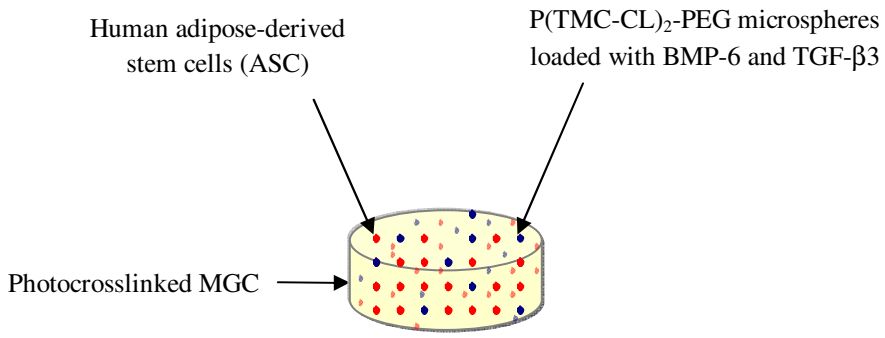

Figure 1. 3. A delivery system for cartilage regeneration.

MGC was chosen as the cell delivery vehicle for the following reasons. The MGC prepolymer is photopolymerizable to form a hydrogel *in situ* that contains more than 80% water. Chitosan is a non-physiologic glycosaminoglycan that has been demonstrated to be biocompatible [110, 225, 226], to accelerate wound healing [227, 228], have antimicrobial properties [229-232] and support the growth and function of chondrocytes [105, 233]. The MGC is soluble in water at neutral pH, allowing for cell incorporation, and we have recently demonstrated the non-cytotoxicity of this prepolymer towards chondrocytes [234].

As growth factor effects on cellular transduction activities is both concentration- and time-dependent [142, 235], ASC chondrogenesis was induced by a local and sustained delivery of chondrogenic growth factors from polymeric microspheres within the MGC gel. Desirable features of the microspheres were considered to be: 1) composed of biodegradable polymers with a history of use *in vivo*, 2) easily dispersible within the aqueous pre-gel solution, 3) soft at body temperature yet manipulatible, and 4) capable of prolonged delivery of low doses of bioactive growth factor. To satisfy the design criteria, amphiphilic triblock poly(1,3-trimethylene carbonate-*co*-ε-caprolactone)-*b*-poly(ethylene glycol)-*b*-poly(1,3-trimethylene carbonate-co-ε-caprolactone) (P(TMC-CL)$_2$-PEG) was employed to fabricate the microspheres. This polymer was chosen for the following reasons. The homopolymers of ε-caprolactone (PCL) and 1,3-

trimethylene carbonate (PTMC) have been demonstrated to be biocompatible and biodegradable [236-238]. In addition, these polymers hydrolyze slowly without generating significant amounts of acidic degradation products that alter local pH [239, 240]. The PEG central block should allow ready dispersion of the microspheres in the gel by forming a hydrophilic surface upon immersion in water.

P(TMC-CL)$_2$-PEG was synthesized to have a low molecular weight with an onset of melting at around 10ºC and yet be amorphous at 37ºC. In this manner, the microspheres would be soft at body temperature, and yet still readily mixed into the pre-gel solution at lower temperature. Growth factor release from these microspheres was driven by osmotic pressure. In this approach, the growth factor is co-lyophilized with a physiologically acceptable osmotigen such as trehalose, which generates the osmotic pressure that drives the release [241]. The proposed means of release through this mechanism is as follows. Following immersion of the microspheres in an aqueous environment, the surface-resident particles dissolve and are released into the medium. Subsequently, water diffuses into the polymer. Upon contact with an embedded solid particle, the water dissolves the solid at the polymer-particle interface, forming a saturated solution. Under the influence of the enhanced activity gradient, water is drawn towards the particle dissolving more of the solid. The incoming water generates pressure within the microsphere matrix that is resisted by the polymer viscosity. The polymer flows in the direction of least resistance, such as the surface of the microsphere, and a liquid-filled pore is formed that ultimately reaches the surface and releases the dissolved solutes [242, 243]. This release mechanism allows for low particle loading (< 20%), provides long-term and nearly constant release, and has been demonstrated to maintain the bioactivity of encapsulated growth factors [244]. In addition, growth factors loaded in microspheres would protect the growth factors from denaturation during the photocrosslinking process.

BMP-6 and TGF-β3 were used to induce ASC chondrogenesis. In particular, human ASC have been demonstrated to be efficiently transformed towards the chondrocyte lineage by exposure to a combination of bone morphogenetic protein-6 (BMP-6) and transforming growth factor-β3 (TGF-β3) at low doses (5 ng/day) over a period of 4 to 6 weeks [86, 160]. Thus, these delivery specifications of BMP-6 and TGF-β3 were also the target delivery in this study.

CHAPTER 2

OBJECTIVES

The global objective of the project was to determine whether embedded microspheres loaded with growth factors would be effective in inducing ASC chondrogenesis in an MGC gel, due to the localized and sustained delivery of chondrogenic growth factors.

Thus, the specific objectives were:

1. To produce a photocrosslinkable, water-soluble MGC prepolymer and MGC gel.
2. To obtain a high viability and proliferation of encapsulated ASC in a photocrosslinked MGC gel.
3. To generate a slow and complete release of BMP-6 and TGF-β3 from P(TMC-CL)$_2$-PEG microspheres in MGC gel, while still maintaining the bioactive states of the growth factors.
4. To determine the effectiveness of the sustained release of BMP-6 and TGF-β3 in directing ASC towards the chondrocyte lineage in an MGC gel.

CHAPTER 3

MATERIALS AND METHODS

Unless otherwise indicated, all the materials and reagents listed were used as received. The methods were described according to the relevant chapters.

3.1. Materials

Glycol chitosan was purchased from Wako Chemical USA, Inc. Deuterium oxide-d_6 and dimethyl sulfoxide-d_6 were purchased from Cambridge Isotope Laboratories, Inc. Water used was of type I purity, obtained from a Millipore Milli-Q Plus ultrapure water system. Hydrochloric acid, acetic acid, formic acid and Pierce® Bicinchoninic acid (BCA) protein assay reagent were obtained from Fisher Scientific Canada. Sodium nitrate, sodium hydroxide, glycidyl methacrylate, 2-hydroxy-4′-(2-hydroxyethoxy)-2-methylpropiophenone (Irgacure 2959), acrylic acid, ε-caprolactone (CL), poly(ethylene glycol) diol (M_n 950-1050 Da) (PEG), anhydrous 1-octanol (99%), tin (II) 2-ethylhexanoate, anhydrous toluene (99.8%), lysozyme (90%) from chicken egg white, trehalose, albumin from bovine serum, Dulbecco's Modified Eagle's Medium/Ham's Nutrient Mixture F12 (DMEM/F12), Dulbecco's Modified Eagle's Medium/ High modified, fetal bovine serum, antibiotic antimycotic solution, penicillin-streptomycin, Dulbecco's Phosphate Buffered Saline (DPBS), Krebs-Ringer bicarbonate buffer, albumin solution from bovine serum (35% in DPBS), 2-mercaptoethanol, goat serum, Tween®20, sodium azide, collagenase from *Clostridium histolyticum* (type II), HEPES, ammonium chloride, potassium bicarbonate, sodium bicarbonate, glucose, ethylenediaminetetraacetic acid disodium salt dehydrate, carbonate-bicarbonate buffer, human insulin, L-Ascorbic acid 2-phosphate

sesquimagnesium salt hydrate, dexamethasone water soluble, Trisma® base, sodium chloride, ammonium acetate, DL-dithiothreitol, Hoechst 33258, deoxyribonucleic acid from calf thymus, chondroitin sulfate A sodium salt from bovine trachea, 1,9-dimethyl-methylene blue, papain from papaya latex, calcium chloride, 4-nitrophenol solution (10 mM) and p-nitrophenyl phosphate substrate liquid system were all obtained from Sigma-Aldrich, Ltd., Canada. Trimethylene carbonate (TMC) was purchased from Boehringer Ingelheim, Germany. Methanol (99.8%), dichloromethane (99.5%) and anhydrous ethyl alcohol (100%) were obtained from Caledon Laboratory Chemicals, Canada. *N*-(3-dimethylaminopropyl)-*N*'-ethylcarbodiimide hydrochloride was obtained from Acros Organics, USA. Ac-GCGYG**RGD**SPG-NH2 peptide was purchased from Anaspec, Inc, USA. LIVE/DEAD® Viability/ Cytotoxicity for mammalian cells and cell proliferation reagent WST-1 were obtained from Roche Diagnostics, Canada. Recombinant human bone morphogenetic protein-6 (BMP-6, HEK 293 derived), recombinant human transforming growth factor-β3 (TGF-β3, E. coli derived) and recombinant murine interleukin-4 (IL-4, E. coli derived) were purchased from PeproTech Inc., USA. ELISA kits for TGF-β3 detection, biotinylated goat anti-human BMP-6, streptavidin conjugated to horseradish peroxidase and tetramethylbenzidine hydrogen peroxide were purchased from R&D Systems®, USA. RPMI 1640 medium, C2C12 and HT-2 cell lines were obtained from ATCC, USA. Pepsin A from porcine stomach and elastase from porcine pancreas were purchased from Worthington Biochemical Corporation, USA. Human collagen type I and II ELISA kits were purchased from MD Biosciences, USA.

3.2. Methods used in Chapter 4

3.2.1. Glycol chitosan purification

Glycol chitosan (1 g) was dissolved in water (75 mL) and filtered to remove insoluble impurities. The filtrate was then dialysed against water with molecular weight cutoff 50 kDa dialysis tubing for 8 h. Both the membranes and the media were replaced at 4 h. The purified high molecular weight glycol chitosan was frozen at -20 °C for a minimum of 8 h and lyophilized for at least 48 h.

3.2.2. Glycol chitosan methacrylation via glycidyl methacrylate

Glycol chitosan was dissolved in 20 mL of water to give a 1.9 w/v% solution, which was adjusted with 1 M NaOH to pH 9.0. Various volumes of glycidyl methacrylate were added to the glycol chitosan solution to provide initial molar ratios of glycidyl methacrylate: free amine per mol glycol chitosan residue ranging from 0.14 to 0.70 and allowed to react for the given times, up to 48 h. The reaction medium was then neutralized and dialysed with a molecular weight cutoff of 12 kDa dialysis tubing against water for 4 h. The membranes and medium were replaced at 2 h. The *N*-methacrylate glycol chitosan solution was lyophilized to yield a crystalline white powder.

3.2.3. Nuclear magnetic resonance spectroscopy

^{1}H NMR spectra were conducted with a Bruker Avance-600 Ultrashield spectrometer equipped with a 5 mm TBI S3 probe with Z gradient and variable temperature capability. Samples were prepared at 20 mg/mL in deuterium oxide, preheated at 60 °C for 6 h, then adjusted to pH > 10 with 1 M sodium hydroxide (30 µL) prior to analysis. Samples were allowed to equilibrate for 10

min at 90 °C within the spectrometer prior to shimming to ensure a homogeneous sample temperature. All chemical shifts were referenced to the HOD peak as a primary reference and to tetramethylsilane (TMS) as a secondary reference. Spectral data were collected by Bruker's XWINNMR software. ^{13}C NMR was performed at a concentration of 55 mg/mL at 80 °C. Cross-polarization magic angle spinning solid state ^{13}C NMR was performed on photocrosslinked gels dried *in vacuo* and ground using a mortar and pestle. The samples were run on a Bruker 600 MHz Avance spectrometer with a spinning rate of 14050 Hz, contact time of 2 ms, and a relaxation delay of 2 s, using a broadband CP-MAS probe.

3.2.4. Photocrosslinking of *N*-methacrylate glycol chitosan

A concentrated solution of *N*-methacrylate glycol chitosan in deionized water (6 w/v%) containing the photoinitiator I2959 (0.1 w/v%) was poured into a cylindrical Teflon mold (7.5 mm diameter x 6 mm). Irgacure 2959 was used in this study, as it had been demonstrated to be the least cytotoxic to various cells, compared to other photoinitiators [245]. The solution was then exposed to long-wavelength ultraviolet light (320 to 480 nm, EXFO Lite, EFOS Corporation, Mississauga, Canada) at intensities ranging from 25 to 102 mW/cm^2 for up to 7 min to yield the *N*-methacrylate glycol chitosan hydrogels.

3.2.5. Gel permeation chromatography with light scattering

GPC with light scattering data were obtained with a Waters 1525 Binary HPLC pump and a Precision Detectors EnterpriseMDP PD2100 series equipped with refractive index and light scattering detectors with angles of 15 and 90°. GPC was achieved using Waters Ultrahydrogel 2000, 250, and 120 columns connected in series. Samples, dissolved in a 0.8 M Na_2NO_3 solution,

were filtered (0.45 μm) and injected (100 μL) with a Waters 717plus autosampler onto the column at 0.8 mL/min and 25 °C at a concentration of 10 mg/mL. All data were obtained and processed in Precision Detectors' Precision Aquire32 and Discovery32 software programs using an absolute refractive index of 1.3255 mL/g determined on a Wyatt Optilab rEX and a refractive index increment (dn/dc) value of 0.115 mL/g.

3.2.6. Sol determination

Immediately after photocrosslinking, the gels were frozen in liquid nitrogen. The frozen gels were lyophilized, and their dry mass recorded. The gels were then swollen three times in type I purified water at 37 °C, with the water replaced every 45 min. The gels were again frozen in liquid nitrogen, lyophilized, and the final mass recorded. The sol content was calculated as

$$sol = \frac{m_{dry,ini} - m_{dry,fin}}{m_{dry,ini}} \tag{3.1}$$

where $m_{\mathrm{dry,ini}}$ and $m_{\mathrm{dry,fin}}$ represent the mass of the dried gel before and after swelling, respectively.

3.2.7. Equilibrium water content

Sol-removed gels were swollen in pH 7.4 phosphate-buffered saline for 96 h. The wet gels were collected, surface moisture was removed by blotting, and the mass of each gel measured. The equilibrium water content (EWC) was calculated as

$$EWC = \frac{m_{wet} - m_{dry,ini}}{m_{wet}} \tag{3.2}$$

where m_{wet} represents mass of wet gel.

3.2.8. Young's modulus

The Young's modulus of different gels were measured via indentation as described in Jin and Lewis [246], using a TA XT plus texture analyzer from Texture Technologies Corp., New York. Flat-ended cylindrical indenters of 3 and 7 mm diameter were used, and gels were photocrosslinked in a cylindrical mold, covered with a glass coverslip to ensure a flat surface. The sol content of the gels (~12 mm D x ~3.5 mm H) was first removed, and the gels were swollen to equilibrium in pH 7.4 phosphate-buffered saline. The gels were then indented on top and bottom of the gel to measure the indented force on the gel with distance. The force (0.0495 N) was triggered at 0.05 mm/s and the indenters traveled for 0.5 mm. Using two different-sized indenters allows for the measurement of the Poisson ratio, v, via

$$\frac{(p/\omega)_1}{(p/\omega)_2} = \frac{a_1}{a_2}\frac{\kappa_1(a_1/h_1, \upsilon_1)}{\kappa_2(a_2/h_2, \upsilon_2)} \tag{3.3}$$

in which a is the radius of a given indenter, p is the indenting force, ω is the indenting depth, h is the height of the gel, the subscripts refer to a given indenter, and κ is a correction factor that accounts for the finite layer effect, obtained from Hayes et al [247]. In eq 3.3, v is the only unknown. The slope of the resulting force-indentation depth curves was calculated for

indentation using both indenters to provide (p/ω). Solving for v then allows for the calculation of Young's modulus, E, using

$$\frac{p}{\omega} = \frac{2aE\kappa}{(1-\upsilon^2)} \tag{3.4}$$

Three measurements were made per gel, and three gels were prepared for each degree of substitution examined (3.5, 7.4 and 13.6%).

3.2.9. *In vitro* degradation

Hydrogels (7.5 mm D x 4 mm H) were prepared through photocrosslinking 5, 9, and 14% degree of substitution *N*-methacrylate glycol chitosan at 100 mW/cm^2 light intensity for 5 min. The gels were rinsed with distilled water three times then incubated in a mixture of 4 mg/mL lysozyme from chicken egg white and 0.1% (w/v) sodium azide. The lysozyme mixture solution was changed every week. Every month, three gel samples were frozen, lyophilized, and weighed to obtain the final weight after degradation.

3.3. Methods used in Chapter 5

3.3.1. Preparation of RGD-grafted, *N*-methacrylate glycol chitosan

Acrylic acid, which was first activated by *N*-(3-dimethylaminopropyl)-*N*'-ethylcarbodiimide hydrochloride (EDC) in distilled water at pH 6 for 15 min, was reacted with 1.9% w/v vacuum filtered MGC (15% degree of *N*-methacrylation) in distilled water for 2 h at pH 7.5. The product, *N*-methacrylate *N*-acrylamide glycol chitosan (MAGC), was purified and lyophilized as above

and the degree of *N*-acrylamide functionalization was determined via ^{1}H NMR and reported as the number of grafted *N*-acrylamide groups per 100 residues. 1.9% w/v MAGC (15 % *N*-methacrylation, 7.3% *N*-acrylamide) was reacted with Ac-G*C*GYG**RGD**SPG-NH_2 peptide in distilled water at pH 8 for 1 h. The product, MAGC-RGD, was neutralized with 1 M hydrochloric acid and purified using the same method as that of MGC. The percent of RGD grafted onto the backbone of MAGC was measured using ^{1}H NMR, calculated based on the reduction of integration peak of the acrylamide protons (δ = 6.65 and 6.8 ppm).

3.3.2. Sol content of MGC under varying crosslinking conditions

MGC (6.8, 15.1 and 27.8% *N*-methacrylation) dissolved to 6 % w/v in either distilled water, cell culture medium (DMEM/ F12) or medium supplemented with 10% fetal bovine serum (medium-FBS) was well mixed with 10% v/v of 5 mg/mL Irgacure 2959 (I2959) photoinitiator. 0.2 mL of the MGC solution was then transferred into a cylindrical Teflon mold and photocrosslinked with long-wave (320-380 nm) UV light at an intensity of 10.8 mW/cm^2 for 3 min using an EXFO Lite (EFOS Corporation, Mississauga, Canada) UV light source. The MGC hydrogel constructs (6.5 mm D x 2 mm H) were frozen in liquid N_2, lyophilized and weighed to obtain the initial dry weight. The lyophilized gels were then washed with the aqueous media three times for 3 h to remove the sol fraction. After sol removal, the gels were frozen in liquid N_2, lyophilized and weighed to obtain the final dry weight. The sol content of MGC gel (6% w/v in medium-FBS, 6.8% *N*-methacrylation) under varying UV light intensity (10.3 to 20.7 mW/cm^2 for 3 min) was investigated using the same method as described above. Similarly, the sol content of MGC gel (6% w/v in medium-FBS, 6.8 and 15.1% *N*-methacrylation) with varying I2959 photoinitiator concentrations from 0.5 to 1.5 mg/mL was measured using the same procedures as described above.

3.3.3. Measurement of Young's modulus

MGC with degree of *N*-methacrylation of 5.1, 11.3 and 29.3% was dissolved in medium-FBS (6% w/v) and well mixed with 10% v/v of 5 mg/mL I2959 photoinitator. 1 mL of the mixed solution was transferred into a cylindrical Teflon mould and exposed to UV light for 3 min at an intensity of 10.8 mW/cm^2. The photocrosslinked MGC constructs (~12 mm D x ~3.5 mm H) were rinsed with gel solvent three times for 3 h to remove sol. The gels were then indented on top and bottom of the gel using 2 flat-ended cylindrical indenters of 3 and 7 mm in diameter to measure the indented force on the gel with distance. The force (0.0495 N) was triggered at 0.05 mm/s and the indenters traveled for 0.5 mm. The Poisson ratio and Young's modulus were calculated using an equation derived by Hayes et al. [247] as described above. The analysis used the assumption that the gels were isotropic, homogeneous elastic; this was valid for the MGC gel's height of less than 4 mm [234].

3.3.4. ASC isolation

The ASC were obtained from the breast tissue of patients undergoing elective surgery in Kingston General Hospital, Kingston, ON, and were isolated using the method established by Flynn et al. [248]. Briefly, the tissue sample was minced and digested in 25 mL of collagenase type II solution (Kreb's Ringer Buffer solution, 20 mg/mL BSA, 3 mM glucose, 2 mg/mL collagenase type II and 25 mM HEPES) for 45 min at 37^{0}C while agitated at 100 rpm. The digested sample was filtered through a 250 μm pore stainless steel filter followed by adipocyte removal on the upper layer of filtered sample. The collagenase in the remaining sample was neutralized with proliferation media (DMEM/ F12, 10% FBS and 1% antibiotics antimytotic) before centrifugation at 1200 g for 5 min. The cell pellet was re-suspended in erythrocyte lysing buffer (0.154 M ammonium chloride, 10 mM potassium bicarbonate, 0.1 mM

ethylenediaminetetraacetic acid disodium salt dihydrate) for 10 min with gentle agitation before re-centrifugation. The cell suspension was then filtered through 100 μm nylon mesh and re-centrifuged. The isolated ASC were incubated at 37^0C, 5% CO_2 and washed with PBS after 24 h to remove tissue debris. ASC were fed with proliferation media that was changed every 2 days. Passage 4 to 7 ASC were used for cytotoxicity and seeding experiments.

3.3.5. Cytotoxicity of I2959 photoinitator and soluble MGC on ASC

I2959 with varying concentrations from 0.5 to 2 mg/mL was well mixed with ASC in proliferation media at a seeding density of 150,000 cells/mL. 0.1 mL of the mixed suspension was transferred into a 96-well plate and incubated for 22 h at 37^0C, 5% CO_2. 10 μL of WST-1 reagent was added and incubated for another 2 h before the optical density was read at 440 nm in a UV/ Vis spectrophotometer. Cell number was calculated based on the calibration of the control sample (ASC without I2959 photoinitator). Similarly, MGC (5.9, 11.3 and 27.8% *N*-methacrylation) with concentration varying from 0.6 to 12 mg/mL was dissolved in proliferation media. 0.05 mL of MGC solution that was well-mixed with ASC at seeding density of 150,000 cells/mL was transferred into 96-well plate and incubated at 37^0C, 5% CO_2. After 23 h, the ASC were washed with PBS three times and the media replaced with fresh media. 5 μL of WST-1 reagent was added to each well and incubated for 1 h. The optical density was read at a wavelength of 440 nm in a UV/ Vis spectrophotometer. Cell number was calculated based on a calibration of the control sample (ASC without MGC solution). Six replicates were used for the cytotoxicity studies.

3.3.6. Effect of combined photopolymerization parameters on ASC viability

For ASC exposed to UV irradiation, 100,000 ASC in 0.1 mL proliferation media was transferred onto a glass cover slip and exposed to UV light with an intensity of 10.8 mW/cm^2 for 3 min. For UV exposure in the presence of MGC solution, 100,000 ASC in 0.1 mL of 6% w/v MGC solution (15% *N*-methacrylation) in medium-FBS were exposed to UV light on a glass cover slip. Similarly, for ASC exposed to UV light in the presence of I2959 photoinitiator, 100,000 ASC in 0.1 mL proliferation media containing 10% v/v of 5 mg/mL I2959 photoinitiator were exposed to UV light on a glass cover slip. Each experiment was performed with 3 replicates. The cover slips were then incubated in a 6-well plate at 37^{0}C, 5% CO_2. After 2 h incubation, WST-1 was added into the culture and incubated for another 2 h before the optical density was read in a UV/ Vis spectrophotometer (440nm).

3.3.7. ASC encapsulation in MGC and MAGC hydrogels

To incorporate ASC within the MGC hydrogel, the lyophilized MGC solid (6, 12 and 25% *N*-methacrylation) dissolved in proliferation media to 6 %w/v was well mixed with 10% v/v of 5 mg/mL I2959 photoinitator and ASC at a seeding density of 150,000 cells/ gel. 0.1 mL of the mixed suspension was transferred into a cylindrical Teflon mold and exposed to UV light (320 to 480 nm) at an intensity of 10.8 mW/cm^2 for 3 min. The MGC gel constructs (6.5 mm D x 1 mm H) containing encapsulated ASC were transferred into a 24-well plate and fed with proliferation media for 7 days. The viability of the ASC was quantified using LIVE/DEAD® staining and imaged using an Olympus FV 1000 confocal scanning laser microscope. The images of the gels were taken using a mosaic stitch technique, which stitched 25 to 31 images to form one image capturing the whole gel at the specific depth. Five layers of gel were scanned for each sample, each layer separated by 100 to 200 μm. The fluorescent images of ASC were processed using

ImageJ software to calculate the number of live and dead cells. Similarly, the viability of ASC encapsulated in MAGC and MAGC-RGD with seeding density of 500,000 cells/gel was also conducted using the same method as that of MGC for 14 days.

3.3.8. Statistics

The data represented the average values of four samples (unless otherwise stated) with error bars based on the standard deviation within the average. The data were assessed using one-tail ANOVA with a Bonferroni post-hoc test and considered statistically significant at $p < 0.05$.

3.4. Methods used in Chapter 6

3.4.1. Amphilic triblock copolymer synthesis

Polymerization was conducted using 1-octanol or PEG as the initiators and tin (II) 2-ethylhexanoate in anhydrous toluene at 120ºC for 24 h under vacuum. The mol ratio of total monomers to 1-octanol was targeted to be 12 with CL to TMC molar ratios ranging from 3 to 11. For PEG-initiated polymerization, the mol ratio of total monomers to PEG was set to 40.3 and 105.5 to obtain low and high number average molecular weight copolymers with similar thermal properties as those of the copolymer initiated with 1-octanol. The mol ratio of catalyst to total monomers was 0.001, while that of CL to TMC was 3.3 [241, 249, 250]. The resulting copolymers, octanol initiated poly(1,3-trimethylene carbonate-*co*-ε-caprolactone) (Oct-P(TMC-CL)) and poly(1,3-trimethylene carbonate-*co*-ε-caprolactone)-*b*-poly(ethylene glycol)-*b*-poly(1,3-trimethylene carbonate-co-ε-caprolactone) P(TMC-CL)$_2$-PEG, were purified by mixing in methanol for 1 h, freezing at -85ºC for 2 h and decanting the unreacted reactants. The purified copolymers were dried at 40ºC for 48 h, and stored in a dessicator under vacuum at room

temperature.

3.4.2. Copolymer characterization

The molar ratios of the copolymers were determined by ^{1}H Nuclear Magnetic Resonance (NMR) on a Bruker Avance-400 MHz spectrometer. The spectral data were analyzed in Spinworks 3 software and the chemical shifts were referenced to the HOD and DMSO-d_6 peaks. The thermal properties of the copolymers were measured using a Mettler Toledo DSC1. The temperature program consisted of heating to 100ºC followed by cooling to -100ºC and a second heating cycle to 100ºC with a heating/cooling rate of 10ºC/min. The glass transition temperature, T_g, and the onset melting point, T_m, were measured from the first heating cycle. The enthalpy of melting, ΔH_m, was calculated from the area of the melting endotherm. For percent crystallinity determination, the samples were heated to 37ºC, held for 15 min, followed by heating to 100ºC. The percent crystallinity of the polymers at 37ºC was calculated by comparing the enthalpy of melting above 37ºC to the enthalpy of melting of a pure poly(ε-caprolactone) crystal (139.5 J/g) [251]. The number average molecular weight (M_n) and polydispersity index (PDI) of the copolymers were determined via Gel Permeation Chromatography (GPC). The GPC system consisted of a Waters 2690 separation module equipped with four Waters Styragel HR columns in series and a multi-angle laser light scattering Wyatt Technology DAWN EOS detector. Tetrahydrofuran (THF) was used as an eluent at a flow rate of 1 mL/min. The increment of refractive index (0.0669 mL/g) was obtained using a Wyatt Optilab rEX. The viscosities of Oct-P(TMC-CL) copolymers were measured at 37ºC using a TA Instruments AR2000 controlled stress rheometer. For the viscosity measurement of P(TMC-CL)$_2$-PEG, Oct-P(TMC-CL) polymers with TMC:CL mol ratio of 18.5: 5.1 and 30.9: 8.5 were used since these mol ratios represented the composition and molecular weight of the TMC-CL block of the triblock

copolymers. A parallel plate stainless steel fixture with a diameter of 20 mm and a plate gap of 0.5 mm was used.

3.4.3. Lysozyme encapsulation in polymeric microspheres

Initial formulation experiments were done using lysozyme as a model protein. The lysozyme was used directly from the manufacturer's bottle. 40% and 10% w/w lysozyme in trehalose was dissolved in phosphate buffer saline (PBS, pH~ 7.4), frozen in liquid nitrogen and lyophilized. To reduce lysozyme particle size, the lyophilized cake was sieved in a glove box through a Tyler No 325 sieve (< 45 μm), the particles dispersed in dicholoromethane (DCM) at 4% w/v and the suspension vortexed for 2 min at 800 rpm. For lysozyme particle incorporation into polymeric microspheres, the dispersed lysozyme particle suspension was mixed with the high and low M_n P(TMC-CL)$_2$-PEG dissolved in DCM to achieve a final polymer concentration of 80% w/v. The lysozyme particle/copolymer suspension was then electrosprayed into cold ethanol [252]. The lysozyme particle/ copolymer suspension with 2.5 or 5% w/w particle loading was taken up into a 1 mL gas tight syringe, which was connected to clear silicone tubing ending in a blunt 18 gauge hypodermic needle. A positive electrode was clamped to the needle and a ground was applied to an aluminium foil strip immersed within the ethanol bath (cooled in dry ice) 8 cm below the needle. The applied voltage and current were set to 4.5 kV and 0.1 mA, respectively. The suspension flow rate was 0.1 mL/min and the ethanol solution was stirred at 300 rpm (Figure 3.1). The suspension droplets solidified immediately upon entering the collecting ethanol bath. The resulting P(TMC-CL)$_2$-PEG microspheres were held in a -85ºC freezer for 48 h to allow DCM extraction into the ethanol bath. The microspheres were then held in a freezer at -20ºC for 48 h to dry. Three batches of microspheres (N= 3) were fabricated for each release condition.

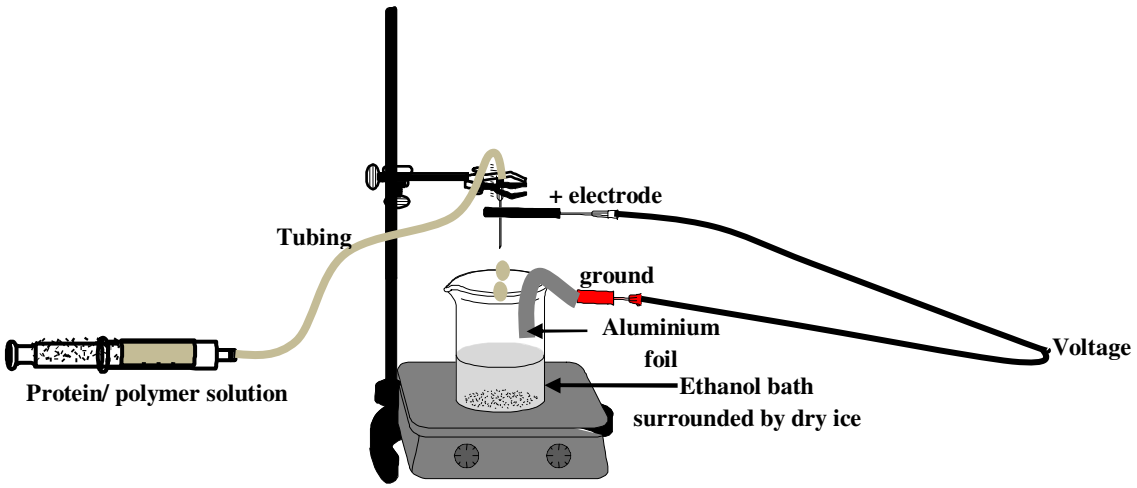

Figure 3. 1. Electrostatic equipment set up for generating protein-loaded P(TMC-CL)$_2$-PEG microspheres.

3.4.4. Protein particle size determination

A 10% bovine serum albumin (BSA) in trehalose mixture was used for incorporating BMP-6 and TGF-β3 into the microspheres, and thus was used to determine the size of the growth factor loaded particles. A lyophilized 10% BSA in trehalose cake was dispersed in DCM (3.5% w/v) and the suspension was vortexed at 1000 rpm for 10 min. The particle size was measured from scanning electron microscope (SEM) images using Sigma Scan Pro 5 software calibrated for each magnification with an image scale.

3.4.5. Encapsulation efficiency and microsphere size determination

5 mg of lysozyme-loaded microspheres (N= 3) were dissolved in 1 mL DCM in an Eppendorf tube. The solution was centrifuged at 9,300 g for 5 min, the supernatant carefully removed and the remaining solid air-dried. The protein/trehalose particles were dissolved in phosphate buffer saline (PBS) and the dissolved protein content was measured using a Pierce® Bicinchoninic acid

protein assay colorimetrically at 562 nm in a μQuant microplate reader (BioTek Instruments, Inc.). The amount of protein was then calculated using a calibration curve. Lysozyme encapsulation efficiency was calculated relative to the lysozyme to polymer weight ratio in the suspension used to prepare the microspheres. During fabrication, microspheres dispersed in ethanol were collected and micrographs of them captured through a Leica camera mounted on microscope. The diameter of the microspheres was measured from the images using SigmaScan Pro 5 software, calibrated using a micrometer image captured at the same magnification. Four to five images from each microsphere batch (N= 3) were measured. Images of microspheres embedded in the *N*-methacrylate glycol chitosan (MGC) gels were obtained using an Olympus FV 1000 confocal scanning laser microscope using a mosaic stitch technique, which stitched 25 to 31 images together to form one image capturing the whole gel at the specific depth. Five layers of gel were scanned for each sample, each layer separated by 100 to 200 μm.

3.4.6. Lysozyme release

MGC with a degree of substitution (mols methacrylate/100 mols chitosan residues) of 5.5% was prepared as described previously [234]. Polymer microspheres loaded with lysozyme particles of varying lysozyme content (10 and 40% w/w in trehalose) and containing 2.5 or 5% (v/v) particles were dispersed in 6% w/v MGC in PBS containing 10% v/v of 5 mg/mL Irgacure 2959 photoinitiator. 0.1 mL of the suspension was then transferred into a cylindrical Teflon™ mold and photocrosslinked under 320 to 480 nm UV light at an intensity of 10.8 mW/cm^2 for 3 min. The cylindrical MGC hydrogel (6.5 mm D x 1 mm H) containing lysozyme-loaded microspheres thus formed was transferred into a glass vessel and incubated in 1 mL PBS (pH 7.4) at 37ºC on a 360º rotating shaker in an incubator. The release medium was replaced every sampling time and the protein content within the releasate was quantified using a Pierce® BCA assay kit. The

optical density was read at a wavelength of 562 nm in a μQuant UV/Vis spectrophotometer. The amount of protein was then calculated by comparison to the calibration curve. Four replicates were used for each release experiment.

3.4.7. *In vitro* degradation of P(TMC-CL)$_2$-PEG

Approximately 10 mg of microspheres were immersed in distilled water at pH 7.4 and incubated at 37ºC. At specific times, samples of the microspheres were centrifuged at 9,300 g for 10 min, the incubation medium decanted and the microsphere mass washed three times in distilled water before being completely dried on a lyophilizer and weighed to obtain the dry mass. The M_n of the polymer at specific time points was also measured by GPC. Three replicates were used for each time point of the mass loss study.

3.4.8. TGF-β3 and BMP-6 release

Solid particles were prepared by dissolving 0.7% w/w TGF-β3 or BMP-6, 9.3% w/w BSA and 90% w/w trehalose in 5 mM succinate buffer (pH 7.4) followed by freezing in liquid nitrogen then lyophilization and the particle size reduced as described above. The particle size was measured using SEM images. P(TMC-CL)$_2$-PEG dissolved in DCM (70% w/v) was transferred into a vial containing the particles to produce a suspension containing 2.5% w/v solid particles. Microspheres containing TGF-β3 or BMP-6 were then prepared as described in Section 3.4.3 and encapsulated in MGC gel using the procedure described in Section 3.4.6. Two different parallel release experiments were then done; one for growth factor quantification and one for assessing the bioactivity of the released growth factor. The release media for TGF-β3 and BMP-6 quantification consisted of 0.02% Tween®20 and 0.02% sodium azide in PBS, while the media

for the bioactivity assay was 1% BSA and 1% antibiotic/antimycotic in PBS. The quantification release media was analyzed using an ELISA kit for human TGF-β3, according to the manufacturer's protocol, while BMP-6 was analyzed using a direct ELISA procedure as follows. BMP-6 standard and release media were diluted in 0.05 M carbonate-bicarbonate buffer (pH 9.6) and incubated in a 96-well plate with a volume of 100 µL/ well overnight at room temperature. The well plate was blocked with 300 µL 1% BSA in PBS, pH 7.2-7.4 for 2 h. 100 µL of detection antibody (800 ng/mL biotinylated goat anti-human BMP-6 diluted in reagent diluent containing 2% w/v heat inactivated normal goat serum) was then added into each well and incubated for 2 h. The assay plate was washed three times in wash buffer (0.05% Tween®20 in PBS, pH 7.2-7.4). 100 µL of streptavidin conjugated to horseradish-peroxidase was incubated for 20 min followed by a washing step. 100 µL of substrate solution (1:1 tetramethylbenzidine to hydrogen peroxide) was incubated for another 2 h before the enzyme-substrate reaction was quenched with 2 N sulfuric acid. The optical density was measured in a µQuant UV/ Vis spectrophotometer at 450 nm. The amount of growth factor released was calculated by using a calibration curve. Four replicates were used for each release experiment.

3.4.9. Bioactivity of TGF-β3 and BMP-6

Released TGF-β3 bioactivity was assessed through a lymphocyte activation assay [253], while BMP-6 bioactivity was assessed through a myoblast proliferation assay [254]. Mouse spleen T lymphocytes (HT-2 clone A5E cell line) were maintained in RPMI1640 medium supplemented with 10% FBS, 0.05 mM 2-mercaptoethanol, 1% penicillin-streptomycin and 30 ng/mL recombinant murine interleukin-4 (IL-4). 100 µL media containing 7,000 HT-2 cells were transferred to a 96-well plate followed by addition of 100 µL TGF-β3 release media, or serially diluted TGF-β3 as received or lyophilized protein particles obtained following size reduction. A

total of 4 wells per time point or condition were used. The final concentration of the components in the media was 10% FBS, 0.05 mM 2-mercaptoethanol, 30 ng/mL IL-4, 1% penicillin streptomycin and varying amounts of TGF-β3. The cells were incubated at 37ºC, 5% CO_2 for 66 h. 20 µL WST-1 reagent was then added and incubated for 7 h before the optical density was read at 440 nm. TGF-β3 bioactivity was reported relative to the response of the cells to as-received TGF-β3. A mouse myoblast cell line (C2C12) was maintained in high glucose DMEM medium supplemented with 10% FBS and 1% antibiotic antimycotic. 100 µL media containing 5,000 C2C12 cells were added to a 96-well plate followed by addition of 100 µL BMP-6 release media, or serially diluted, as-received BMP-6, or lyophilized protein particles obtained following size reduction. The final concentration of the components in the media was 5% FBS, 0.5% penicillin-streptomycin and varying amounts of BMP-6. The culture was maintained at 37^0C, 5% CO_2 for 72 h. On analysis day, the cells were washed with PBS twice before they were lysed by scraping in PBS, and the resulting suspensions transferred to Eppendorf tubes. The lysed cell suspensions were centrifuged at 12,000 g for 10 min at 4^0C. The standard of alkaline phosphatase activity was established from 10 mM of 4-nitrophenol in 0.02 M sodium hydroxide (NaOH). 50 µL of the standard and supernatant of the sample solution were added into a 96-well plate followed by addition of 100 µL of p-nitrophenyl phosphate substrate. The well plate was incubated at 37ºC, 5% CO_2 for 4 h. The enzyme-substrate reaction was quenched using 100 µL of 3 M NaOH before the optical density was read at 405 nm. The alkaline phosphatase activity was normalized by the total protein content measured using the Pierce® BCA reagent. BMP-6 bioactivity was reported relative to the response of the cells to as-received BMP-6.

3.4.10. Statistics

The data points represent the average values of replicate samples with error bars based on the

standard deviation about the average.

3.5. Methods used in Chapter 7

3.5.1. ASC and growth factor-loaded microspheres incorporation in MAGC-RGD gel

10 mg of P(TMC-CL)-PEG microspheres loaded with TGF-β3 or BMP-6 and blank microspheres were individually dispersed in 6% w/v MAGC-RGD polymer (15% *N*-methacrylation, 8.5% RGD) dissolved in proliferation media containing 10% v/v of 5 mg/mL Irgacure 2959 photoinitiator and 10 million suspended ASC / mL. The final 0.1 mL of the mixed solution was transferred into a cylindrical Teflon™ mold and photocrosslinked under UV light (320 to 480nm) at an intensity of 10.8 mW/cm^2 for 3 min. The cylindrical MAGC-RGD gel constructs (~6.5mm D x 1 mm H) containing blank or TGF-β3/ BMP-6 loaded microspheres thus formed and ASC were transferred into a 24-well plate and fed with 0.7 mL media. The conditions of MAGC-RGD gels incorporated with P(TMC-CL)$_2$-PEG microspheres and ASC were summarized on Table 3.1.

Table 3. 1. The conditions of MAGC-RGD gel samples incorporated with P(TMC-CL)$_2$-PEG microspheres

Gel ID	Microsphere Loading	Soluble GF in media
No GF	Blank	None
GF media	Blank	14.5 ng/mL TGF-β3 +14.5 ng/mL BMP-6
GF microspheres	TGF-β3/ BMP-6	None

GF = growth factor

The encapsulated ASC in each gel condition were fed with chondrogenic media (DMEM/ F12, 10% FBS, 1% antibiotics antimytotic, 100 nM dexamethasone, 6.25 μg/mL human insulin and 50 μg/mL $_L$-Ascorbic acid 2-phosphate sesquimagnesium salt hydrate). The media was changed

every two days. ASC encapsulated in the gels of GF media were fed with chondrogenic media and supplemented with 14.5 ng/mL of TGF-β3 and BMP-6 to attain 5 ng/ day of each soluble growth factor (Table 3.1). ASC encapsulated in the gels of No GF and GF microspheres were fed with chondrogenic media without soluble growth factor supplementation. The gels (n= 4) containing blank microspheres and ASC were sacrificed on day 0 to quantify the initial average per gel deoxyribonucleic acid (DNA) and glycosaminoglycan (GAG) content. Eight samples were sacrificed on each time point (day 14 and 28) to quantify DNA and GAG content (n= 4), and the amount of collagen type I and II (n= 4) produced.

3.5.2. DNA quantification

At each time point (day 0, 14 and 28), MAGC-RGD gels (n= 4) containing ASC and blank or growth factor-loaded microspheres were freeze-dried in liquid nitrogen and lyophilized. The lyophilized samples were then homogenized and digested with papain (40 μg/mL in 35.3 mM ammonium acetate, 1 mM ethylenediaminetetraacetic acid disodium salt dehydrate, 2 mM DL-dithiothreitol, pH 6.2) for 72 h at 65^0C. The samples were stored at -85^0C until analysis. The DNA content in MAGC-RGD constructs was determined using the Hoechst 33528 dye assay [255]. Briefly, 50 μL of the diluted, digested samples were added into a black 96-well plate followed by 200 μL Hoechst 33528 dye (0.1 μg/mL in 10 mM Trisma® base, 1 mM ethylenediaminetetraacetic acid disodium salt dehydrate, 0.1 mM sodium chlroide, pH 7.4). The amount of DNA was measured in a fluorometer at excitation/ emission wavelengths of 350/ 450 nm and calculated by comparison to the calibration curve generated from the standards (0 to 6 μg/mL) using DNA from calf thymus.

3.5.3. GAG quantification

The papain-digested samples from DNA quantification were also used to determine GAG content using 1,9-dimethyl-methylene blue (DMMB) dye binding assay [256, 257]. Briefly, 10 µL of the digested samples were added into a 96-well plate followed by addition of 200 µL DMMB dye (16 µg/mL in 1% v/v of 100% ethanol and 99% v/v of 0.2% formic acid, pH 5.3). The GAG content was measured in µQuant (BioTek Instruments, Inc.) UV/ Vis spectrophotometer at a wavelength of 525 nm and calculated by comparison to the calibration curve generated from the standards (0 to 120 µg/mL) using chondroitin sulfate A from bovine trachea.

3.5.4. Collagen type I and type II quantification

The content of collagen types I and II was determined using ELISA kits for human collagen type I and II, according to the manufacturer's protocol. At each time point (day 14 and 28), MAGC-RGD gels (n= 4) containing ASC and blank or growth factor-loaded microspheres were freeze-dried in liquid nitrogen and lyophilized. The lyophilized samples were then homogenized in 0.05 M acetic acid (pH 2.8-3.0) and digested with pepsin (10 mg/mL in 0.05 M acetic acid) for 72 h at 4^0C on an orbital shaker. After pepsin digestion, 10x TBS buffer (1 M Trisma® base, 2 M sodium chloride, 50 mM calcium chloride, pH 7.8-8.0) was added to the samples and the pH was increased to 8 using 1 M NaOH. The samples were further digested with pancreatic elastase (1 mg/mL in 1x TBS, pH 7.8-8.0) for 48 h at 4^0C on an orbital shaker to hydrolyze collagen into intra- and inter- crosslinkages molecules. After the two-step digestion, the samples were centrifuged at 9,300 g for 5 min at room temperature. The supernatant of the samples were diluted accordingly before being analyzed using the respective ELISA kits.

3.5.5. Statistics

The data represented the average values of four samples with error bars based on the standard deviation within the average. The data were assessed using one-tail ANOVA with a Bonferroni post-hoc test and considered statistically significant at $p < 0.05$.

CHAPTER 4

N-METHACRYLATE GLYCOL CHITOSAN AS A PHOTOPOLYMERIZABLE BIOMATERIAL

4.1. Introduction

Photopolymerization to form hydrogels has attracted considerable interest in the field of tissue engineering and drug delivery. The reason for this interest is that gel constructs have similar water contents to the extracellular matrix and thus allow for efficient nutrient transport, which is important for maintaining cell viability, as well as contributing to biocompatibility by reducing mechanical irritation to the surrounding tissue. In tissue engineering applications, photopolymerization can be used for the rapid entrapment of cells with minimal cell death and to prepare scaffolds in a variety of geometries, and judicious choice of the photopolymerizable macromonomer can allow for effective cell attachment and proliferation [96, 258-260]. In recent years, there has been increasing interest in developing photopolymerized materials for protein drug delivery applications [67, 68, 261-268]. For both tissue engineering and drug delivery, advantages of photopolymerizable gels are that gelation can be performed at physiologic temperature and *in situ* with minimal heat generation.

As glycosaminoglycans comprise a significant portion of, and play important roles within, the extracellular matrix, they are obvious choices for the preparation of photopolymerizable hydrogel constructs. A number of different approaches have been taken to prepare photopolymerizable glycosaminoglycans. For example, cinnamate [269] and methacrylate [96, 98, 258, 260] functional groups have been grafted to both hyaluronate and chondroitin sulfate, while hyaluronate has been styrenated [270]. However, these polysaccharides are generally expensive and so alternative materials have been investigated.

Chitosan is a nonphysiologic glycosaminoglycan that has been demonstrated to be biocompatible [225, 226, 271], to accelerate wound healing [227, 228], has antimicrobial properties [229-232], and supports the growth and function of human osteoblasts and bovine chondrocytes [105, 233]. It is therefore a potentially useful biomaterial for use in the preparation of photopolymerizable hydrogels as tissue engineering constructs and drug delivery matrices. Photopolymerizable chitosan derivatives have been prepared previously through styrenation [270] and methacrylation using reactive aldehyde intermediates [272]. The styrene grafting approach resulted in only a 12% gel yield when the reaction was done with low molecular weight chitosan, while methacrylation via reactive aldehydes required the synthesis of methacrylated vanillin or hydroxybenzaldehydes. Further, the degradation of chitosan *in vivo* is slow, with degradation times in excess of 20 weeks depending on its degree of deacetylation [273, 274], which has been attributed to its low solubility at physiologic pH and its crystallinity [225]. For tissue engineering applications, it is often desirable to encapsulate cells directly in the hydrogel matrix, and this would not be possible with chitosan-only gels due to their low water content at pH 7.4. Thus, a useful property of a chitosan-based photopolymerizable prepolymer would be solubility in aqueous solution at neutral pH.

A water soluble photopolymerizable chitosan has previously been prepared by grafting 4-azidobenzoic acid to available free amine groups of lactose modified chitosan [275]. A possible disadvantage of this approach is that exposure to UV irradiation converts the azide group to nitrene groups that are highly reactive with amino groups. Nonspecific interactions of these nitrenes with amino groups during photopolymerization may result in protein denaturation and grafting of the protein to the chitosan itself. This is likely the reason for the observed incomplete bovine serum albumin and fibroblast growth factor-2 release from matrices in which the modified chitosan was photopolymerized in the presence of these proteins in solution [276].

In this chapter the potential of methacrylated glycol chitosan as an alternative photopolymerizable chitosan is explored. Glycol chitosan (Figure 4.1) is soluble over a wide range of pH and, in the few reports to date, has been found to be cytocompatible. For example, Carreño-Gómez and Duncan saw only mild concentration-independent (up to 2.5 $mg \cdot mL^{-1}$) levels of toxicity of glycol chitosan toward a murine melanoma cell line. They also observed reduced hemolysis in a 24 h incubation with red blood cells compared against other chitosan forms [277]. Furthermore, it has recently been found that glycol chitosan is not only noncytotoxic, but stimulates chondrocyte growth at low concentrations [278]. The glycol chitosan was made photopolymerizable by methacrylation through the reaction of glycol chitosan with glycidyl methacrylate. Glycidyl methacrylate has been used to modify chitosan[279] and oligochitosan [280]; however, methacrylated chitosan was not soluble at physiologic pH, while significant water solubility of methacrylated oligochitosan was obtained only for tetramers. Furthermore, these materials were not investigated as photopolymerizable prepolymers.

Methacrylated glycol chitosan was prepared at different molar ratios of glycidyl methacrylate to free amine/glycol chitosan residue. Hydrogels prepared from the methacrylated glycol chitosan were characterized in terms of their sol content as influenced by degree of methacrylation, UV intensity, time of irradiation, and gel depth. The equilibrium swelling capacity of low-sol–gels was measured in water, and their mechanical properties were determined using indentation.

4.2. Results and Discussion

The structure of glycol chitosan, as determined from ^{1}H NMR [278], is shown in Figure 4.1, along with that of methacrylated glycol chitosan. Glycol chitosan has both hydroxyl and amine groups that will undergo a nucleophilic substitution reaction with glycidyl methacrylate.

The most favorable nucleophile is the primary amine [281], as the reaction of the epoxide with the hydroxyl groups requires high pH conditions (typically 11–12) and typically low degrees of substitution are achieved [282].

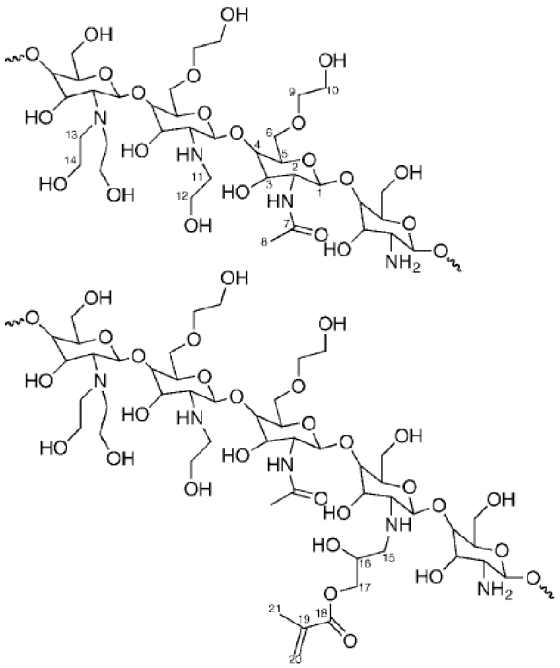

Figure 4. 1. Structure of glycol chitosan (top) and *N*-methacrylate glycol chitosan (bottom)

^{1}H NMR of methacrylated glycol chitosan is provided in Figure 4.2. Methacrylation is achieved, as evidenced by peaks arising at 5.85 ppm and 6.2 ppm due to protons on the vinyl carbon and a peak at 2.45 ppm due to the methyl group on the methacrylate. The same groups in unreacted glycidyl methacrylate appear at 6.3, 6.7, and 2.55 ppm, respectively. *N*-methacrylation can be discerned in the spectrum, as a reduction in peak area at 3.25 ppm (H-2 proton for the deacetylated residues) and the appearance of a small peak centered at 3.35 ppm corresponding to H-2 for the *N*-methacrylate residue. There is also a concurrent reduction in the H-1 peak for the deacetylated residue (5.05 ppm) and the appearance of a new peak at 5.1 ppm corresponding to

H-1 for the *N*-methacrylate residue. The *N*-methacrylation of glycol chitosan was confirmed using ^{13}C NMR, as shown in Figure 4.3. Peaks corresponding to the vinyl carbons appear at 128 and 137 ppm, for the methyl carbon on the methacrylate at 18 ppm, and the carbonyl carbon of the methacrylate at 171 ppm.

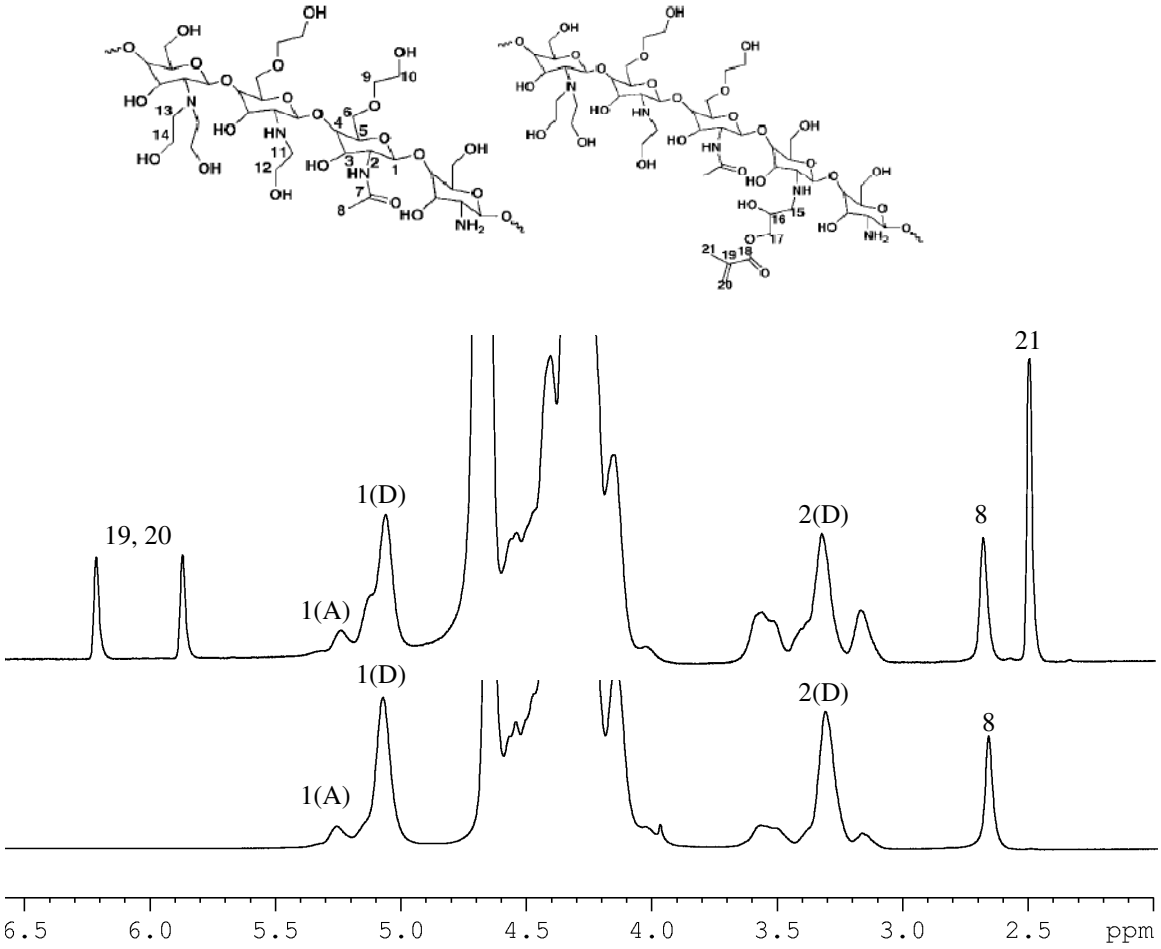

Figure 4. 2. ^{1}H NMR spectra of unmodified and methacrylated glycol chitosan. Peak assignments correspond to ^{1}H designations in Figure 4.1. The (D) refers to deacetylated residues, while the (A) refers to acetylated residues.

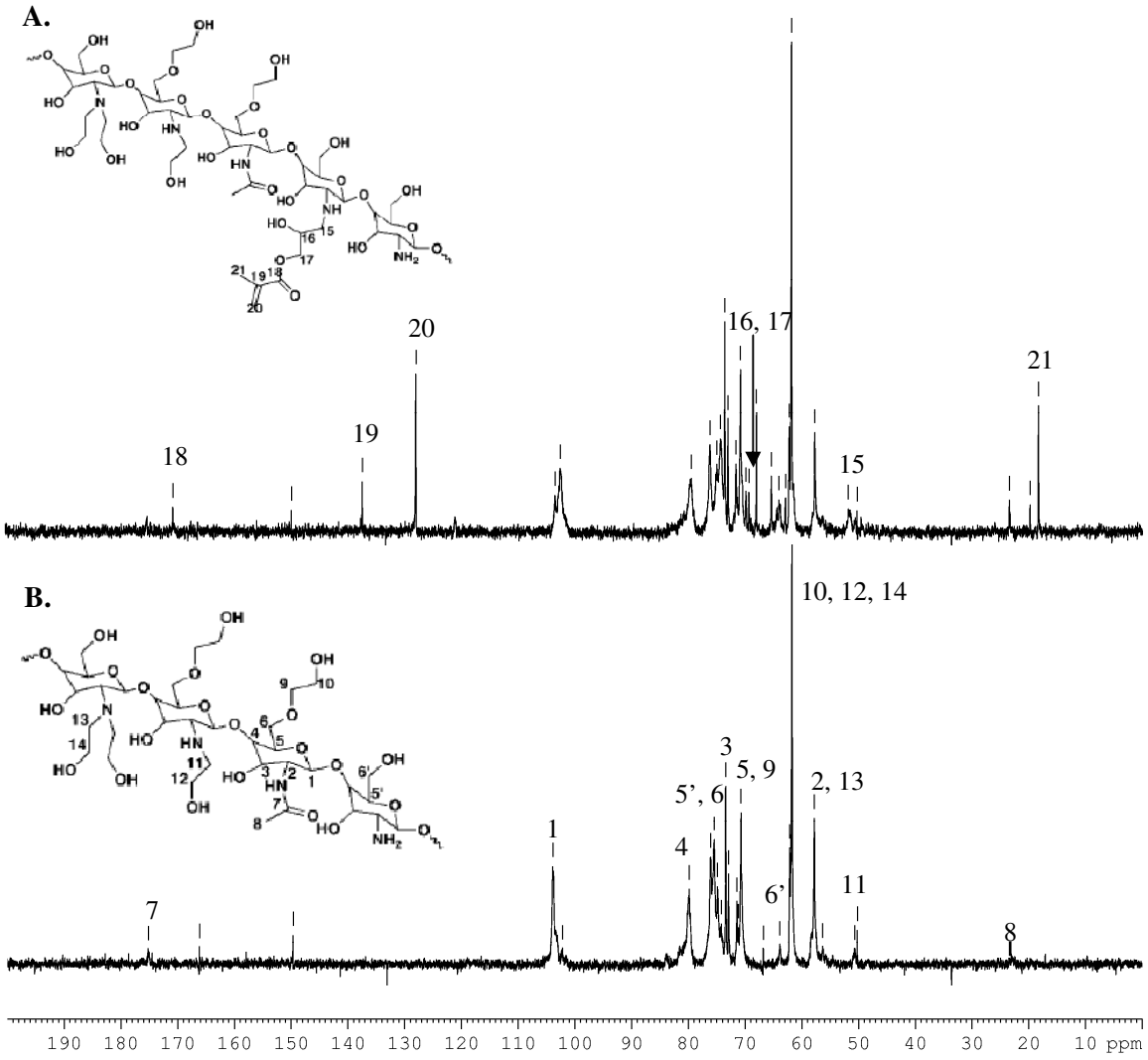

Figure 4. 3. ^{13}C NMR spectra of glycol chitosan (A) and *N*-methacrylate glycol chitosan (B). Peak assignments correspond to designations in Figure 4.1.

The reaction conditions were investigated by monitoring the degree of substitution with time and as a function of molar excess of glycidyl methacrylate to reactive amine/residue. The degree of substitution (DOS) of methacrylate groups onto the glycol chitosan backbone was calculated as

$$DOS = \frac{(I_{5.8}+I_{6.2})/2}{I_{5.05}+I_{5.2}} \times 100\% \quad (4.1)$$

wherein *I* represents the integration of the peak corresponding to the subscript ^{1}H NMR ppm. This DOS is effectively the number of grafted methacrylate groups per 100 residues. The moles of reactive amine per mol residue was calculated as

$$NH_2/residue = \frac{I_{3.25}}{I_{5.05}+I_{5.2}} \quad (4.2)$$

The reaction proceeds relatively quickly initially, then slows with time (Figure 4.4A), reaching a maximum conversion by 48 h, although little increase in DOS is obtained by running the reaction past 24 h. These results are consistent with those of Abo-Shosha and Ibrahim who examined the reaction of cellulose-poly(glycidyl methacrylate) with methylamine in water under basic conditions [283] and are attributed to the competing reaction of the hydrolysis of the epoxide ring. The DOS is readily controlled by the molar excess of glycidyl methacrylate to reactive amine/residue (GMA/NH_2); DOS increases linearly as the initial GMA/NH_2 ratio increases (Figure 4.4B), which is again consistent with the results of Abo-Shosha and Ibrahim [283].

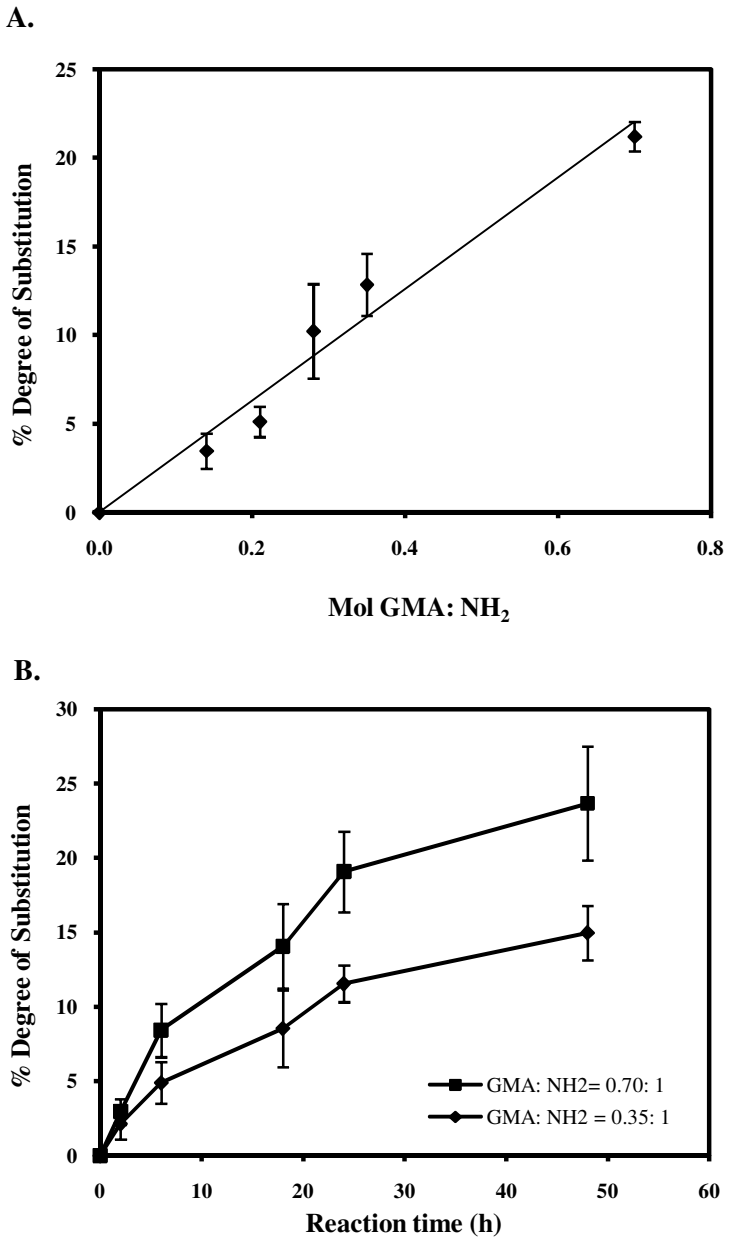

Figure 4. 4. Influence of reaction conditions on degree of substitution. (A) Reaction time and (B) initial molar excess GMA (DOS at 24 h).

The possibility of a Michael-type addition reaction occurring between the unprotonated amine and the already grafted vinyl group was also considered. This reaction has been shown to proceed slowly at room temperature in aqueous media and was not expected to be significant [284]. As Table 4.1 shows, the increase in molecular weight of glycol chitosan upon

methacrylation can be readily attributed to the degree of substitution, and the polydispersity index does not increase significantly. Thus, it is not likely that considerable Michael-type addition reactions occurred during the methacrylation reaction time.

Table 4. 1. Change in number average molecular weight (M_n) and polydispersity (PDI) of glycol chitosan upon methacrylation

M_n Initial (kDa)	PDI initial	% DOS	M_n after (kDa)	PDI after
96.3	2.2	10.2	106.9	2.1
96.3	2.2	25.4	116.4	2.1

An important parameter in the manufacture of hydrogel constructs for tissue engineering using a photocrosslinkable material is the sol content of the network formed. A low sol content is indicative of efficient cross-linking. The influence of prepolymer solution depth, irradiation time, and irradiation intensity on sol content were examined, and the results are given in Figure 4.5. As would be expected, prepolymer solutions of greater depth require longer times to reach minimal sol contents at a given irradiation time and light intensity (Figure 4.5A). The 6 mm deep prepolymer solutions required 5 min at 102 mW/ cm^2 intensity to reach a sol content of 6.0 ± 2.7%, whereas 4 mm deep prepolymer solutions produced gels with similar sol contents (6.8 ± 2.6%) after only 1 min at 102 mW/cm^2 intensity. For the 4 mm deep prepolymer solutions, there was little change in sol content with longer gelation times, with 5 min at 102 mW/cm^2 resulting in gels with a sol content of 3.3 ± 1.3%. For the 6 mm deep prepolymer solutions, there was no significant change in sol content after 5 min of irradiation at 102 mW/cm^2. Figure 4.5B shows that there is little influence of DOS on gel sol content at a given photocrosslinking condition, as there is no significant difference between sol contents of gels prepared with 5% DOS versus 21% DOS. Furthermore, sol contents decreased as irradiation intensity increased for a 5 min irradiation time, up to an irradiation intensity of 73 mW/cm^2, after which intensity had no

noticeable effect. However, gels with low sol contents (8.8 ± 1.3%) were obtained at the lowest intensity accurately measurable of 25 mW/cm^2. The low sol contents indicate that the photocrosslinking conditions were effective at producing networks.

The hydrogels contained significant amounts of water, as reflected in their equilibrium water content. The equilibrium water content was higher in gels prepared from prepolymers of lower DOS (Figure 4.5B), with little effect of irradiation intensity at a fixed irradiation time of 5 min. Gels prepared from greater prepolymer solution heights had higher equilibrium water contents (EWC) at given cross-linking conditions (Figure 4.5A). For example, at cross-linking conditions of 102 mW/cm^2 and 3 min, 4 mm thick gels had an EWC of 88.4 ± 1.1%, while 6 mm thick gels had an EWC of 94.8 ± 0.7%. As the sol had been removed prior to swelling to equilibrium, the difference in EWC is likely due to a difference in cross-link density within the lower regions of the 6 mm thick gels. Free-radical generation decreases with penetration depth due to radiation absorbance, and so, the lower regions of the 6 mm thick gels had a lower cross-link density. Thus, the gels should be prepared with thickness less than 6 mm to avoid a heterogeneous structure.

Interestingly, as the irradiation time increased beyond 5 min for an irradiation intensity of 102 mW/cm^2, the EWC increased for both 4 mm and 6 mm thick gels, although the sol contents for both thicknesses remained essentially constant (Figure 4.5A). This result indicates that the cross-link density decreases as radiation time increases beyond 5 min, while a network is still effectively formed. This result is attributed to free-radical cleavage of the chitosan backbone through photoinduced production of radicals that can no longer be consumed by carbon-carbon double bonds. This reasoning arises from the fact that chitosan and glycol chitosan can be readily depolymerized through free radical attack of the glycosidic bond using potassium persulfate free-radical generation [278, 285].

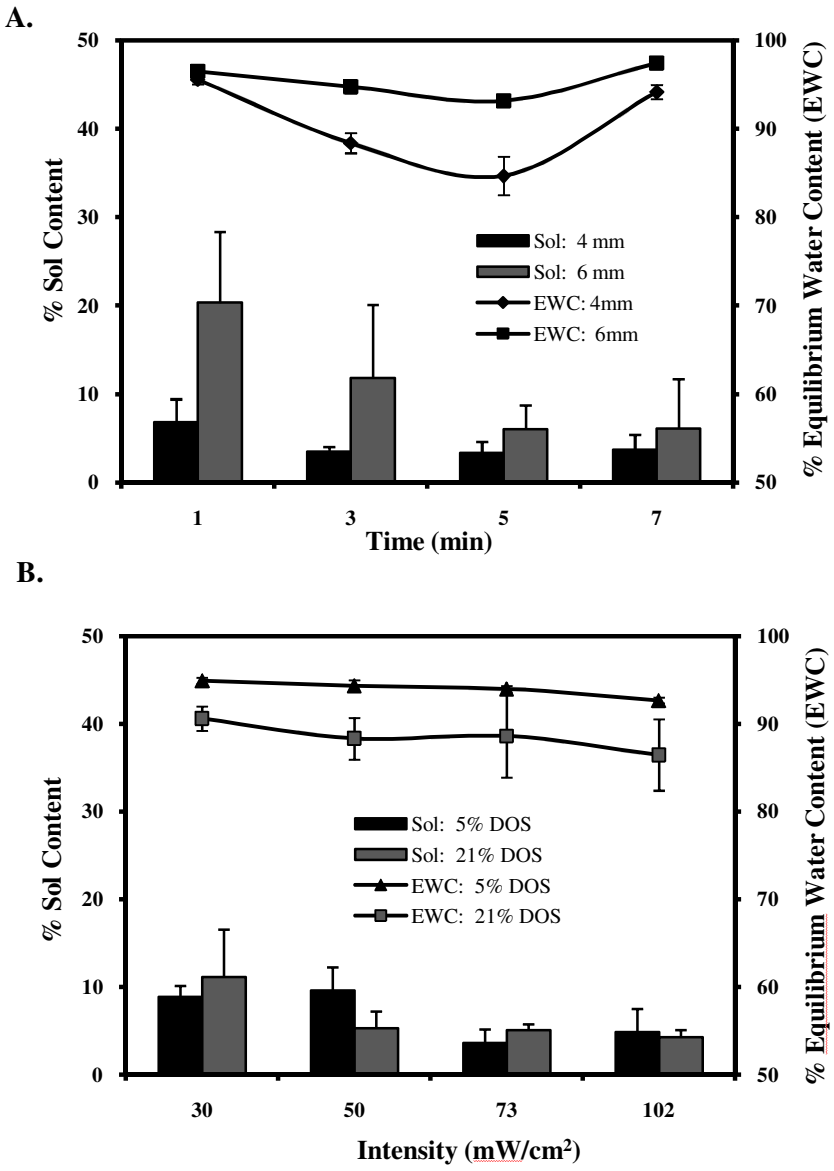

Figure 4. 5. Influence of (A) time variation and prepolymer solution depth of gels (6% w/v, 21% DOS) exposed to irradiation intensity of 102 mW/cm^2 and (B) irradiation intensities and degree of *N*-methacrylate substitution (DOS) of gels (6 w/v%, 4 mm depth) obtained after 5 min of irradiation time, on sol content and equilibrium water content.

As one possible use of the photocrosslinked glycol chitosan gels under investigation is as a scaffold for regenerating articular cartilage, it was important to know the Young's modulus of the gels. It is generally accepted that to produce de novo tissue of appropriate biological and physical properties, the scaffold used should have mechanical properties that are consistent with

the mechanical properties of the tissue. Indentation testing is commonly used to measure the mechanical properties of articular cartilage [246], and so, it was applied to the photocrosslinked glycol chitosan gels. The Young's moduli were calculated from force-indentation depth curves for the two different-sized indenters and 4 mm thick gels as a function of DOS (Figure 4.6). The analysis used assumes that the gel is an isotropic, homogeneous elastic. The Poisson ratio measured for the gels remained essentially constant at between 0.12–0.17. This value is lower than the often assumed value of 0.5 for hydrogels, but is expected, given the large EWC of >90% of the gels measured. This value also compares favorably with those obtained by Goldsmith et al. for hydrogels composed of poly(*N*-vinylpyrrolidone-comethyl methacrylic acid) with cellulose acetate (0–0.30), which had an EWC of 50% [286]. The calculated instantaneous Young's modulus, *E*, increases as the DOS of the prepolymer used to prepare the gel increases, but the increase in *E* diminishes in extent beyond a DOS of 7% when the variability in the measurement is taken into account. The maximum *E* value measured was 0.44 MPa. This value is much smaller than that of human tibial articular cartilage, which has been reported to be 1–10 MPa [287]. Thus, the mechanical properties of this gel may need to be further increased if it is to be used as a scaffold for regeneration of articular cartilage, and it does not appear that this can be achieved through increasing the DOS of the glycol chitosan prepolymer. The possibility of cocrosslinking with another polymer is currently being pursued.

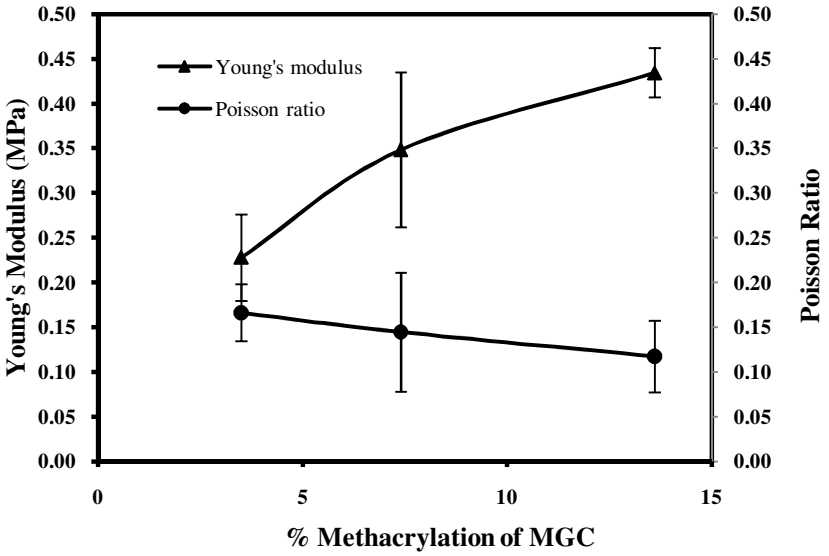

Figure 4. 6. Young's Modulus (E) and Poisson ratio of MGC gels (75 mW/cm^2, 5 min) with varying degree of *N*-methacrylation of the prepolymer solution.

Solid state ^{13}C NMR on the sol-removed gels was done to determine the degree of double-bond conversion during photocrosslinking. The spectrum obtained from a gel prepared using 21% DOS methacrylated glycol chitosan, and a photocrosslinking time of 5 min is given in Figure 4.7. There are no peaks present between 120 and 140 ppm that would correspond to carbon–carbon double bonds, while all other ^{13}C peaks noted in Figure 4.3 are present, albeit broadened. It can, therefore, be concluded that, within the network, there are no unconsumed double bonds that could potentially lead to cytotoxicity.

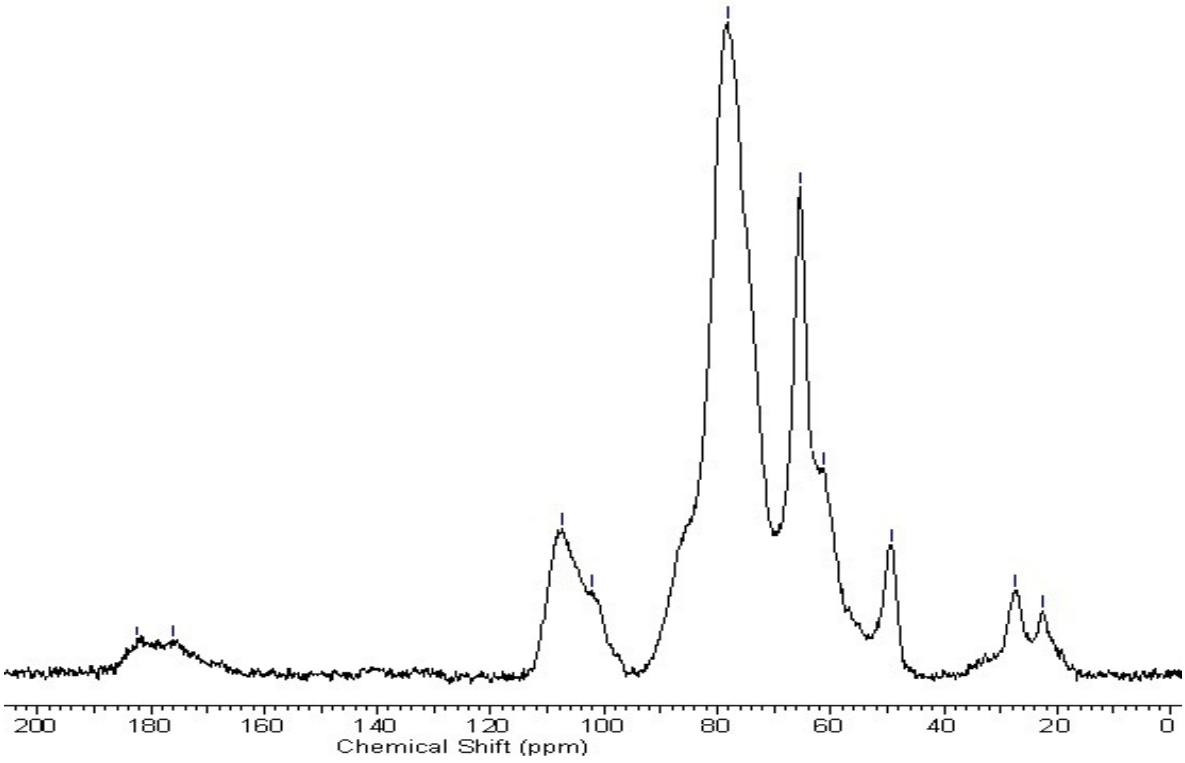

Figure 4. 7. CP-MAS ^{13}C NMR spectrum of photocrosslinked MGC gel (21% DOS) after sol removal.

Chitosan is known to be degraded *in vitro* by lysozyme [288], which is ubiquitous *in vivo*. The rate of degradation of chitosan increases as the degree of deacetylation decreases and as the water solubility of chitosan derivatives increases [289]. However, there have been no reports to date on the *in vitro* degradation of glycol chitosan via lysozyme. To determine the influence of cross-link density of the photocrosslinked hydrogels on *in vitro* degradation rate, hydrogels prepared from varying %DOS were incubated in PBS containing 4 mg/mL lysozyme at 37 °C. The results are shown in Figure 4.8.

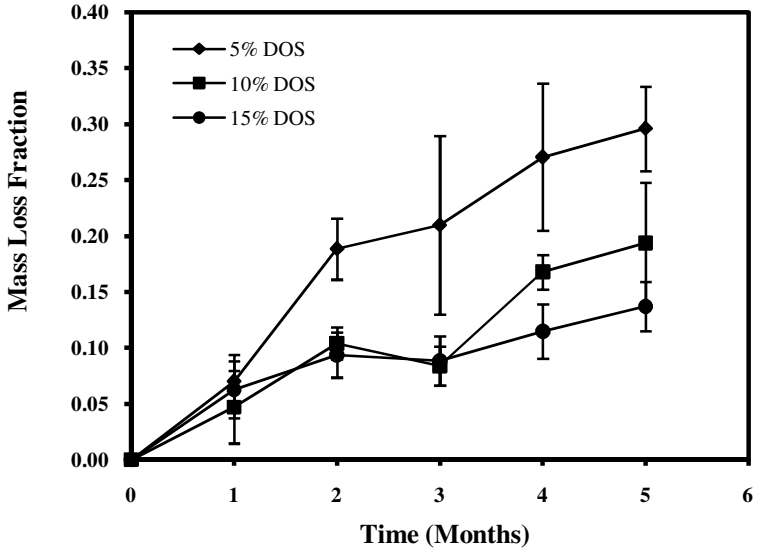

Figure 4. 8. ***In vitro*** **degradation kinetics of MGC gel with varying percent DOS using lysozyme in PBS at 37^{0}C.**

All the hydrogels lost mass during the degradation period, with the extent and rate of mass loss increasing as the crosslink density decreased, that is, as % DOS decreased. A lower cross-link density allows for more ready access of the enzyme to the polymer backbone as the molecular weight between crosslinks increases, as the active binding site of lysozyme binds 6 sugar rings [290]. Moreover, the penetration of the enzyme into the hydrogel bulk would increase as the cross-link density decreased. Both of these effects would increase the rate of degradation. The degradation rates under these conditions were slow, with the greatest mass loss achieved only approximately 30% after 5 months. *In vivo* degradation is likely to be very different, as the gels will be attacked by other enzymes [288] as well as oxidative species [290] and will experience mechanical stress. Nevertheless, the results of this *in vitro* study provide an idea of the expected influence of cross-link density on the degradation rate.

4.3. Conclusions

Glycol chitosan can be reacted with glycidyl methacrylate to yield a water-soluble, photopolymerizable prepolymer that can be used to prepare hydrogels of low sol content. The degree of methacrylation can be readily manipulated by adjusting the molar excess of glycidyl methacrylate to glycol chitosan reactive amine ratio and the reaction time. The hydrogels degraded slowly in the presence of lysozyme at a rate that increased as the cross-link density of the gels decreased. *N*-methacrylate glycol chitosan thus appears to be a promising biomaterial for use in tissue engineering and drug delivery.

CHAPTER 5

ADIPOSE-DERIVED STEM CELL PHOTOENCAPSULATION IN RGD-GRAFTED *N*-METHACRYLATE GLYCOL CHITOSAN GELS

5.1. Introduction

Hydrogels are desirable scaffolds for tissue engineering applications and drug delivery depots as they have high water content and allow homogenous incorporation of cells, drugs and bioactive macromolecules. For cell encapsulation, the highly hydrated environment of hydrogels provides efficient nutrient transport to the embedded cells and thus promotes cell viability [291-293]. The high hydration property of hydrogels also generally induces minimal irritation to the surrounding tissue following implantation [294, 295]. The pre-polymer of a gel can also be tailored to contain bioactive stimuli to enhance cell attachment, migration and proliferation [296-298].

One method to form a hydrogel construct is to photopolymerize a photosensitive polymer solution under visible or ultraviolet (UV) light in the presence of photoinitiators [299-301]. There are numerous advantages of photopolymerization. It can be done in a minimally invasive manner by injecting pre-polymer solution into a defect site, and gels can be formed *in situ* with minimal heat generation [302]. Photopolymerizable gels are generally stable and mechanically strong, due to their covalent crosslinking [300]. For these reasons, in recent years, photopolymerization of hydrogels has been extensively employed for *in situ* controlled release of bioactive growth factors and tissue engineering applications [69, 303-307].

The effects of photopolymerization parameters, such as UV irradiation and photoinitiator concentration, on cell viability have been explored [245, 308-310]. The assessments have

included gel monolayers as well as 3D hydrogels and have examined various cell lines and stem cells. These studies showed that cell viability was not only determined by the photopolymerization parameters, but was also influenced by cell type [245, 308, 311, 312], hydrogel properties (i.e. permissive hydrogels that provide no cues and simply permit cell encapsulation, or hydrogels that mimic extracellular matrix environments)[311] and photoinitiator selection [308]. Moreover, covalently grafted and interpenetrated bioactive macromolecules within the gels promote cell viability and, specifically for stem cells, differentiation to certain lineages [313, 314]. Therefore, judicious examination of these parameters is essential for effective cell encapsulation in photopolymerizable hydrogels.

Previously, pre-polymer photosensitive *N*-methacrylate glycol chitosan (MGC) and its gel were demonstrated to be cytocompatible using an immortalized chondrocyte cell line, but without cell incorporation [234]. In this study, MGC was photopolymerized to form hydrogels encapsulating human adipose-derived stem cells (ASC). The photocrosslinking parameters for fabricating MGC gel, such as sol content, UV irradiation intensity, I2959 photoinitiator concentration, degree of *N*-methacrylation and parameter combination were evaluated for ASC viability and proliferation. Furthermore, the cell ligand binding RGD peptide motif was grafted onto MGC to improve cell attachment and thus viability. This grafting was accomplished by first grafting acrylamide groups to the free amine groups along the MGC backbone, followed by employing a Michael-type addition reaction between the grafted *N*-acrylamide and a thiol on a cysteine within the peptide Ac-G*C*GYG**RGD**SPG-NH_2. Viability, cellularity and distribution of ASC in the MGC gels with and without grafted RGD were investigated.

5.2. Results and Discussion

The influence of photopolymerization parameters, such as solvent conditions, UV light intensity and I2959 photoinitiator concentration, were examined by measuring the sol content of MGC gels formed. A lower sol content indicates a higher efficiency of photocrosslinking. The sol content of MGC gels in aqueous solvents, such as water, medium and medium supplemented with FBS was measured to study the solvent effects on the photocrosslinked gels. Figure 5.1A shows that the sol content of MGC gels when prepared in water was significantly lower than that of the gels prepared in cell culture medium or in medium-FBS. In addition, the sol content decreased with increasing degree of *N*-methacrylation of the MGC for the gels prepared in water. On the other hand, the sol content of MGC in medium and medium-FBS were similar with an average of 28.1%, regardless of MGC percent *N*-methacrylation. Thus, the increase in sol content was due to a compound present in the culture medium. The DMEM/ F12 medium contains linoleic acid, which contains 2 *cis* carbon-carbon double bonds that likely reacted with the free radicals generated during photocrosslinking resulting in the higher sol content of MGC gels in medium. Since the study aimed to investigate the viability of encapsulating ASCs in the gels and FBS did not have an effect on photocrosslinking efficiency, the pre-polymer MGC was dissolved in medium-FBS to form gel constructs for the remainder of the study.

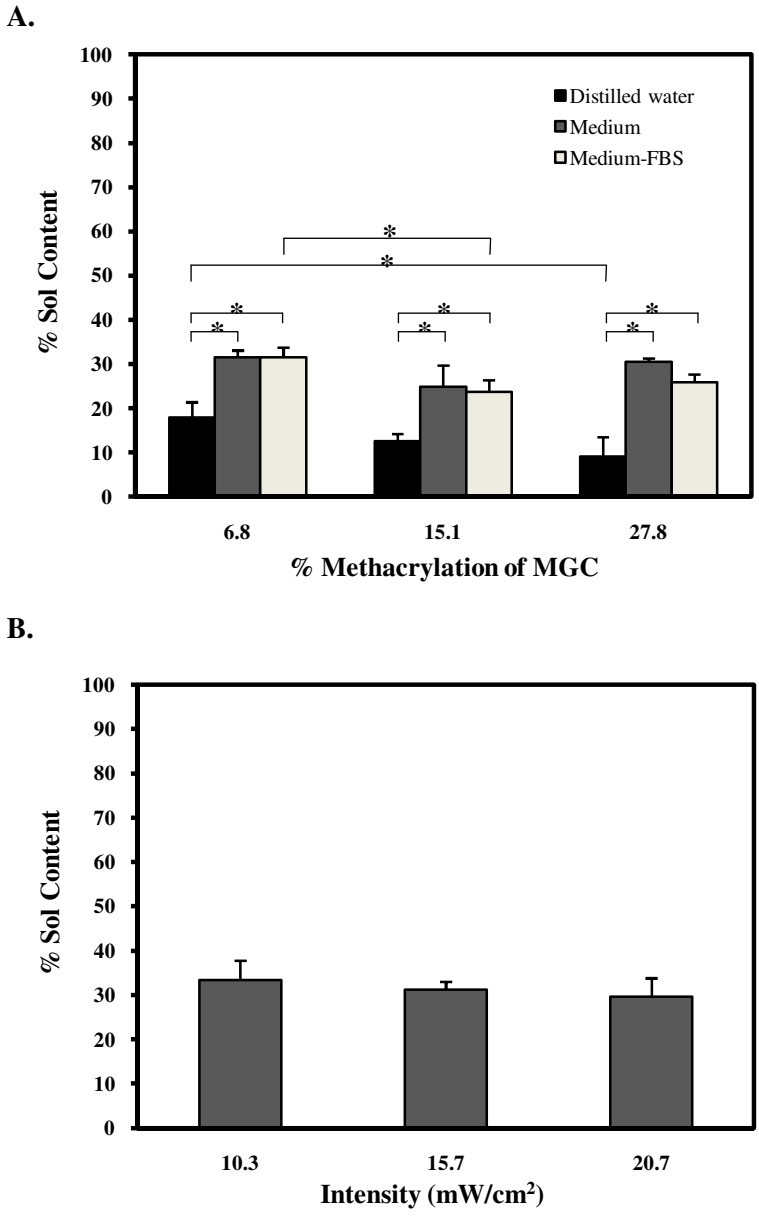

Figure 5. 1. Influence of (A) *N*-methacrylation degree, MGC solvent conditions and (B) UV light intensity for gels prepared in medium-FBS on sol content from MGC of 15.0% *N*-methacrylation. The photocrosslinking conditions were UV exposure of 10.8 mW/cm^2 for 3 min in the presence of 0.5 mg/mL I2959 (n=4, *: p< 0.05).

Varying the UV intensity from 10.3 to 20.7 mW/cm^2 did not influence the sol content of the MGC gels when prepared in medium-FBS (Figure 5.1B). Similarly, the I2959 photoinitiator concentration did not alter the sol content of the gels with high and low degree of *N*-methacrylation, over the range studied (0.5 to 1.5 mg/mL) (Figure 5.2A). In addition, ASC were

highly viable in media containing up to 1 mg/mL I2959 photoinitiator, but viability decreased at concentrations greater than 1.5 mg/mL. The number of ASC in rounded morphology was higher in media containing 2 mg/mL I2959 compared to that in 0.5 mg/mL (Figure 5.2B and C). Without UV irradiation, the I2959 photoinitiator molecules do not form free radical species that react with cellular components and hence did not induce cell damage.

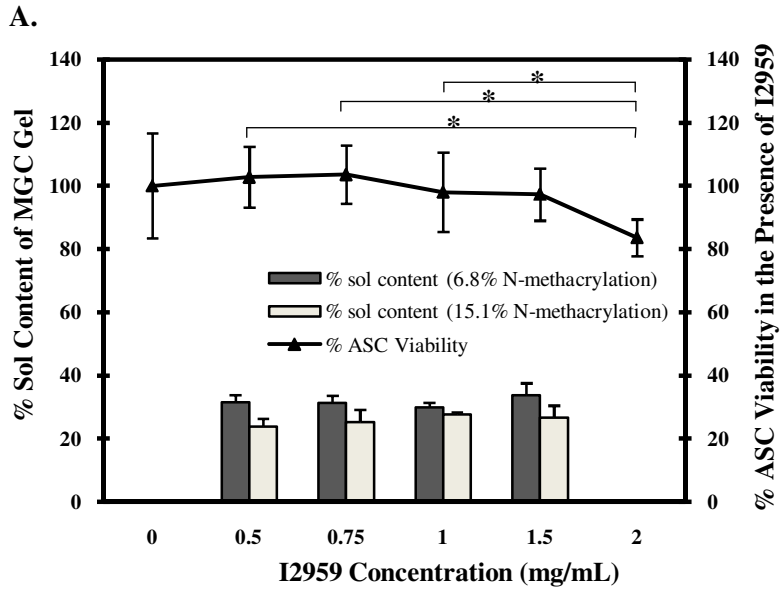

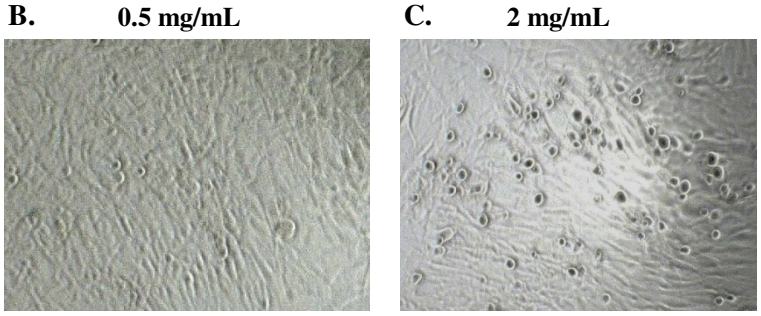

Figure 5. 2. (A) Influence of I2959 concentrations on sol content for gel in medium-FBS and ASC viability. The photocrosslinking conditions of 6% w/v MGC solution were 10.8 mW/cm^2 UV irradiation for 3 min in the presence of 0.5 mg/mL I2959 (sol content: n= 4 , ASC viability: n= 6, *: p< 0.05). Brightfield images of ASC exposed to (B) 0.5 mg/mL and (C) 2 mg/mL I2959 photoinitiator, after 24h.

As the unreacted MGC present in the gels as sol may influence ASC viability following photoencapsulation, ASC were cultured in the presence of MGC prepolymer solution at varying concentrations for 24 h and their viability was measured. Figure 5.3 shows that ASC were more viable at lower MGC concentrations and with MGC prepolymers of lower degrees of *N*-methacrylation. For prepolymers with a degree of *N*-methacrylation of 6%, ASC remained highly viable up to MGC concentrations of 12 mg/mL. However, for prepolymers with degrees of *N*-methacrylation of 11 and 28%, ASC viability decreased to 58.9% and 66.2% at MGC concentrations of 6 mg/mL, respectively. For these higher degrees of *N*-methacrylation, the influence of MGC concentration on ASC viability was essentially the same. The higher number of methacrylate groups present likely increased the possibility of adverse interactions between the MGC and membrane proteins on the cell surface. The average sol content of the MGC gels in the presence of media with serum was 30%, which translates to a concentration of 2.25 mg/mL free MGC within the gels. At this concentration, ASC viability as per the cytotoxicity assay was 115.4 ± 16.3%, 71.7 ± 8.0% and 82.7 ± 13.3% for gels with 6%, 11% and 28% *N*-methacrylation, respectively. It would therefore be expected that gels prepared with higher *N*-methacrylated MGC would exhibit poorer ASC viability, but that the viability would still be acceptable.

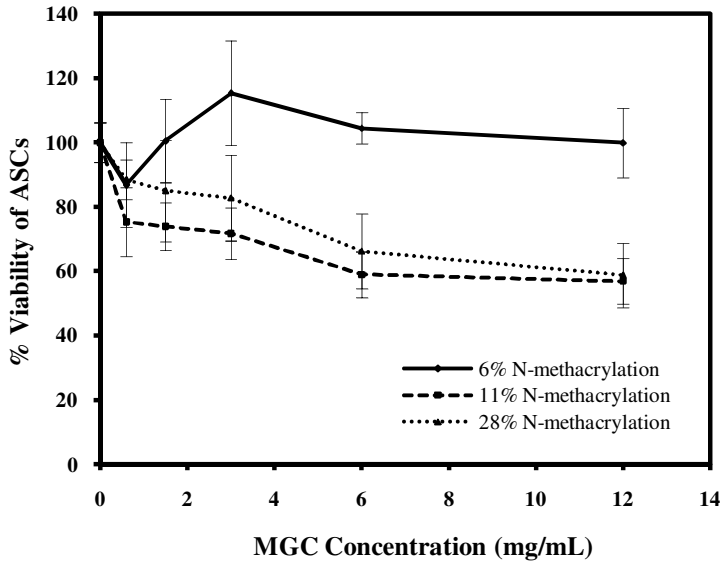

Figure 5. 3. Influence of MGC concentrations and degree of *N*-methacrylation on ASC viability (n=6).

As an individual photopolymerization parameter did not significantly influence ASC viability, parameter combinations were examined to determine potential detrimental effects on ASC viability. Figure 5.4 shows that ASC were highly viable (87.7 ± 3.2 %) when exposed to UV light at the intensity of 10.8 mW/cm^2 for 3 min. On the other hand, when ASC were UV-irradiated in the presence of I2959 or MGC solution, their viability was reduced to 53.4 ± 2.7 and 57.1 ± 5.9 %, respectively. During photopolymerization, UV light homolytically splits photoinitiator molecules to free radical species. In the absence of a polymer containing a reactive vinyl group, the free radicals react with phospholipids of cell membrane and form oxygen reactive species, leading to lipid peroxidation and damage to protein and DNA [315, 316]. Similar studies have demonstrated that goat bone marrow mesenchymal stem cells were more than 80% viable under similar photocrosslinking conditions, except the UV intensities were lower (4 and 6 mW/cm^2) [245, 311]. Nevertheless, different cell types could have variable responses under the same photopolymerization conditions [245]. When ASC were exposed to the MGC prepolymer in the presence of UV irradiation, ASC death was due principally to the high

concentration of highly methacrylated MGC (7.5 mg/mL, 15% *N*-methacrylation). As shown on Figure 5.3, ASC were 58.9 ± 7.1 % viable for 6 mg/mL MGC solution with 11.3% *N*-methacrylation, which is statistically equivalent to the viability obtained in the presence of UV irradiation (57.1 ± 5.9 %).

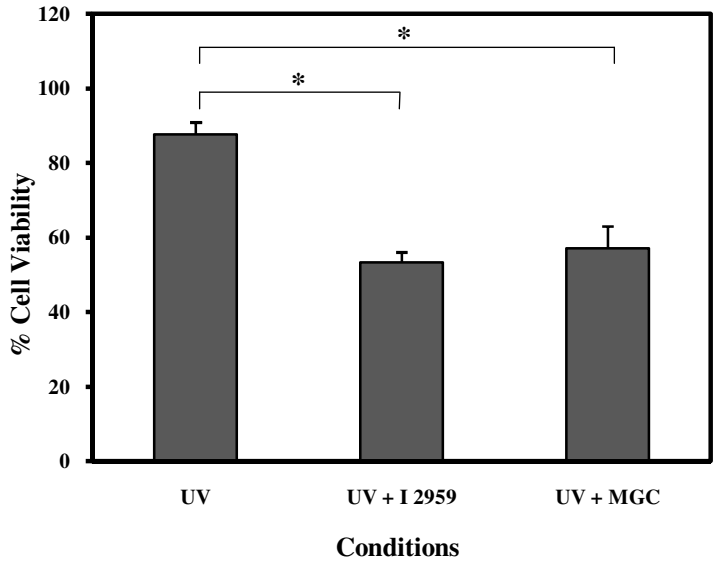

Figure 5. 4. ASC viability after 4 h: Exposed to UV light alone (10.8 mW/cm^2), or exposed to UV light in the presence of I2959 (0.5 mg/mL) or MGC solution (6% w/v in medium-FBS, 15% *N*-methacrylation) (n= 4, *: p< 0.05).

With an understanding of the influence of the photoencapsulation parameters on ASC survival, the viability of ASC incorporated into MGC gels via photopolymerization was investigated. For these experiments, the MGC was dissolved in proliferation media to a final concentration of 6 %w/v and which contained 0.5 mg/mL I2959. Figure 5.5A shows the influence of degree of *N*-methacrylation of the MGC on ASC viability at 24 h post-encapsulation. Following photoencapsulation, the viability of ASC encapsulated in MGC gel was low for all gels, and statistically equivalent with respect to the influence of degree of *N*-methacrylation of the

MGC prepolymer. As time progressed, ASC viability decreased, however, the extent of change in ASC viability was a function of the degree of *N*-methacrylation of the MGC prepolymer used. For gels prepared with 6% *N*-methacrylation MGC, cell viability rapidly decreased with time, dropping from 53.9 ± 8.2 % at day 1 to 29.3 ± 13.8 % at day 4, to only 3.1 ± 0 % by day 7. In contrast, ASC viability decreased only slightly with time for gels prepared with MGC of 12% and 25% *N*-methacrylation; after 24 h ASC viability was 69 ± 9 and 69.5 ± 7 %, respectively, while by day 7, ASC viability in these gels was 51.7 ± 7.8 and 40.7 ± 11.3 %, respectively. The slight difference in initial cell death with respect to degree of *N*-methacrylation of the MGC prepolymer used was considered to be due to the fact that a constant photoinitiatior concentration was used in each case. As a result, the ratio of free radicals initially generated to methacrylate groups was higher for MGC with lower degree of *N*-methacrylation, and so the number of free radicals available to react with cellular components was higher and thus led to an increase in cell death. In addition, the average number of ASC within a given plane in the gel was statistically similar for MGC gels for high and low % *N*-methacrylation on day 1 (Figure 5.5B). However, it was significantly lower on day 4 and 7, regardless of the degree of *N*-methacrylation of the MGC used. On day 7, MGC gels prepared with the MGC of 6% *N*-methacrylation retained the least number of ASC, while gels prepared with MGC of 12% and 25% *N*-methacrylation retained greater, and similar, numbers of ASC.

These results can be explained by ASC response to gel stiffness. The Young's moduli of the gels increased with the degree of *N*-methacrylation of the MGC (Figure 5.5C). It has been demonstrated that stiffer gels allow better cell adhesion and spreading [317-319]. ASC are anchorage-dependent cells and so ASC adhesion on gels prepared with MGC of 12 and 25% *N*-methacrylation was most likely higher than that of gels prepared with MGC of 6% *N*-methacrylation, and thus led to an increase cell viability and cell number within the stiffer gels.

A.

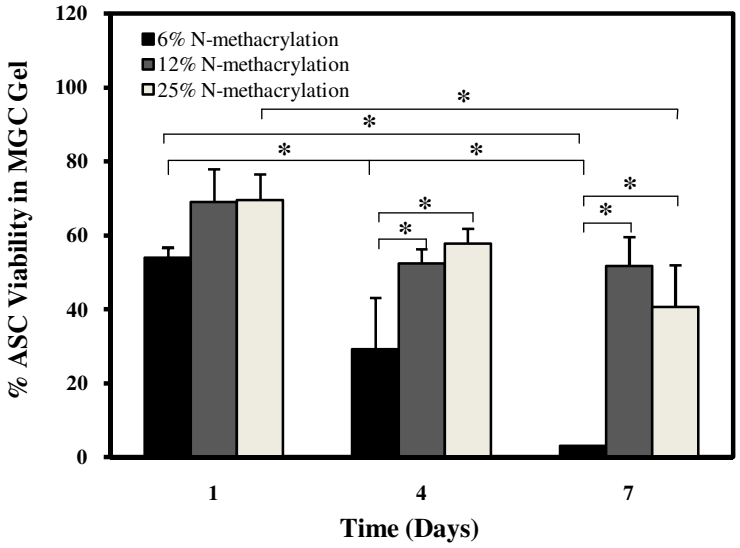
6% N-methacrylation
12% N-methacrylation
25% N-methacrylation
% ASC Viability in MGC Gel
120
100
80
60
40
20
0
1
4
7
Time (Days)
*

B.

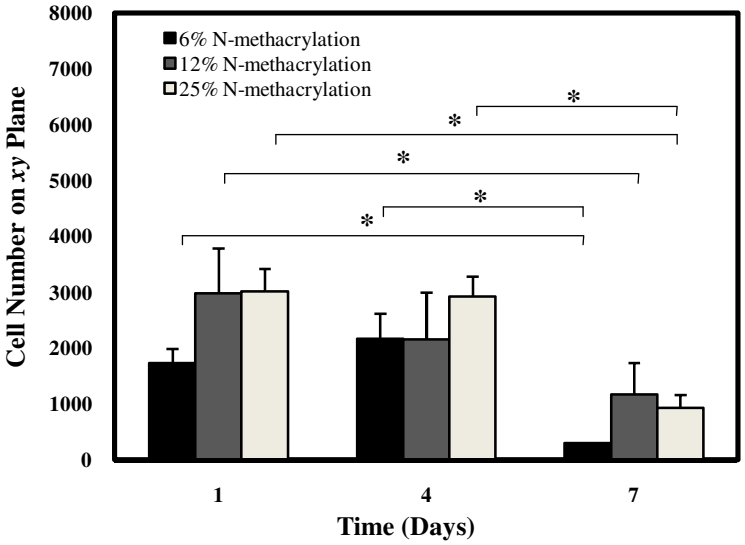
6% N-methacrylation
12% N-methacrylation
25% N-methacrylation
Cell Number on xy Plane
8000
7000
6000
5000
4000
3000
2000
1000
0
1
4
7
Time (Days)
*

C.

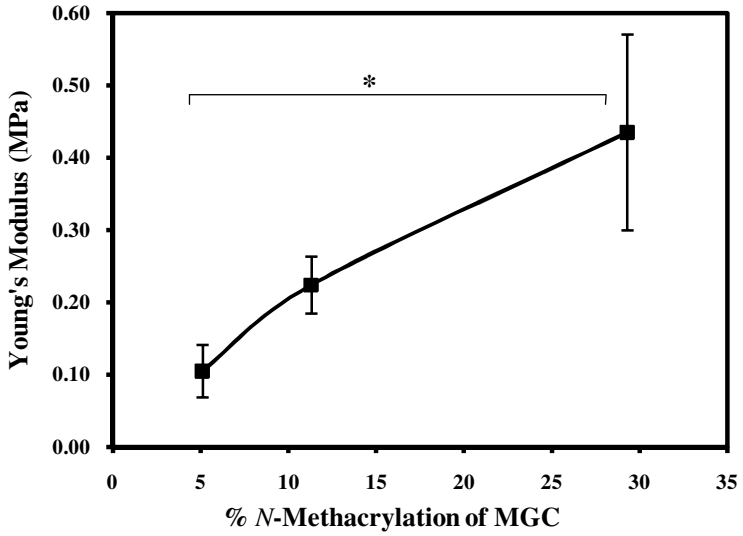

Figure 5. 5. (A) Viability and (B) number of ASC encapsulated in photocrosslinked MGC gels. (C) Young's modulus of MGC gels in medium-FBS as a function of degree of *N*-methacrylation (n= 4, *: p< 0.05).

It was reasoned that the lack of adhesive cell ligands within the MGC gel resulted in the low ASC viability. The use of peptide sequences derived from components of the extracellular matrix is effective at promoting cell attachment as the active sites are exposed to cells in greater concentrations and in better orientation than can be achieved through protein adsorption. Thus, a peptide containing the RGD (Arg-Gly-Asp) adhesive peptide sequence, which has been extensively studied for cell attachment, was grafted onto the MGC polymer chains.

To facilitate peptide grafting, 15% degree of *N*-methacrylation MGC was first modified to contain an *N*-acrylamide group by grafting acrylic acid to the free amine groups on MGC through conventional carbodiimide (EDC) chemistry. The grafted polymer, *N*-methacrylate, *N*-acrylamide glycol chitosan (MAGC), was then reacted with an RGD peptide sequence containing a free thiol on a cysteine residue (G**C**GYG**RGD**SPG) in a Michael-type addition reaction under basic conditions. An acrylamide group was grafted first for this reaction as it undergoes Michael addition significantly faster than does pendant methacrylate [320]. This grafting approach was

chosen because the Michael addition reaction occurs selectively between the acrylamide and the thiol, and it can be done effectively with high yield in aqueous media at physiologic pH.

The presence of the grafted *N*-acrylamide was confirmed by ^{1}H NMR; protons of the acrylamide vinyl group appeared at 6.25, 6.65 and 6.8 ppm. Following acrylamide reaction with the cysteine thiol of the peptide, the proton peaks of acrylamide were absent and peaks of the grafted peptide sequence were present (e.g. at 1.7, 1.9, 2.8 ppm representative of protons on the alkane region of the arginine group, at 2.4 and 3.75 ppm representative of protons on the proline ring, at 3, 3.05 ppm and 6.7 ppm representative of the tyrosine group) (Figure 5.6). In this manner, two different GCGYG**RGD**SPG grafting densities were achieved: 1.8 and 4.9% with grafting efficiency of 50 and 67%, respectively.

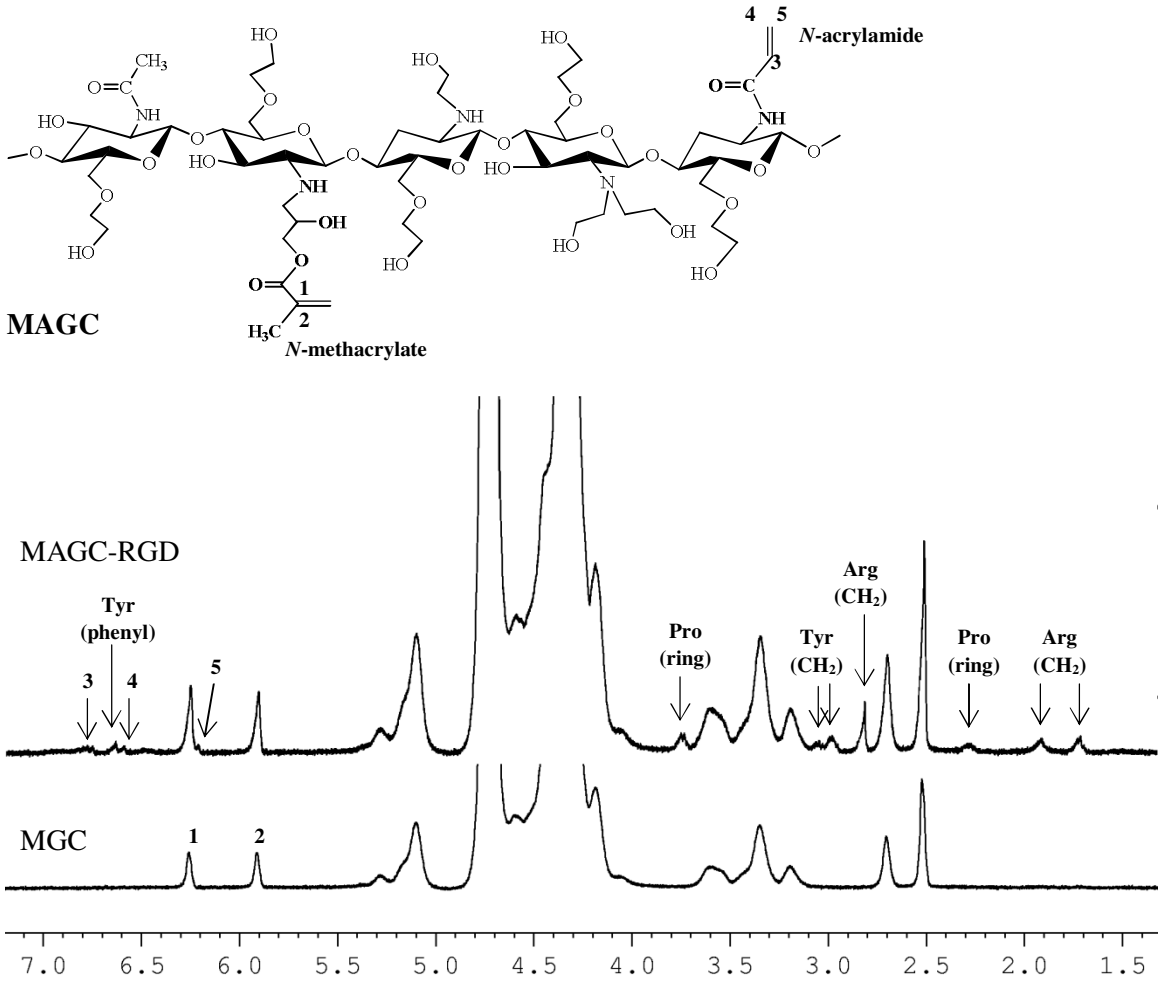

Figure 5. 6. Representative ^{1}H NMR spectra of MGC and MAGC-RGD obtained in D_2O at 90^{0}C.

Others have grafted an RGD-containing peptide onto chitosan in solution using different chemical approaches. For example, Han et al. employed a bifunctional heterolinker, *N*-succinimidyl 3-(2-pyridyldithio)-propionate (SPDP), to covalently link chitosan and cyclic RGD, c[RGDfK (Ac-SCH_2CO)], and reported 60% conjugation yield [321]. Another group reacted RGD peptide containing polyethylene glycol derivative (aldehyde end terminal) with chitosan at low pH and 4.6% grafting was achieved [322]. The bifunctional photosensitive crosslinker sulfosuccinimidyl-6-(4'-azido-2'-nitrophenylamino) hexanoate (sulfo SANPAH) was also employed to react with GRGDY and chitosan under UV light (290-370nm) irradiation [323]. However, the percentage and efficiency of RGD grafting was not reported. Another approach

was to derivatize chitosan with 2-iminothiolane followed by RGDSGGC grafting through disulfide formation initiated by dimethyl sulfoxide (DMSO) and the obtained DOS was 25% [324]. In comparison to our approach, these conjugation routes and purification steps are more time consuming. In addition, the degree and efficiency of grafting was similar, except for the last conjugation method, which required extensive time for DMSO removal.

The ability of the grafted GCGYG**RGD**SPG peptide to support ASC adhesion within the gel was evaluated with respect to ASC viability, cellularity and morphology following photoencapsulation. ASC viability in MAGC gels grafted with GCGYG**RGD**SPG was significantly improved over that attained within MGC gels, and the viability was maintained above 85% throughout the 14 day culture period (Figure 5.7A). On the other hand, the viability of ASC incorporated in MAGC alone (15.1% *N*-methacrylate, 7.3% *N*-acrylamide) was 62.2% averaged over the 14 days, which was significantly lower than that in the gels containing grafted GCGYG**RGD**SPG. ASC viability also decreased with time and followed a similar trend to that in MGC gels prepared with 12 and 25% *N*-methacrylated MGC (Figure 5.5A). The average ASC viability in MAGC gels grafted with 4.9% GCGYG**RGD**SPG was consistently slightly higher than that of gels containing 1.8% GCGYG**RGD**SPG, however the difference was not significant.

In addition, the number of viable ASC in MAGC gels did not significantly decrease with time and was slightly lower than ASC encapsulated in gels containing grafted GCGYG**RGD**SPG (Figure 5.7B). Conversely, the number of viable cells in MAGC grafted with 1.8% and 4.9% RGD peptides remained effectively constant. This result indicates that ASC incorporated in MAGC gels with and without GCGYG**RGD**SPG did not proliferate. Cell proliferation in hydrogels containing RGD sequence is highly dependent on the density of the peptide per volume of the constructs. The RGD concentration itself in a hydrogel depends on the type of hydrogel, cells, species, age of various cells and molecular interactions between the cells and the hydrogel [325]. There has been only one other study concerning human ASC encapsulated in a gel

modified to contain the RGD sequence. Duggal et al. employed alginate grafted with 43.3 μM RGD to encapsulate human ASC [326]. In that study, the number of ASC encapsulated within the gels remained constant over 21 days. In our study, MAGC grafted with 1.8% and 4.9% RGD peptides corresponding to 15.3 μM and 41.3 μM RGD, respectively, also showed constant cell number for 14 days. Increasing RGD grafting density in the gel would promote ASC proliferation, if it were necessary for a specific objective. Another possible explanation of the low proliferative capability of the encapsulated ASC is inactive cell cycle after photopolymerization. Severe UV exposure has been demonstrated to prolong the lag phase of stem cells' inactive state [311]. Nevertheless, the presence of the grafted RGD peptide sequence significantly improved ASC viability.

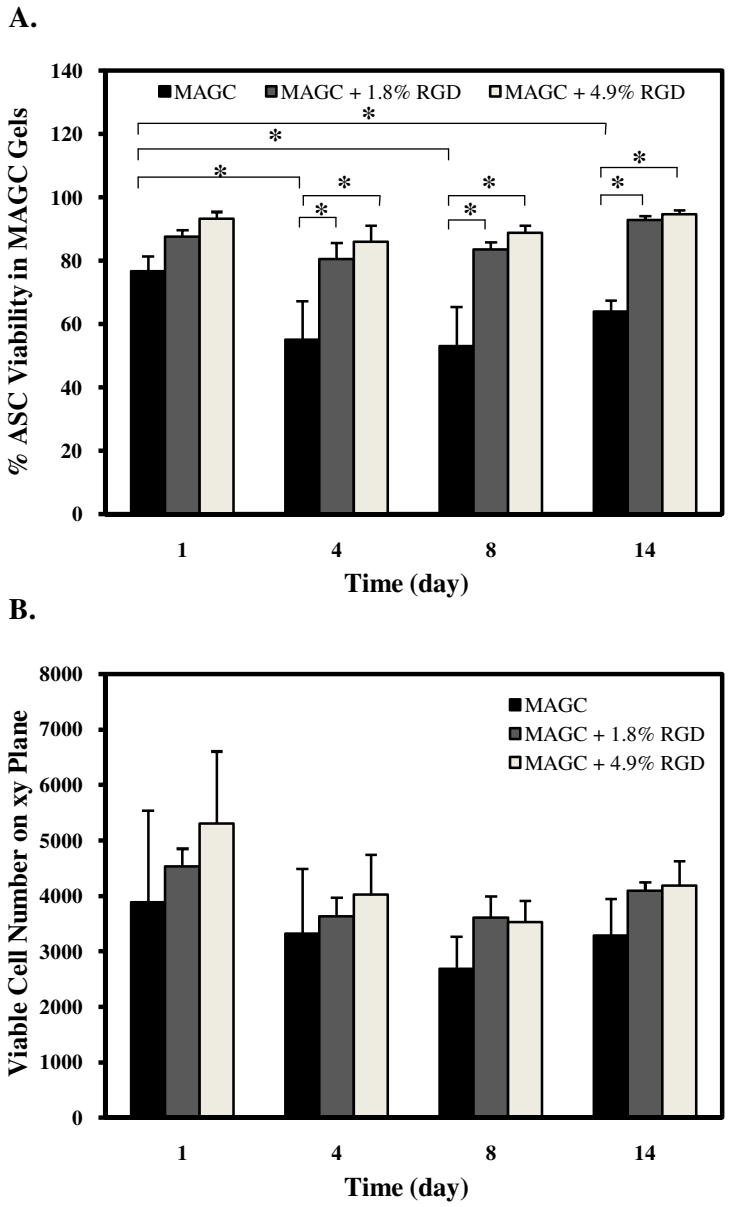

Figure 5. 7. (A) Percent viability and (B) viable number of ASC encapsulated in photocrosslinked MAGC and MAGC-RGD gels (n= 4, *: p< 0.05).

ASC distribution within different layers of the gels was also examined. The number of ASC initially located at the top of the gels was significantly lower than within lower layers of the gels (Figure 5.8A). In addition, the number of ASC situated near the top and middle layers of the gels decreased significantly with time. In contrast, the number of ASC present at the bottom of

the gels increased from day 8 to 14. This may be due to dead cells from other layers settling to the bottom of the gel, in which the number of dead cells remained high throughout the culture period (Figure 5.8B). The LIVE/DEAD images of ASC in MAGC-RGD gel on day 1 showed that ASC were highly distributed on the bottom of the gels (Figure 5.8 C-E). This was attributed to the influence of gravitational force during the 3 min gel irradiation. In addition, ASC on the bottom of the gel were more uniformly distributed throughout the *xy* plane, in comparison to other layers. For ASC located on the middle and top layers, the densely populated area was located at the edge of the gel, suggesting ASC migration towards this direction.

A.

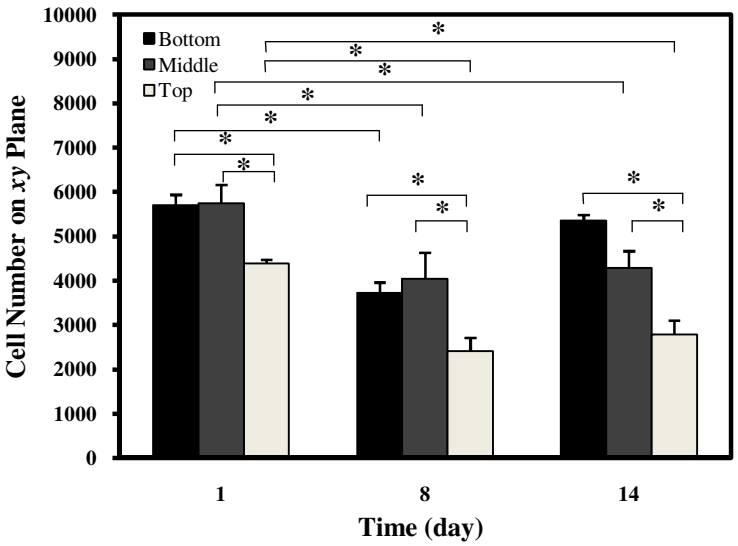
Bottom
Middle
Top
Cell Number on xy Plane
10000
9000
8000
7000
6000
5000
4000
3000
2000
1000
0
1
8
14
Time (day)

B.

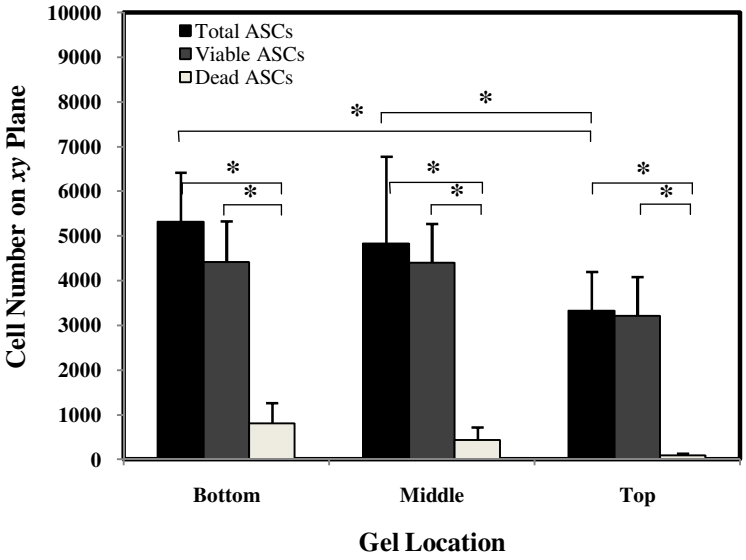
Total ASCs
Viable ASCs
Dead ASCs
Cell Number on xy Plane
10000
9000
8000
7000
6000
5000
4000
3000
2000
1000
0
Bottom
Middle
Top
Gel Location

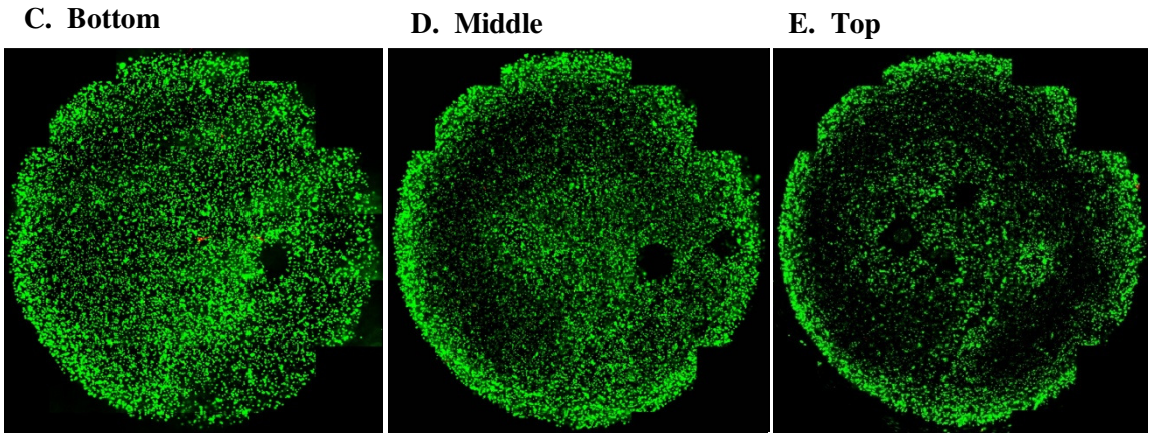

Figure 5. 8. (A) ASC distribution in MAGC gel grafted with 4.9% RGD, (B) ASC viability on different locations of the gel throughout culture period (n= 4, *: p< 0.05). Images of ASCs on the (C) bottom, (D) middle and (E) top of the gel on day 1.

5.3. Conclusions

In this study, we have examined the potential of photoencapsulating adipose-derived stem cells within *N*-methacrylate glycol chitosan prepolymer. The prepolymer can be photopolymerized at room temperature to form a hydrogel construct at low I2959 photoinitiator concentration and light intensity. Concentrations of *N*-methacrylate glycol chitosan consistent with the sol content of the gels formed, and I2959 concentrations up to 1mg/mL, were not cytotoxic to adipose-derived stem cells. In gels that did not contain RGD grafted peptide, the viability of adipose-derived stem cells remained constant for 7 days when incorporated in gels prepared with prepolymer of a high degree of *N*-methacrylation. Cell number decreased with time for all gels and the least number of cells was retained in gels prepared with prepolymers of a low degree of *N*-methacrylation. The crosslinking density and thus stiffness of the gel determined the viability and number of cells retained in the gels; higher gel stiffness resulted in increased cell viability and number with time. In the presence of grafted RGD peptide in the gel, the encapsulated adipose-derived stem cells were highly viable (~90%) and their number remained constant for 14 days. As injectable, *in situ* gelation biomaterials are attractive for tissue

engineering and drug delivery applications, *N*-methacrylate, *N*-acrylamide glycol chitosan grafted with a cell adhesive peptide may prove to be a useful material.

CHAPTER 6

LOW MELTING POINT AMPHIPHILIC MICROSPHERES FOR DELIVERY OF BONE MORPHOGENETIC PROTEIN-6 AND TRANSFORMING GROWTH FACTOR-β3 IN A HYDROGEL MATRIX

6.1. Introduction

As discussed in the Introduction and Literature Review, human ASC can be efficiently transformed towards the chondrocyte lineage by exposure to a combination of bone morphogenetic protein-6 (BMP-6) and transforming growth factor-β3 (TGF-β3) at low doses (5 ng/day) over a period of 4 to 6 weeks [86, 160]. One strategy to induce differentiation of ASC within a gel *in situ* using these growth factors is to co-deliver them by means of polymeric microspheres.

Desirable features of the microspheres to be used were considered to be: 1) composed of biodegradable polymers with a history of *in vivo* use, 2) easily dispersible within the aqueous pre-gel solution, 3) soft at body temperature yet possessing good handling properties at room temperature, and 4) capable of prolonged delivery of low doses of bioactive growth factor. To satisfy the design criteria, amphiphilic triblock poly(1,3-trimethylene carbonate-*co*-ε-caprolactone)-*b*-poly(ethylene glycol)-*b*-poly(1,3-trimethylene carbonate-co-ε-caprolactone) (P(TMC-CL)$_2$-PEG) was employed to fabricate the microspheres. This polymer was chosen for the following reasons. The homopolymers of ε-caprolactone (PCL) and 1,3-trimethylene carbonate (PTMC) have been demonstrated to be biocompatible and biodegradable [237, 238]. In addition, these polymers hydrolyze slowly without accumulating significant amounts of acidic degradation products that alter local pH [239, 240]. The PEG central block should allow ready

dispersion of the microspheres in the gel by forming a hydrophilic surface upon immersion in water. Finally, low molecular weight homopolymers of ε-caprolactone possess a melting point of 40-41ºC [249]. By copolymerizing with trimethylene carbonate, it should be possible to generate a low molecular weight polymer with an onset of melting of around 10ºC and that would be amorphous at 37ºC, by utilizing the principle of melting point depression induced by copolymerization, expressed as [327],

$$\frac{1}{T_f} - \frac{1}{T_f^o} = \frac{RX_B}{\Delta H_f} \tag{6.1}$$

wherein T_f is the melting point of the copolymer, T_f^o is the melting point of the crystallizable homopolymer in its pure state, R is the gas constant, X_B is the mole fraction of noncrystallizable comonomer, and ΔH_f is the heat of fusion per mole of crystalline copolymers. In this manner, the microspheres would be soft at body temperature, and yet still readily mixed into the pre-gel solution at lower temperature.

Growth factor release from these microspheres will be driven by osmotic pressure. In this approach, the growth factor is co-lyophilized with a physiologically acceptable osmotigen such as trehalose, which generates the osmotic pressure that drives the release [241]. For the *in situ* setting hydrogel delivery vehicle, *N*-methacrylate glycol chitosan was used. The objective of this work was to examine the potential of the P(TMC-CL)$_2$-PEG microspheres embedded within a hydrogel matrix for the individual delivery of BMP-6 and TGF-β3 while maintaining their bioactivity.

6.2. Results and Discussion

6.2.1. Characterization of Oct-P(TMC-CL) and P(TMC-CL)$_2$-PEG copolymers

A primary design criterion of the microspheres was that they were to have a melting temperature (T_m) range such that there were solid at storage temperatures of less than 10ºC, but would be a viscous liquid at body temperature. To determine the molar ratios of CL to TMC (CL: TMC) in the final polymers that yielded such a melting point range, preliminary studies were performed using 1-octanol as an initiator, because it is effective at initiating the polymerization [241] and because the PEG used had a melting point range of 34 to 43ºC and so would interfere with the analysis. Increasing the molar ratio of CL:TMC in Oct-P(TMC-CL) polymer from 3.3:1 to 5.7:1, while keeping the molecular weight of approximately constant at 1500 Da, increased the onset of melting from -7 to 11ºC (Table 6.1). Furthermore, the crystallinity of the polymers at 37ºC range from 0 to 17.6% as the CL:TMC ratio increased, and the T_g was decreased from -62 to -71ºC for CL:TMC molar ratio from 3.3 to 5.7, respectively. Thus, an increased CL:TMC molar ratio lowers the T_g of the polymer. With a CL:TMC ratio of 5:1, the polymer melting range was 10 to 47ºC, and had a degree of crystallinity of only 3.9% at 37ºC. This composition complied with the desired thermal properties of microspheres for the intended purpose, and was therefore used in further polymer development.

Table 6. 1. Compositions and thermal properties of Oct-P(TMC-CL) copolymers

Target CL:TMC:Oct molar ratio	*CL:TMC:Oct molar ratio*	*CL/TMC*	*M_n (Da)*	*PDI*	*T_g (ºC)*	*ΔH_m (J/g)*	*T_m range (ºC)*	*%X (37ºC)*
9: 3: 1	10.7: 3.2: 1	3.3	1580	1.5	-62	56.4	-7 – 44	0
10: 2: 1	10.8: 2.2: 1	4.9	1430	1.1	-64	51.4	10 – 47	3.9
11: 1: 1	11.9: 2.1: 1	5.7	1460	1.5	-71	57.2	11-51	17.6

PEG diol with a molecular weight of ~ 1000 Da was employed to form a triblock copolymer with a central PEG region. The CL:TMC molar ratio was designed to be 5:1, based on the preliminary work with 1-octanol initiated copolymers, while the number average molecular weight of the TMC-CL block was targeted to be roughly similar to that of the 1-octanol initiated polymers, to three times that molecular weight (Table 6.2). The resulting high M_n P(TMC-CL)$_2$-PEG triblock (9910 Da) had TMC-CL blocks that were 3 times longer than that of the Oct-P(TMC-CL), as targeted, while the TMC-CL block of the low M_n copolymer (5940 Da) was 1.7 times longer. This difference from the targeted molecular weight is attributed to loss of the low molecular weight polymer fraction during purification. The P(TMC-CL)$_2$-PEG copolymers were synthesized to attain similar CL to TMC molar ratios but differing M_n, and the M_n played a key role in determining polymer thermal properties. There were two melting endotherms present, one of which overlapped with the melting range of pure PEG, indicating that there were PEG-rich regions phase separated within the polymer bulk. The crystallinity contributed by the PEG regions was expected to disappear once the microspheres were incubated in aqueous solution. The low M_n copolymer was amorphous at 37ºC, while the high M_n polymer contained 39.2% crystallinity, which was contributed by both PEG and P(TMC-CL). The higher molar ratio of CL to TMC in the 9910-Da P(TMC-CL)$_2$-PEG copolymer resulted in a slightly lower T_g, despite its higher molecular weight.

As it was anticipated that the thermal properties of the polymeric microspheres would differ once equilibrated with water, the thermal properties of microspheres incubated in PBS for 24 h were measured. A crystallization peak was not observed in microspheres made from the PEG-initiated triblock copolymers, indicating that the PEG regions had indeed been dissolved. The T_g for P(TMC-CL)$_2$-PEG copolymers soaked in PBS decreased as a result of the dissolution of the crystalline PEG as well as the plasticizing effect of water (Table 6.3). The zero shear rate viscosities at 37ºC of Oct-P(TMC-CL) of similar molecular weight as the P(TMC-CL) blocks in

the low and high M_n P(TMC-CL)$_2$-PEG were 7.6 and 39.5 Pa.s, respectively. Thus, the copolymers were viscous liquids at body temperature.

Table 6. 2. Compositions and thermal properties of triblock P(TMC-CL)$_2$-PEG copolymers

Target CL:TMC:PEG	*Actual CL: TMC:PEG*	*CL/ TMC*	*M_n (Da)*	*PDI*	*T_g (°C)*	*ΔH_m (J/g)*	*T_m range (°C)*	*%X (37°C)*
0:0:1	-	-	995	-	-	132.4	34-43	0
30.9: 9.4: 1	36.1: 7.2: 1	5.0	5940	1.3	-59	18.7	6-31	0
						23.8	35-41	
81: 24.5: 1	80.2: 13.6: 1	5.9	9910	1.2	-62	1.8	14-29	39.2
						54.7	44-51	

Table 6. 3. Thermal properties of P(TMC-CL)$_2$-PEG microspheres after 24-hr incubation in PBS

M_n (Da)	*T_g (°C)*	*T_m range (°C)*	*ΔH_m (J/g)*	*%X (37°C)*	*η_{37C} (Pa.s)*
5940	-63	19-34	10.2	0	7.6*
9910	-72	35-42	14.5	10.4	39.5*

* Viscosity of Oct-P(TMC-CL) of a the same molecular weight as the P(TMC-CL) block in the triblock copolymer.

6.2.2. Microsphere fabrication

Both high and low M_n triblock P(TMC-CL)$_2$-PEG copolymers were employed to manufacture microspheres for lysozyme release studies. Lysozyme was used as a model protein to determine formulation parameters influencing protein release as well as fabrication parameters influencing microsphere properties before incorporating Bone Morphogenetic Protein-6 (BMP-6) and Transforming Growth Factor-β3 (TGF-β3). Lysozyme is a single polypeptide with a M_n of 14.3 kDa [328], while BMP-6 is a homodimeric polypeptide with a M_n 26.2 kDa [329]. TGF-β3 is an homodimeric polypeptide protein with a M_n (25.0 kDa [330]) similar to BMP-6.

The average diameter of the lysozyme particle-containing microspheres was between 65 and 85 μm (Table 6.4), which was sufficiently large to provide control over growth factor release and yet still be injectable through a needle. Since microspheres as a delivery vehicle are fairly small, the particle size of the loaded protein must be reduced to allow uniform dispersion within the microspheres. The resulting average particle diameter for lysozyme was 2.3 ± 0.6 μm (Figure 6.1). The content of BMP-6 and TGF-β3 in the lyophilized-cake formulation (9.3% BSA and 90% trehalose) was less than 1% w/w. Therefore, it was considered unlikely that the presence of the growth factors would affect the average particle diameter. The average size of 9.3% w/w BSA-trehalose particles was on the order of that of the lysozyme particles.

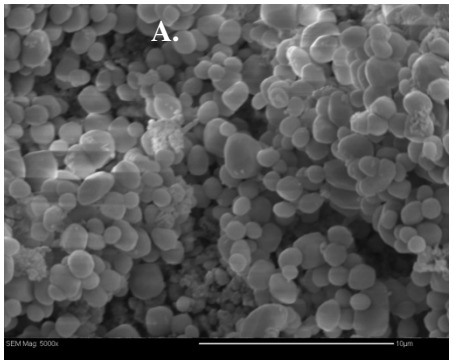

Figure 6. 1. Representative SEM image of lysozyme in DCM (4% w/v), after being sieved through a Tyler No 325 sieve (< 45 μm) and vortexed at 800 rpm for 2 min. (Scale bar = 10 μm)

Microspheres prepared from low M_n P(TMC-CL)$_2$-PEG were obtained in low yield, while P(TMC-CL)$_2$-PEG with M_n of 9910 Da resulted in reasonably high microsphere yield and lysozyme encapsulation efficiency (Table 6.4). The low yield was attributed to the average microsphere diameter being smaller than the mesh size of the sieve (D_{mesh}= 45 μm) used to collect the microspheres from the ethanol bath. This indicates that these microspheres were generally smaller to begin with, before being collected on the sieve, a result that is likely due to reduced

polymer solution surface tension. A possible explanation for the lower encapsulation efficiency obtained for low M_n P(TMC-CL)$_2$-PEG microspheres loaded with 10% w/w lysozyme in trehalose is the greater shrinkage of these microspheres during solvent extraction leading to greater loss of encapsulated particles from the microsphere surface.

Table 6. 4. Microsphere fabrication parameters of P(TMC-CL)$_2$-PEG copolymers

Mn (Da)	*% w/w lysozyme in trehalose in particles*	*% Particle loading in microspheres*	*% Yield*	*% Encapsulation efficiency*	*Average Diameter (μm)*
5540	10	5	29.9 ± 4.5	86.8± 15.9	64.9 ± 5.7
	40	5	30.9 ± 8.7	102.5 ± 39.3	65.3 ± 27.4
	10	2.5	55.5*	45.9*	59.3 ± 14.2**
9910	10	2.5	72.1*	128.8*	84.9 ± 32.9**

Unless otherwise noted, each microsphere condition was prepared in three replicate batches

* No replicates ** No replicates, standard deviation within the sample.

6.2.3. Microsphere dispersibility in MGC hydrogels

It was expected that the hydrophilic PEG molecules at the microsphere surface would orient themselves outward into the aqueous medium to provide a hydrophilic surface allowing good dispersibility of the microspheres within the hydrogel carrying vehicle. Preliminary studies on the dispersibility of the microspheres within the MGC gel demonstrated this to be true. Oct-P(TMC-CL) and low M_n P(TMC-CL)$_2$-PEG microspheres aggregated within the MGC gels (Figures 6.2A-D), while the high M_n P(TMC-CL)$_2$-PEG microspheres were uniformly distributed throughout (Figures 6.2E, F). Although the hydrophilic PEG aided the dispersion of the microspheres within MGC gel, this effect was countered in part by the degree of crystallinity and viscosity of the amorphous regions of the copolymer used. Both Oct-P(TMC-CL) and low M_n P(TMC-CL)$_2$-PEG were nearly amorphous at the crosslinking conditions and had low viscosity

(Tables 6.1 and 6.3) and thus had low resistance to aggregation during mixing in the MGC pre-gel solution. The higher viscosity of the amorphous regions and the presence of crystals in the bulk phase allowed the high M_n P(TMC-CL)$_2$-PEG microspheres to remain separated.

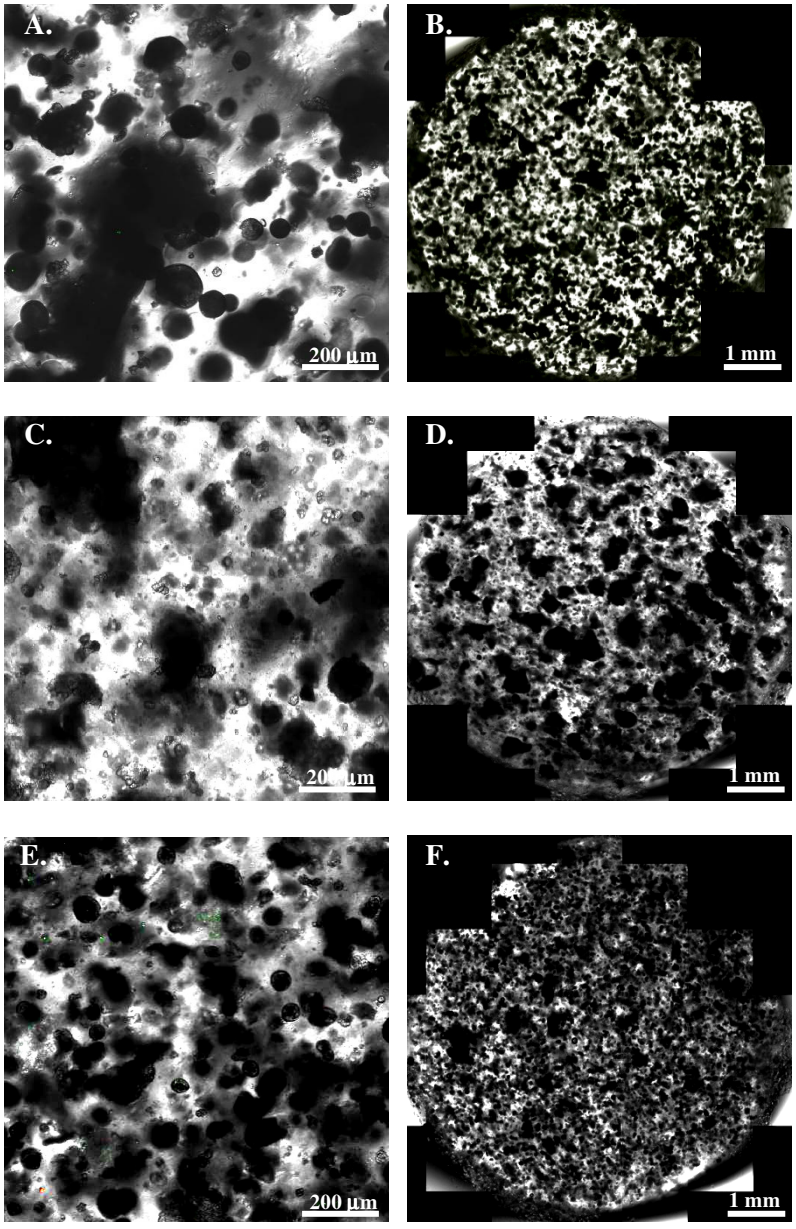

Figure 6. 2. Images of microspheres embedded in MGC hydrogels (5.5% *N*-methacrylation). Microspheres made from: (A, B) Oct-P(TMC-CL), (C, D) 5940-Da P(TMC-CL)$_2$-PEG and (E, F) 9910-Da P(TMC-CL)$_2$-PEG. (A), (C) and (E): 100x magnification; (B), (D) and (F): Stitched images of the MGC gel with embedded microspheres.

6.2.4. Protein release kinetics

The effect of trehalose content of the incorporated solid particles on the release of lysozyme from P(TMC-CL)$_2$-PEG microspheres was investigated using the 5940 Da polymer to form the microspheres. Figure 6.3 shows that the initial burst for particles loaded in the microspheres at 5% w/w was similar (32 to 34%), regardless of the trehalose content of the particles. Following the burst, lysozyme release was sustained and completed on day 48 when the particles consisted of 90% w/w trehalose. On the other hand, only 64.5% of the initially loaded protein was released by 45 days from microspheres containing particles consisting of 60% w/w trehalose. As lysozyme carries a net positive charge and chitosan is a polycation, and because the water content of the gel was high (~ 95%), there was negligible contribution of the gel phase to the release, and release from the microspheres was considered to be rate-limiting.

That the protein release was dependent on the content of hygroscopic trehalose suggested that the release of the protein was governed by the osmotic pressure driven mechanism [241, 242]. The proposed means of release through this mechanism is as follows. Following immersion of the microspheres in an aqueous environment, the surface-resident particles dissolve and are released into the medium. Subsequently, water diffuses into the polymer. Upon contact with an embedded solid particle, the water dissolves the solid at the polymer-particle interface, forming a saturated solution. Under the influence of the enhanced activity gradient, water is drawn towards the particle dissolving more of the solid. The incoming water generates pressure within the microsphere matrix that is resisted by the polymer viscosity. The polymer flows in the direction of least resistance, such as the surface of the microsphere, and a liquid-filled pore is formed that ultimately reaches the surface and releases the dissolved solutes.

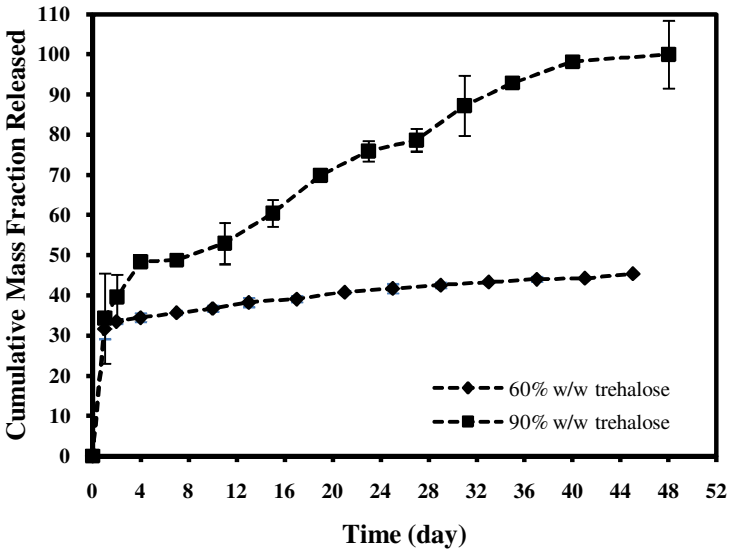

Figure 6. 3. Release profile of lysozyme from microspheres prepared with the 5940 Da P(TMC-CL)$_2$-PEG as a function of trehalose content in the dispersed particles. The particle loading was 5% w/w.

As an increase in particle loading in the delivery vehicle increases the amount of particles dispersed on the surface of polymer matrix and thus the initial burst [196, 331], the particle loading in low M_n P(TMC-CL)$_2$-PEG microspheres was reduced to 2.5 % w/w in an effort to reduce the initial burst. Figure 6.4A shows that a 2.5% w/w loading lowered the initial burst to 6.3 and 4.8% for the situation wherein 5 mg and 2.5 mg microspheres were loaded into MGC gel, respectively, and prolonged the release period to 63 days. In addition, the lower initial burst lengthened the duration of protein release. Nevertheless, the lysozyme release from microspheres prepared with low M_n P(TMC-CL)$_2$-PEG exhibited large variability. The contributing factor was microsphere aggregation in the MGC gel (Figure 6.2C, D). As a result, the aggregated microspheres were larger in size and generated a slower release rate.

A similar release trend was observed for lysozyme release from microspheres prepared from high M_n P(TMC-CL)$_2$-PEG loaded into the gels, but with less variability in the released amount at a given time (Figure 6.4B). The release profile of 2.5 and 5 mg microspheres encapsulated into the MGC gel was identical, with 12% initial burst and an average release of

1.44%/day over a 70 day period. The release was zero order beyond the initial burst, as indicated by a linear regression to the data (coefficient of determination: $R^2 = 0.96$). Thus, high M_n P(TMC-CL)$_2$-PEG microspheres were better able to deliver protein in a controlled manner.

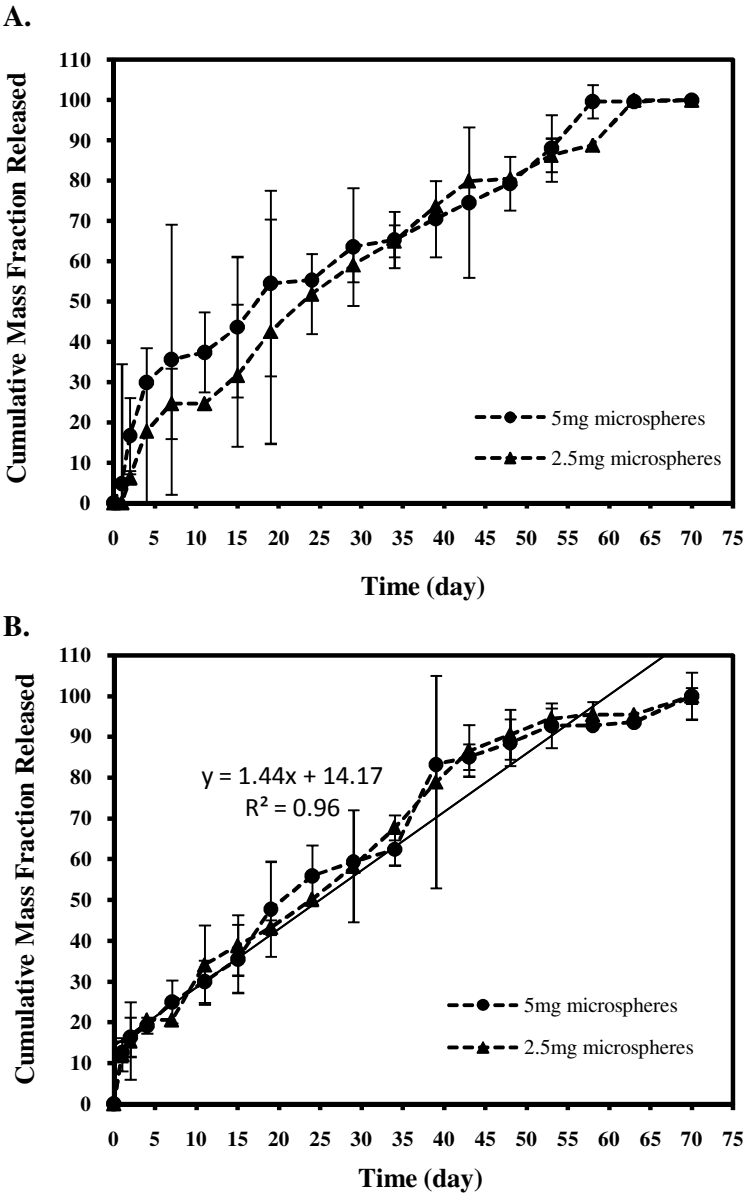

Figure 6. 4. Release profiles of MGC gels containing microspheres with 2.5% loaded 10% w/w lysozyme in trehalose particles with 2.5 and 5 mg of microspheres loaded/MGC gel. Lysozyme released from microspheres with P(TMC-CL)$_2$-PEG Mn of (A) 5940 and (B) 9910 Da. The solid line in (B) represents a linear regression from 1 to 53 days.

6.2.5. Polymer degradation

To determine whether polymer degradation by hydrolysis influenced lysozyme release, the mass loss and M_n change of microspheres immersed in water (pH~7.4) only were also measured. The M_n decrease and mass loss of the 9910-Da P(TMC-CL)$_2$-PEG microspheres after 28 weeks was 30.7% and 5%, respectively (Figure 6.5), while the M_n decrease and mass loss of 5940-Da P(TMC-CL)$_2$-PEG microspheres were 15% and 3.6%, respectively. Thus, the degradation of the P(TMC-CL)$_2$-PEG was slow and not appreciably affected by polymer molecular weight over the time frame examined. That a decrease in molecular weight occurred with little appreciable mass loss is consistent with a bulk degradation mechanism. The greater change in M_n of the higher molecular weight polymer is attributed to the necessity for a greater number of ester bonds along the backbone to be cleaved in order to generate a water-soluble degradation product. Slow *in vitro* degradation of 150 kDa P(TMC-CL) with a similar molar ratio of CL:TMC as used in this study has been reported by Pego et al [332]. It was reasoned, however, that the low molecular weight used in this study would produce a greater degradation rate. These results indicate that there is a compromise between obtaining a low melting point polymer based on the use of TMC and CL, and an appreciable degradation rate.

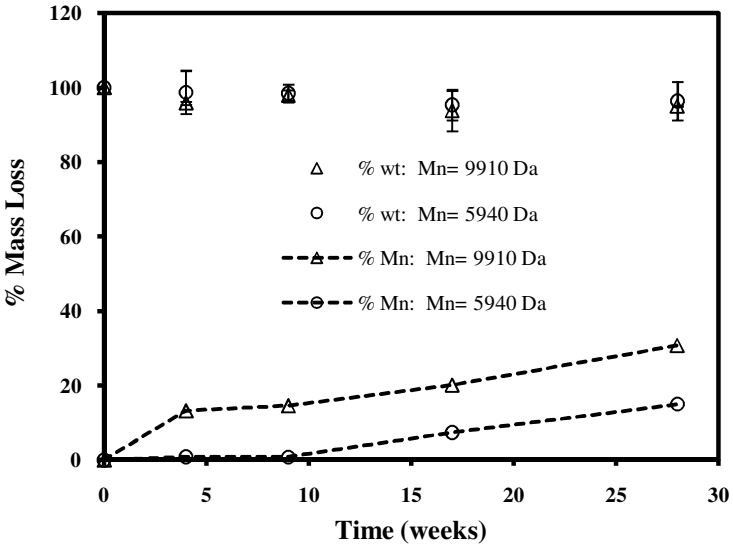

Figure 6. 5. Degradation in water at pH 7.4 of microspheres prepared using different molecular weight P(TMC-CL)$_2$-PEG expressed as percent mass loss and M_n decrease.

6.2.6. BMP-6 and TGF-β3 release studies

Since P(TMC-CL)$_2$-PEG microspheres with M_n of 9910 Da uniformly distributed in MGC gel, did not aggregate, and generated a nearly constant release profile, this copolymer was employed for individual encapsulation of BMP-6 and TGF-β3. The formulation of a mixed protein solid particle was similar to that used with lysozyme; 90% w/w trehalose and 10% w/w protein. The targeted doses of BMP-6 and TGF-β3 were based on the study by Diekman et al., who used 5 ng/day of each growth factor to promote chondrogenesis of adipose-derived stem cells [86]. According to the release profile of the model protein lysozyme at 2.5% particle loading in the microspheres and 5 mg microspheres loaded in the gel, the content of BMP-6 and TGF-β3 in the mixed protein particle was calculated to be less than 1% w/w to achieve the targeted dose. BSA was incorporated to both stabilize the growth factors and make up the remaining 10% w/w of the protein formulation. Both growth factors were initially formulated to be at 0.7% w/w in the lyophilized cake. Table 6.5 shows that the BMP-6 content (0.48% w/w) in

the mixed protein formulation after lyophilization was lower than that of TGF-β3 (0.81% w/w). It was likely that BMP-6 content was lower in the as-received lyophilized powder, resulting in the lower amount of BMP-6 in the lyophilized cake. The encapsulation efficiency and yield of BMP-6 loaded microspheres were higher than those obtained for TGF-β3 loaded microspheres. A possible reason for the low encapsulation efficiency of TGF-β3 was that the average microsphere diameter obtained was smaller and thus led to higher number of particles dispersed on the periphery of microspheres and thus protein loss in ethanol extraction phase. In addition, smaller microspheres resulted in lower microsphere yield as the microspheres were collected on a 45 μm Tyler No 325 sieve.

Table 6. 5. The formulation of BMP-6 and TGF-β3 and manufacturing efficiency

Protein content	% w/w in lyophilized solid	Wt (ng)/ gel	% encapsulation efficiency	% microsphere yield
BMP-6	0.48	472	77.9 ± 16.8	66.5
BSA	8.6		79.3 ± 15.8	
TGFβ-3	0.81	294	25.6 ± 4.6	45.5
BSA	8.4		50.2 ± 10.4	

The release profiles of BMP-6 and TGF-β3 along with BSA are shown in Figures 6.6A and 6.6B. The release of BMP-6 was more sustained than that of the incorporated BSA; BMP-6 was continuously released for 60 days, while BSA release only lasted for 20 days (Figure 6.6A). The release period of BMP-6 and BSA was preceded by initial bursts of 14.3% and 23.6%, respectively. For TGF-β3 loaded microspheres, both TGF-β3 and BSA generated identical release kinetics (Figure 6.6B). A sustained release period for TGF-β3 and BSA lasted for 20 days before the release slowed down. The release of TGF-β3 and BSA were initiated with similar bursts of 32.9% and 33.3%, respectively. Although the total amount of TGF-β3 loaded in the

microspheres was one third less than that of BMP-6, the release of TGF-β3 was faster. As a result, both BMP-6 and TGF-β3 were released at an average of approximately 5 ng/day for 20 days after the initial burst before the release profiles deviated (Figure 6.6C).

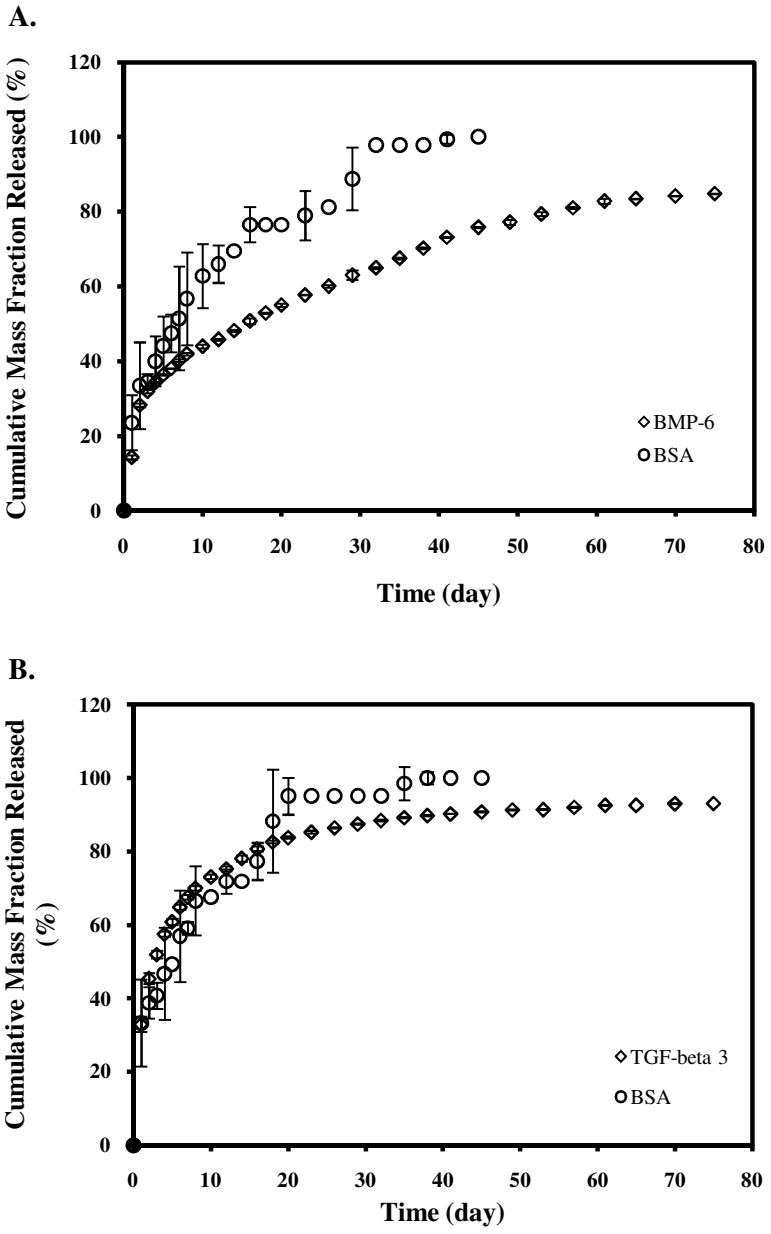

C.

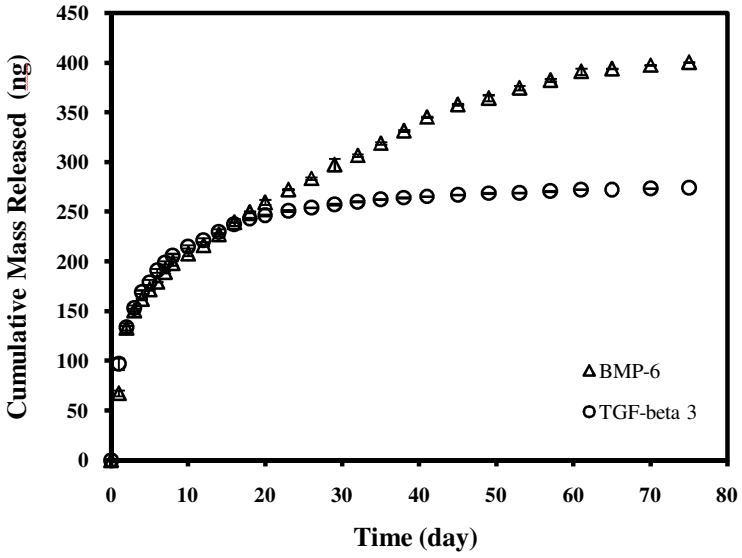

Figure 6. 6. Cumulative mass fraction released of (A) BMP-6 and BSA, (B) TGF-β3 and BSA encapsulated in 9910-Da P(TMC-CL)$_2$-PEG microspheres, and (C) comparative cumulative mass of BMP-6 and TGF-β3 released.

The release profiles of both growth factors and bulking agent BSA are compared to that of lysozyme in Figure 6.7, while the isoelectic point (pI) and M_n of each protein are listed in Table 6.6. Since the P(TMC-CL)$_2$-PEG copolymer employed for encapsulating the microspheres was the same, the physical properties of the proteins contributed to their different release kinetics. The pI values of BSA and TGF-β3 are both below 7, and thus they carry a net negative charge under the release conditions, and they both generated similar release profiles. In contrast, the release of BMP-6 and lysozyme were maintained for a longer period of time and the pI values of both proteins are above 7, and thus they carry a net positive charge. Moreover, the M_n of the proteins did not affect the release rates. As the hydrogel used is positively charged, this difference in release rate cannot be attributed to differences in protein interaction with the MGC following release from the microspheres. It is possible that the positively charged proteins are interacting with the P(TMC-CL)$_2$-PEG, or its negatively charged degradation products, which are likely present at the protein solution/polymer interface, despite the slow degradation rate of the

polymer. Thus, protein adsorption followed by desorption may be slowing down the release of positively charged proteins within the microspheres.

Table 6. 6. The physical properties of the proteins examined

Protein	pI	M_n (kDa)
Lysozyme	11.3 [333]	14.3 [328]
BMP-6	8.6 [329]	26.2 [329]
TGF-β3	6.5 [330]	25.0 [330]
BSA	4.9 [334]	66.4 [335]

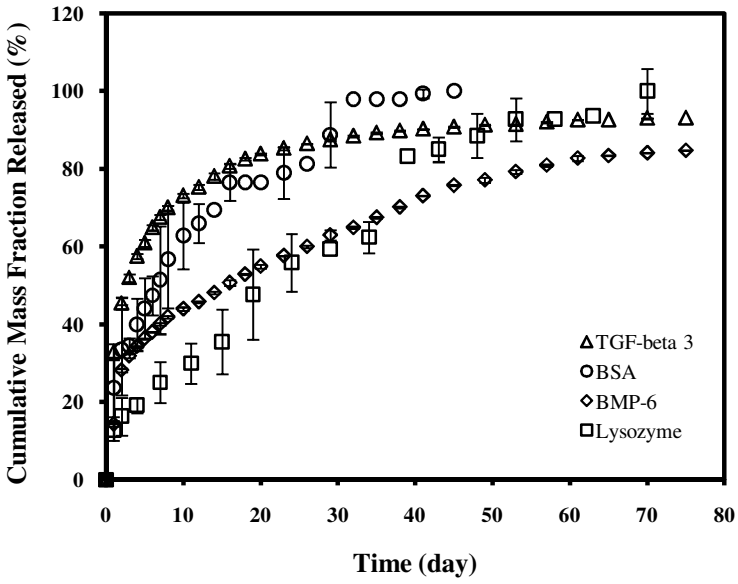

Figure 6. 7. Comparative release profiles of the different proteins released from 9910-Da P(TMC-CL)$_2$-PEG microspheres embedded in MGC gels.

The stability of the released therapeutic protein is an important parameter to determine the effectiveness of the delivery approach. The bioactivities of BMP-6 and TGF-β3 released from P(TMC-CL)$_2$-PEG microspheres were analyzed using cell-based assays. BMP-6 and TGF-β3 were 78.6 ± 1.0% and 89.1 ± 12.3% bioactive as compared to as-received growth factor, respectively, after being lyophilized with trehalose and BSA and vortexed in polymer solvent

(DCM) for 10 min. The bioactivities of the released BMP-6 and TGF-β3 were normalized to these values. Figure 6.8 shows that the average bioactivity of BMP-6 and TGF-β3 over the release period remained high.

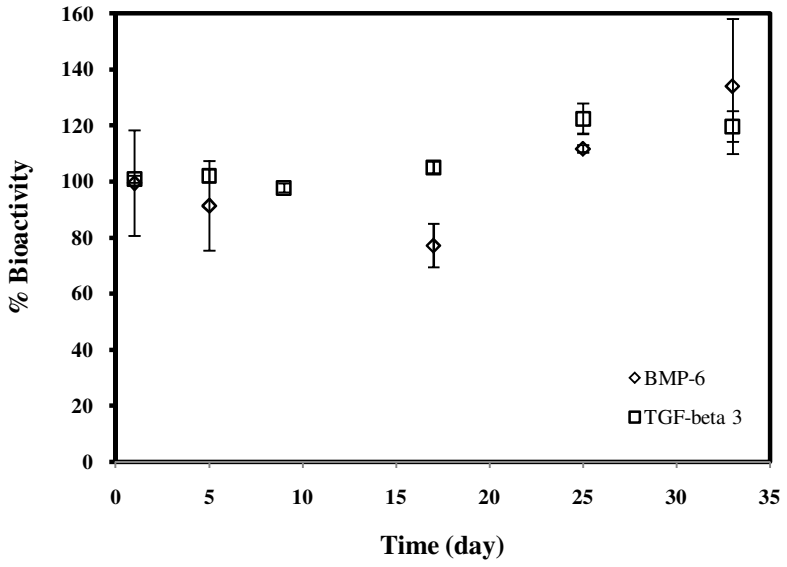

Figure 6. 8. Bioactivities of BMP-6 and TGF-β3 released from P(TMC-CL)$_2$-PEG microspheres (M_n= 9910 Da).

6.3. Conclusions

Triblock P(TMC-CL)$_2$-PEG copolymers can be used to form microspheres that are easily dispersible within a pregel solution, the microspheres have good handling characteristics, and are viscous liquids at body temperature and so may not elicit a strong inflammatory response if they escape into the synovial space. Protein release from these microspheres, embedded within a hydrogel delivery vehicle, can be prolonged and nearly linear when driven by osmotic effects. Protein release kinetics from the microspheres was influenced by the protein isoelectric point, with positively charged proteins releasing at a slower rate from the microspheres than negatively

charged proteins. This result is proposed to be due to positively charged proteins adsorbing to a greater extent on the surface of the P(TMC-CL)$_2$-PEG. Promisingly, this formulation approach delivered these proteins in a sustained manner, while maintaining the proteins in a highly bioactive state.

CHAPTER 7

GROWTH FACTOR DELIVERY FROM POLYMERIC MICROSPHERES IN A HYDROGEL MATRIX INDUCES ASC CHONDROGENESIS

7.1. Introduction

Cell adhesive peptide RGD grafting to *N*-methacrylate glycol chitosan (MGC) backbone is essential to ensure high viability of adipose-derived stem cells (ASC) in photoencapsulated MGC gel. In addition, a localized delivery of chondrogenic growth factor in MGC hydrogel is required to direct ASC to chondrocyte lineage. It has been demonstrated that a release rate of 5 ng/day of Transforming Growth Factor-β3 (TGF-β3) and Bone Morphogenetic Protein-6 (BMP-6) beyond initial burst can be obtained from vicious liquid microspheres embedded within an MGC gel matrix.

Thus, the objective of this chapter was to assess whether ASC chondrogenesis could be enhanced with a localized, controlled delivery of BMP-6 and TGF-β3 loaded in P(TMC-CL)$_2$-PEG microspheres that were embedded in a photopolymerizable MGC gel. To determine whether the proposed approach was potentially useful, ASC were encapsulated within RGD-grafted MGC matrices and grown in static culture for 4 weeks. At specific times the cellularity and ECM composition (glycosaminoglycan (GAG), collagen type I and II) were quantitatively determined.

7.2. Results and Discussion

To determine whether the proposed approach for inducing chondrogenesis of the ASC *in situ* was feasible, samples comprised of MAGC-RGD gels incorporated with ASC and blank P(TMC-CL)$_2$-PEG microspheres without growth factor supply (negative control, Gel ID= No GF), with BMP-6 and TGF-β3 supplemented in media (positive control, Gel ID= GF media) and microspheres loaded with BMP-6 and TGF-β3 (Gel ID= GF microspheres) were compared. Figure 7.1A shows that the DNA content was similar for all sample conditions throughout the culture period, indicating an absence of ASC proliferation. The presence of BMP-6 and TGF-β3 in the culture (GF media and GF microspheres) did not induce ASC proliferation, whereas ASC encapsulated in RGD-grafted MGC gels without growth factor supply (No GF) have been demonstrated to only improve ASC viability without increasing cell number with time (Figure 5.7A and B). Nevertheless, non-proliferation does not necessarily decrease ASC capacity to differentiate within the gel.

The GAG content normalized to DNA (GAG/DNA) was higher for all samples on day 14 and 28, in comparison to day 0 (Figure 7.1B). The GAG/DNA amount was 17.7 ± 9.0, 30.9 ± 5.7, 34.1 ± 7.5 μg/μg on day 14, 14.7 ± 2.6, 16.2 ± 4.2, 22.8 ± 4.6 μg/μg on day 28 for No GF, GF media and GF microspheres samples, respectively, and 15.1 ± 3.2 μg/μg on day 0. The GAG/ DNA content was significantly higher for ASC stimulated with BMP-6 and TGF-β3 (GF media and GF microspheres samples) on day 14, in comparison to that of ASC without growth factor supplementation (No GF). However, the GAG/DNA was similar, regardless of the methods of growth factor administration (GF media and GF microspheres). Diekman et al. showed that GAG/ DNA content was similar to the control (chondrogenic media without growth factor and dexamethasone) when 5 ng/day of both TGF-β3 and BMP-6 were added to culture media of ASC encapsulated in alginate beads [86]. On the other hand, using a similar dose of combination

growth factors, ASC seeded in cartilage-derived matrix produced significantly higher GAG/ DNA, in comparison to the control (chondrogenic media supplemented with 100 nM dexamethasone) [86]. This result implies that ASC and scaffold interaction might have attributed to the degree of GAG synthesized by ASC. Furthermore, the study also demonstrated that GAG/DNA content was highly increased when high dose BMP-6 (250 ng/day) was added to the culture media of ASC encapsulated in alginate beads [86]. This suggests that the type of growth factor and its dose also influences GAG production by ASC.

Furthermore, the GAG/DNA content on day 28 was significantly higher for ASC induced with sustained delivery of BMP-6 and TGF-β3 (GF microspheres), when compared to those of ASC induced with soluble BMP-6 and TGF-β3 (GF media) and without growth factor stimulation (No GF). The results suggest that sustained delivery of BMP-6 and TGF-β3 was more effective in inducing ASC towards chondrogenesis. However, the GAG/DNA content was lower for all samples on day 28, in comparison to that on day 14. This might be attributed to the GAG loss in the culture media, instead of being retained within the gel.

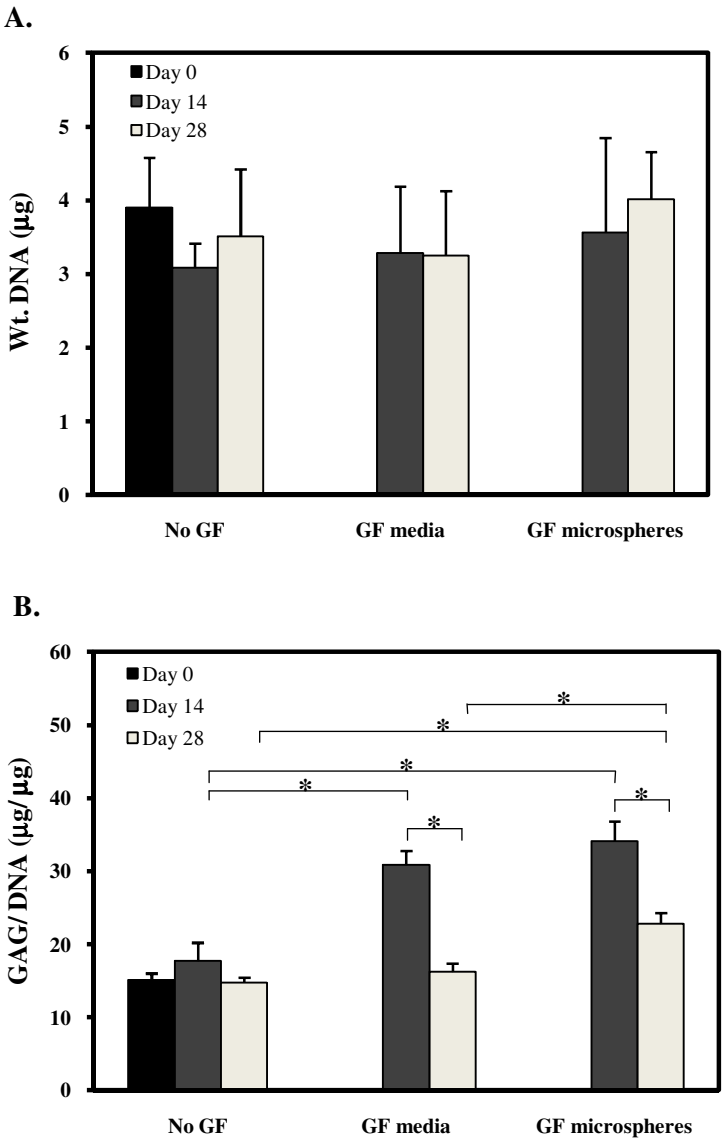

Figure 7. 1. (A) DNA content and (B) GAG normalized to DNA of encapsulated ASC in MAGC-RGD gel incorporated with blank P(TMC-CL)$_2$-PEG microspheres supplemented with no soluble growth factors (no GF), growth factors in media (GF media) and growth factor-loaded in polymeric microspheres (GF microspheres) (n= 4, *: p< 0.05).

As the ratio of collagen type II to type I normalized to DNA (Col II/ Col I/ DNA) is indicative of the production of hyaline-like cartilage and thus an indicator of chondrogenesis, the ratio of collagen type II to I normalized to DNA (Col II/ Col I/ DNA) content was quantified on day 14 and 28. Figure 7.2 shows that the ratios were significantly higher for all samples on day

28, in comparison to those on day 14. In addition, day 14 ratios were significantly higher for encapsulated ASC induced with growth factors released from embedded microspheres loaded with growth factors (GF microspheres: 0.0022 ± 0.0008 ng/ng/μg), in comparison with ASC induced with soluble growth factors added to the culture media (GF media: 0.0008 ± 0.0004 ng/ng/μg) and without growth factor (No GF: 0.0004 ± 0 ng/ng/μg). Previous results demonstrated that chondrogenesis of human bone marrow-derived stem cells (BMSC) seeded on RGD-immobilized alginate gels was inhibited initially (after 7 days) when induced with soluble TGF-β1 [336]. On the other hand, the chondrogenic induction was enhanced after 21 days when BMSC were seeded on a macroporous, RGD-grafted alginate scaffold [337]. Another study showed that cleavable RGD in photopolymerized PEG gels enhanced chondrogenesis of encapsulated BMSC based on the matrix production, in comparison to non-cleavable RGD gels after 21 days [119]. Similarly, it was demonstrated that large molecule chimeric RGD embedded in alginate beads enhanced chondrogenesis of encapsulated rat ASC in the presence of TGF-β3 [338], due to the release of the chimeric RGD from the scaffold. These findings were in contrast with the present study that showed that chondrogenesis of ASC encapsulated in MGC gels grafted with non-cleavable RGD was increased for ASC induced with BMP-6 and TGF-β3 (GF media and GF microspheres samples) at later time points (day 14 and 28). However, the results were not compared with a control of ASC incorporated in the gels without RGD grafting, which was not included in the study due to low ASC viability. In addition, the present study also demonstrated that the ratio of Col II/ Col I/ DNA for ASC in the gels without growth factor supply (No GF) was similar to that of encapsulated ASC induced with soluble growth factors (GF media) on day 28. This finding suggests that ASC without BMP-6 and TGF-β3 induction also underwent chondrogenesis, possibly by the influence of RGD peptide alone in the gel matrix. These disparities might be attributed to the fact that chondrogenesis of adult stem cells depends

on the types of chondrogenic growth factors employed, the chemical and mechanical properties of the scaffold and the source of the stem cells utilized.

ASC in scaffolds containing GF releasing microspheres had significantly higher Col II/ Col I/ DNA ratio than those in GF media samples on day 14, and slightly higher on day 28, but this difference was not statistically significant. It is reasoned that BMP-6 and TGF-β3 released from microspheres with the gel was in closer proximity to ASC, while the growth factors supplemented in culture media might require more time to diffuse to the gel matrix and bind to the membrane receptors of ASC. Nevertheless, the ratio on day 28 was not significantly higher and this might be attributed to the slow down in release of TGF-β3 from microspheres after day 20 (Figure 6.6C), resulting in the release of BMP-6 alone. It is speculated that the rate of BMP-6 release alone at 5 ng/ day after day 20 was not sufficient to induce further ASC chondrogenesis. To date, studies that used dual growth factors of BMP-6 and TGF-β3 with a dose of 5 ng/day performed the analysis of ASC chondrogenesis by immunohistochemical staining and gene expression on days 28 and 42 [86, 339]. Regardless of the slow down in release of TGF-β3, the slight increase of the ratio on day 28 suggests that ASC did not de-differentiate. Furthermore, the controlled release of BMP-6 and TGF-β3 from microspheres on both analysis days (14 and 28) suggested that ASC were directed to a chondrocyte-like lineage and would differentiate to chondrocytes when BMP-6 and TGF-β3 were both continuously released from microspheres for an extended period of time. In the future, the dose of these growth factors should be varied to optimize chondrogenesis.

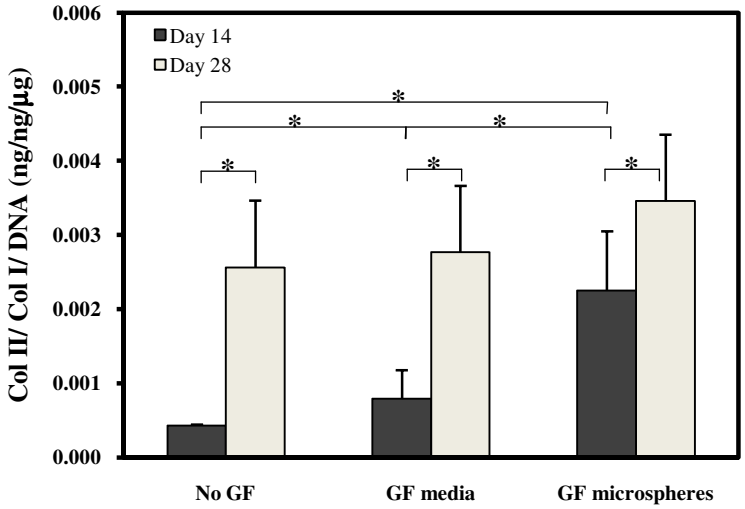

Figure 7. 2. Ratio of collagen type II to collagen type I normalized to DNA content in MAGC-RGD gels incorporated with ASC and blank P(TMC-CL)$_2$-PEG microspheres supplemented with no soluble growth factor (no GF), growth factor fed in media (GF media) and growth factor-loaded in polymeric microspheres (GF micropsheres) (n= 4, *: p< 0.05).

7.3. Conclusions

P(TMC-CL)$_2$-PEG microspheres containing BMP-6 and TGF-β3 were embedded along with ASC in MAGC-RGD *in situ* gels to induce chondrogenesis. The ASC did not proliferate throughout the 28-day culture period; however, the ASC produced significantly higher amount of GAG normalized to DNA, when induced with BMP-6 and TGF-β3 loaded in microspheres. The chondrogenesis indication from the Col II/ Col I/ DNA ratio implied that ASC were directed towards the chondrocyte phenotype more rapidly when induced with a sustained and local release of BMP-6 and TGF-β3 from the embedded microspheres. Thus, localized co-delivery of BMP-6 and TGF-β3 loaded in microspheres for ASC chondrogenesis MAGC-RGD gel matrix may be promising for *in vivo* applications and may be an applicable design for clinical setting wherein implantation is done in a non-invasive manner.

CHAPTER 8

SUMMARY AND CONCLUSIONS

The co-delivery of ASC and P(TMC-CL)$_2$-PEG microspheres loaded with BMP-6 and TGF-β3 in a photocrosslinked MGC gel was able to induce ASC chondrogenesis. This design strategy is advantageous since the MGC pre-gel solution is injectable and thus can be applied through minimally invasive means so that the chondrogenesis can be induced at the defect site.

The initial polymer glycol chitosan and glycol chitosan grafted with *N*-methacrylate (MGC) were well-characterized in ^{1}H and ^{13}C NMR. The reaction kinetics of *N*-methacrylate grafting onto glycol chitosan backbone were dependent on the reaction time and mol ratio of glycidyl methacrylate to amine group in glycol chitosan. The number average molecular weight (M_n) of glycol chitosan was 96.3 kDa and the M_n of MGC was increased with increasing degree of *N*-methacrylation. Without cell incorporation, the optimum photocrosslinking conditions of MGC gel in water were determined to be 73 to 102 mW/cm^2 of UV light intensities for 5 minutes. In addition, the thickness of the gel should not be more than 4 mm to achieve a sol content below 5%. The Young's modulus of the MGC gel in water reached a maximum value of approximately 0.35 MPa at 13.6% *N*-methacrylation. The equilibrium water content of MGC constructs was above 80%, regardless of percent DOS, thickness of the constructs, light intensities and time exposure to UV light. The *in vitro* degradation rate of MGC constructs was slow and dependent on the degree of crosslinking.

The MGC prepolymer with ASC incorporation could be photopolymerized at room temperature to form a hydrogel construct at low I2959 photoinitiator concentration (0.5 mg/ mL) and light intensity (10.8 mW/cm^2) with short duration time (3 min). In addition, medium serum was used as the aqueous solution to form MGC gels incorporated with ASC and the gels had a sol

content of 30%, regardless of the degree of *N*-methacrylation. The concentrations of MGC consistent with the sol content of the gels formed and I2959 concentrations up to 1 mg/mL were not cytotoxic to ASC. ASC viability was low and remained constant for 7 days, when encapsulated in MGC gels prepared with high degree of *N*-methacrylation and without RGD grafted peptide. The cell number decreased with time for all gels and the least number of cells was retained in gels prepared with prepolymers of a low degree of *N*-methacrylation. The crosslinking density and thus stiffness of the gel determined the viability and number of cells retained in the gels; higher gel stiffness resulted in increased cell viability and number with time. In the presence of grafted RGD peptide in the gel, the encapsulated ASC were highly viable (~90%) and their number remained constant for 14 days.

For growth factor delivery vehicle, triblock P(TMC-CL)$_2$-PEG copolymers were synthesized to have M_n of about 10,000 Da and a melting range close to physiological temperature. These copolymers were employed to fabricate microspheres with average diameters below 100 μm. A model protein lysozyme was mixed with trehalose and encapsulated into the fabricated polymeric microspheres using a low-temperature electrospray technique. Particles containing 90% w/w trehalose co-lyophilized with lysozyme allowed a sustained release of lysozyme from the microspheres in the gel. A low loading (2.5% w/w) of mixed trehalose/protein particles in the microspheres decreased the initial burst. Varying the microsphere loading in the gel did not affect the release kinetics. High molecular weight P(TMC-CL)$_2$-PEG (M_n= 9910 Da) microspheres in the gel were uniformly distributed, did not aggregate and generated a consistent and linear lysozyme release profile. Hence, the chondrogenic growth factors (BMP-6 and TGF-β3) in the presence of stabilizing BSA and 90% w/w trehalose were individually encapsulated in microspheres made from this polymer. The BMP-6 was released at similar rates as was lysozyme, while TGF-β3 and BSA generated similar release kinetics. The protein release rate was dependent on the protein charge, with positively charged proteins

releasing at a slower rate from the microspheres than negatively charged proteins. Both growth factors released from P(TMC-CL)$_2$-PEG microspheres were highly bioactive.

Finally, P(TMC-CL)$_2$-PEG microspheres containing BMP-6 and TGF-β3 were embedded along with ASC in RGD-grafted MGC gels with the objective of assessing whether local release of these growth factors could induce differentiation of the ASC towards chondrocytes. The ASC did not proliferate throughout the 28 day culture period examined. ASC induced with soluble BMP-6 and TGF-β3 supplemented in media as well as loaded in microspheres produced similar amount of GAG normalized to DNA (GAG/DNA) at 14 days. However, the GAG/DNA content was significantly higher at 28 days for ASC stimulated with growth factors loaded in micropsheres. The chondrogenesis indication from Col II/ Col I/ DNA ratio suggested that ASC was slightly better directed towards chondrocyte-like when induced with sustained released of BMP-6 and TGF-β3 from microspheres. Thus, localized co-delivery of BMP-6 and TGF-β3 loaded in microspheres for ASC chondrogenesis MAGC-RGD gel matrix showed promising *in vivo* applications and more applicable design for clinical settings in a non-invasive manner.

Recommendations for future work:

1. *In vitro* degradation rate of MGC gel can be improved by grafting enzyme-degrading molecules on MGC prepolymer. The other approach is to study whether chondrocytes can degrade the MGC backbone to avoid enzyme-degrading molecules incorporation. The degradation of hydrogels has been demonstrated to improve the extracellular matrix (ECM) deposition within the gel [340, 341]. It was reasoned that hydrogel degradation allows more space for cells to deposit the newly synthesized ECM within the gel matrix. In addition, native tissues are always undergoing re-structuring, such as matrix degradation and synthesis

simultaneously. Therefore, the gel's degradation mimics the environment of native cartilage. This would improve ECM deposition and thus tissue regeneration.

2. Increasing the grafting density of RGD in MGC prepolymer might enhance ASC proliferative activity [342]. This study may also confirm whether ASC cellularity is dependant to RGD grafting density or inactive cell cycle following photopolymerization. In addition, increasing RGD has also been shown to enhance chondrogenesis of human MSC in a dose-dependent manner [343]. Further, an increase number of RGD molecules on MGC prepolymer might reduce ASC settling to the bottom of the gels and better retain ASC in the gel since the integrins of ASC might immediately bind to RGD during photocrosslinking process.

3. Another route of grafting RGD peptide on the MGC backbone should be employed without a competing reaction to obtain high yield of RGD grafting. The current grafting method was achieved by reacting the thiol molecules of cysteine amino acid in RGD sequence with *N*-acrylamide group of MGC polymer (Figure 5.6). Although thiol group in RGD is more highly reactive towards *N*-acrylamide molecules grafted in MGC, the amine group in MGC can also react with *N*-acrylamide group at slower rate. As a result, the availability of *N*-acrylamide groups of MGC may be reduced to react with the thiol group in RGD. One of the possible chemical approaches for RGD grafting on MGC backbone is to use bifunctional crosslinker, such as sulfosuccinimidyl-4-(*N*-maleimidomethyl)cyclohexane-1-carboxylate. It consists of amine reactive *N*-hydroxysuccinimide (NHS ester) to react with primary amine of MGC and sulfhydryl-reactive maleimide group that can react with thiol of cysteine amino acid in RGD peptide.

4. The loading of TGF-β3 in microspheres should be lowered to reduce the initial burst and thus prolong the release period. The prolonged release of TGF-β3, along with BMP-6, would continuously induce ASC chondrogenesis.

5. Varying the concentration of BMP-6 and TGF-β3 for optimal ASC differentiation towards chondrocyte lineage in MGC gel should be explored.

6. Gene expressions should be examined to confirm ASC chondrogenesis using semi-quantitative RT-PCR and qualitative immunohistochmeistry staining techniques.

REFERENCES

[1] T.D. Bell, Y.H. An, R.J. Friedman, Repair of Articular Cartilage Defects Using Biomaterials and Tissue Engineering Methods, Marcel Dekker, Inc., New York, NY, 2000.

[2] J.A. Buckwalter, H.J. Mankin, Articular cartilage .2. Degeneration and osteoarthrosis, repair, regeneration, and transplantation. Journal of Bone and Joint Surgery-American Volume 79A(4) (1997) 612-632.

[3] HCUP Nationwide Inpatient Sample (NIS). Healthcare Cost and Utilization Project (HCUP). Available at http://hcup-us.ahrq.gov/reports/statbriefs/sb34.jsp.

[4] V.C.A. Vacanti J.P., The History and Scope of Tissue Engineering, Academic Press, San Diego, CA, 2000.

[5] J. Schiller, B. Fuchs, K. Arnold, The molecular organization of polymers of cartilage in health and disease. Current Organic Chemistry 10(14) (2006) 1771-1789.

[6] D.R. Eyre, Collagen structure and function in articular cartilage: metabolic changes in the development of osteoarthritis. In Osteoarthritic Disorders, The American Academy of Orthopaedic Surgeons, Rosemont, Illinois, 1995.

[7] D.R. Eyre, J.J. Wu, P. Woods, Cartilage-specific collagens. Structural studies. In Articular Cartilage and Osteoarthritis, Raven Press, New York, 1992.

[8] L.J. Sandell, Molecular biology of collagens in normal and osteoarthritic cartilage. In Osteoarthritic Disorders, The American Academy of Orthopaedic Surgeons, Rosemont, Illinois, 1995.

[9] P. Bruckner, M. Mendler, B. Steinmann, S. Huber, K.H. Winterhalter, The structure of human collagen type-IX and its organization in fetal and infant cartilage fibrils. Journal of Biological Chemistry 263(32) (1988) 16911-16917.

[10] M. Diab, J.J. Wu, D.R. Eyre, Collagen type IX from human cartilage: A structural profile of intermolecular cross-linking sites. Biochemical Journal 314 (1996) 327-332.

[11] H. Hagiwara, C. Schroterkermani, H.J. Merker, Localization of collagen type-VI in articular cartilage of young and adult mice. Cell and tissue research 272(1) (1993) 155-160.

[12] J. Marcelino, C.A. McDevitt, Attachment of articular-cartilage chondrocytes to the tissue form of type-VI collagen. Biochimica Et Biophysica Acta-Protein Structure and Molecular Enzymology 1249(2) (1995) 180-188.

[13] J.A. Buckwalter, H.J. Mankin, Articular cartilage .1. Tissue design and chondrocyte-matrix interactions. Journal of Bone and Joint Surgery-American Volume 79A(4) (1997) 600-611.

[14] T.E. Hardingham, A.J. Fosang, J. Dudhia, Aggrecan, the chondroitin/keratan sulfate proteoglycan from cartilage. In Articular Cartilage and Osteoarthritis, Raven Press, New York, 1992.

[15] L.C. Rosenberg, Structure and function of dermatan sulfate proteoglycans in articular cartilage. In Articular Cartilage and Osteoarthritis, Raven Press, New York, 1992.

[16] L.C. Rosenberg, J.A. Buckwalter, Cartilage proteoglycans. In Articular Cartilage Biochemistry, Raven Press, New York, 1986.

[17] P.J. Roughley, E.R. Lee, Cartilage proteoglycans- structure and potential functions. Microscopy Research and Technique 28(5) (1994) 385-397.

[18] J.S. Temenoff, A.G. Mikos, Review: tissue engineering for regeneration of articular cartilage. Biomaterials 21(5) (2000) 431-440.

[19] X. Chevalier, N. Groult, B. Largetpiet, L. Zardi, W. Hornebeck, Tenascin distribution in articular-cartilage from normal subjects and from patients with osteoarthritis and rheumatoid-arthritis. Arthritis and Rheumatism 37(7) (1994) 1013-1022.

[20] T. Hayashi, E. Abe, H.E. Jasin, Fibronectin synthesis in superficial and deep layers of normal articular cartilage. Arthritis and Rheumatism 39(4) (1996) 567-573.

[21] D.K. Heinegard, E.R. Pimentel, Cartilage matrix proteins. In Articular Cartilage and Osteoarthritis, Raven Press, New York, 1992.

[22] J. Mollenhauer, J.A. Bee, M.A. Lizarbe, K. Vondermark, Role of anchorin-CII, a 31,000-mol-wt membrane-protein, in the interaction of chondrocytes with type-II collagen. Journal of Cell Biology 98(4) (1984) 1572-1579.

[23] J.A. Buckwalter, E.B. Hunziker, L.C. Rosenberg, R.D. Coutts, M.E. Adams, D.R. Eyre, Articular cartilage. Composition and structure. In Injury and Repair of the Musculoskeletal Soft Tissues, The American Academy of Orthopaedic Surgeons, Park Ridge, Illinois, 1988.

[24] V.C. Mow, M.P. Rosenwasser, Articular cartilage. Biomechanics. In Injury and Repair of the Musculoskeletal Soft Tissues, The American Academy of Orthopaedic Surgeons, Park Ridge, Illinois, 1988.

[25] V. Roth, V.C. Mow, The intrinsic tensile behavior of the matrix of bovine articular-cartilage and its variation with age. Journal of Bone and Joint Surgery-American Volume 62(7) (1980) 1102-1117.

[26] B. Dozin, M. Malpeli, L. Camardella, R. Cancedda, A. Pietrangelo, Response of young, aged and osteoarthritic human articular chondrocytes to inflammatory cytokines: molecular and cellular aspects. Matrix Biology 21(5) (2002) 449-459.

[27] D. Nesic, R. Whiteside, M. Brittberg, D. Wendt, I. Martin, P. Mainil-Varlet, Cartilage tissue engineering for degenerative joint disease. Advanced Drug Delivery Reviews 58(2) (2006) 300-322.

[28] S. Hashimoto, K. Takahashi, D. Amiel, R.D. Coutts, M. Lotz, Chondrocyte apoptosis and nitric oxide production during experimentally induced osteoarthritis. Arthritis and Rheumatism 41(7) (1998) 1266-1274.

[29] H.A. Kim, Y.J. Lee, S.C. Seong, K.W. Choe, Y.W. Song, Apoptotic chondrocyte death in human osteoarthritis. Journal of Rheumatology 27(2) (2000) 455-462.

[30] F.H. Gannon, L. Sokoloff, Histomorphometry of the aging human patella: histologic criteria and controls. Osteoarthritis Cartilage 7(2) (1999) 173-181.

[31] E.B. Hunziker, Articular cartilage repair: basic science and clinical progress. A review of the current status and prospects. Osteoarthritis Cartilage 10(6) (2002) 432-463.

[32] M. Brittberg, A. Lindahl, A. Nilsson, C. Ohlsson, O. Isaksson, L. Peterson, Treatment of deep cartilage defects in the knee with autologous chondrocyte transplantation. New England Journal of Medicine 331(14) (1994) 889-895.

[33] M. Brittberg, L. Peterson, E. Sjogren-Jansson, T. Tallheden, A. Lindahl, Articular cartilage engineering with autologous chondrocyte transplantation - A review of recent developments. Journal of Bone and Joint Surgery-American Volume 85A (2003) 109-115.

[34] P. Behrens, T. Bitter, B. Kurz, M. Russlies, Matrix-associated autologous chondrocyte transplantation/implantation (MACT/MACI) - 5-year follow-up. Knee 13(3) (2006) 194-202.

[35] M.-H. Zheng, C. Willers, L. Kirilak, P. Yates, J. Xu, D. Wood, A. Shimmin, Matrix-induced autologous chondrocyte implantation (MACI): biological and histological assessment. Tissue Engineering 13(4) (2007) 737-746.

[36] M. Marcacci, E. Kon, S. Zaffagnini, G. Filardo, M. Delcogliano, M.P. Neri, F. Iacono, A.P. Hollander, Arthroscopic second generation autologous chondrocyte implantation. Knee Surgery Sports Traumatology Arthroscopy 15(5) (2007) 610-619.

[37] M. Marcacci, S. Zaffagnini, E. Kon, A. Visani, F. Iacono, I. Loreti, Arthroscopic autologous condrocyte transplantation: technical note. Knee Surgery Sports Traumatology Arthroscopy 10(3) (2002) 154-159.

[38] G.J.V.M. van Osch, M. Brittberg, J.E. Dennis, Y.M. Bastiaansen-Jenniskens, R.G. Erben, Y.T. Konttinen, F.P. Luyten, Cartilage repair: past and future - lessons for regenerative medicine. Journal of Cellular and Molecular Medicine 13(5) (2009) 792-810.

[39] J. Malda, C.G. Frondoza, Microcarriers in the engineering of cartilage and bone. Trends Biotechnol. 24(7) (2006) 299-304.

[40] X. Guo, C. Wang, C. Duan, M. Descamps, Q. Zhao, L. Dong, S. Lu, K. Anselme, J. Lu, Y.Q. Song, Repair of osteochondral defects with autologous chondrocytes seeded onto bioceramic scaffold in sheep. Tissue Engineering 10(11/12) (2004) 1830-1840.

[41] C.J. Hunter, M.E. Levenston, Maturation and integration of tissue-engineered cartilages within an in vitro defect repair model. Tissue Engineering 10(5-6) (2004) 736-746.

[42] E. Tognana, F. Chen, R.F. Padera, H.A. Leddy, S.E. Christensen, F. Guilak, G. Vunjak-Novakovic, L.E. Freed, Adjacent tissues (cartilage, bone) affect the functional integration of engineered calf cartilage in vitro. Osteoarthritis and Cartilage 13(2) (2005) 129-138.

[43] C.W. Archer, S. Redman, I. Khan, J. Bishop, K. Richardson, Enhancing tissue integration in cartilage repair procedures. Journal of Anatomy 209(4) (2006) 481-493.

[44] A.P. Hollander, S.C. Dickinson, T.J. Sims, P. Brun, R. Cortivo, E. Kon, M. Marcacci, S. Zanasi, A. Borrione, C. De Luca, A. Pavesio, C. Soranzo, G. Abatangelo, Maturation of tissue engineered cartilage implanted in injured and osteoarthritic human knees. Tissue Engineering 12(7) (2006) 1787-1798.

[45] D.E.T. Shepherd, B.B. Seedhom, The 'instantaneous' compressive modulus of human articular cartilage in joints of the lower limb. Rheumatology 38(2) (1999) 124-132.

[46] A. Thambyah, A. Nather, J. Goh, Mechanical properties of articular cartilage covered by the meniscus. Osteoarthritis and Cartilage 14(6) (2006) 580-588.

[47] J. Raghunath, H.J. Salacinski, K.M. Sales, P.E. Butler, A.M. Seifalian, Advancing cartilage tissue engineering: the application of stem cell technology. Current Opinion in Biotechnology 16(5) (2005) 503-509.

[48] B. Obradovic, I. Martin, R.F. Padera, S. Treppo, L.E. Freed, G. Vunjak-Novakovic, Integration of engineered cartilage. Journal of Orthopaedics Research 19(6) (2001) 1089-1097.

[49] P.D. Benya, J.D. Shaffer, Dedifferentiated chondrocytes reexpress the differentiated collagen phenotype when cultured in agarose gels. Cell 30(1) (1982) 215-224.

[50] F. Dell'Accio, C. De Bari, F.P. Luyten, Molecular markers predictive of the capacity of expanded human articular chondrocytes to form stable cartilage in vivo. Arthritis and Rheumatism 44(7) (2001) 1608-1619.

[51] K. Vondermark, V. Gauss, H. Vondermark, P. Muller, Relationship between cell-shape and type of collagen synthesized as chondrocytes lose their cartilage phenotype in culture. Nature 267(5611) (1977) 531-532.

[52] M. Kayakabe, S. Tsutsumi, H. Watanabe, Y. Kato, K. Takagishi, Transplantation of autologous rabbit BM-derived mesenchymal stromal cells embedded in hyaluronic acid gel sponge into osteochondral defects of the knee. Cytotherapy 8(4) (2006) 343-353.

[53] Y. Oshima, N. Watanabe, K.-i. Matsuda, S. Takai, M. Kawata, T. Kubo, Behavior of transplanted bone marrow-derived GFP mesenchymal cells in osteochondral defect as a simulation of autologous transplantation. Journal of Histochemistry and Cytochemistry 53(2) (2005) 207-216.

[54] M. Radice, P. Brun, R. Cortivo, R. Scapinelli, C. Battaliard, G. Abatangelo, Hyaluronan-based biopolymers as delivery vehicles for bone-marrow-derived mesenchymal progenitors. Journal of Biomedical Materials Research 50(2) (2000) 101-109.

[55] M.F. Pittenger, Multilineage potential of adult human mesenchymal stem cells. Science (Washington, D. C.) 285(5428) (1999) 665.

[56] S.W. O'Driscoll, Articular cartilage regeneration using periosteum. Clinical orthopaedics and related research(367) (1999) S186-S203.

[57] A.F. Steinert, S.C. Ghivizzani, A. Rethwilm, R.S. Tuan, C.H. Evans, U. Noth, Major biological obstacles for persistent cell-based regeneration of articular cartilage. Arthritis Research and Therapy 9(3) (2007).

[58] C. De Bari, F. Dell'Accio, F.P. Luyten, Failure of in vitro-differentiated mesenchymal stem cells from the synovial membrane to form ectopic stable cartilage in vivo. Arthritis and Rheumatism 50(1) (2004) 142-150.

[59] Y. Sakaguchi, I. Sekiya, K. Yagishita, T. Muneta, Comparison of human stem cells derived from various mesenchymal tissues - Superiority of synovium as a cell source. Arthritis and Rheumatism 52(8) (2005) 2521-2529.

[60] S. Shirasawa, I. Sekiya, Y. Sakaguchi, K. Yagishita, S. Ichinose, T. Muneta, In vitro chondrogenesis of human synovium-derived mesenchymal stem cells: Optimal condition and comparison with bone marrow-derived cells. Journal of Cellular Biochemistry 97(1) (2005) 84-97.

[61] P.A. Zuk, M. Zhu, H. Mizuno, J. Huang, J.W. Futrell, A.J. Katz, P. Benhaim, H.P. Lorenz, M.H. Hedrick, Multilineage cells from human adipose tissue: Implications for cell-based therapies. Tissue Engineering 7(2) (2001) 211-228.

[62] H.-Y. Cheung, K.-T. Lau, T.-P. Lu, D. Hui, A critical review on polymer-based bio-engineered materials for scaffold development. Composites, Part B: Engineering 38B(3) (2007) 291-300.

[63] V.L. Tsang, S.N. Bhatia, Three-dimensional tissue fabrication. Advanced Drug Delivery Reviews 56(11) (2004) 1635-1647.

[64] T.B.F. Woodfield, J.M. Bezemer, J.S. Pieper, C.A. van Blitterswijk, J. Riesle, Scaffolds for tissue engineering of cartilage. Critical Reviews in Eukaryotic Gene Expression 12(3) (2002) 209-236.

[65] R.R. Chen, D.J. Mooney, Polymeric growth factor delivery strategies for tissue engineering. Pharmaceutical Research 20(8) (2003) 1103-1112.

[66] B.V. Slaughter, S.S. Khurshid, O.Z. Fisher, A. Khademhosseini, N.A. Peppas, Hydrogels in Regenerative Medicine. Advanced Materials 21(32-33) (2009) 3307-3329.

[67] Y.J. An, J.A. Hubbell, Intraarterial protein delivery via intimally-adherent bilayer hydrogels. Journal of Controlled Release 64(1-3) (2000) 205-215.

[68] S.M. Chowdhury, J.A. Hubbell, Adhesion prevention with ancrod released via a tissue-adherent hydrogel. J. Surg. Res. 61(1) (1996) 58-64.

[69] S. Lu, W.F. Ramirez, K.S. Anseth, Photopolymerized, multilaminated matrix devices with optimized nonuniform initial concentration profiles to control drug release. Journal of Pharmaceutical Sciences 89(1) (2000) 45-51.

[70] H.G. Schild, Poly (N-isopropylacrylamide)- experiment, theory and application. Progress in Polymer Science 17(2) (1992) 163-249.

[71] H.K. Ju, S.Y. Kim, S.J. Kim, Y.M. Lee, pH/temperature-responsive semi-IPM hydrogels composed of alginate and poly(N-isopropylacrylamide). Journal of Applied Polymer Science 83(5) (2002) 1128-1139.

[72] C.-C. Lin, A.T. Metters, Hydrogels in controlled release formulations: Network design and mathematical modeling. Advanced Drug Delivery Reviews 58(12-13) (2006) 1379-1408.

[73] Y.S. Choi, M.W. Im, C.S. Kim, M.H. Lee, S.E. Noh, S.M. Lim, S.L. Kim, C.G. Cho, D.I. Kim, Chondrogenic differentiation of human umbilical cord blood-derived multilineage progenitor cells in atelocollagen. Cytotherapy 10(2) (2008) 165-173.

[74] U. Noth, L. Rackwitz, A. Heymer, M. Weber, B. Baumann, A. Steinert, N. Schutze, F. Jakob, J. Eulert, Chondrogenic differentiation of human mesenchymal stem cells in collagen type I hydrogels. J. Biomed. Mater. Res. Part A 83A(3) (2007) 626-635.

[75] A. Yokoyama, I. Sekiya, K. Miyazaki, S. Ichinose, Y. Hata, T. Muneta, In vitro cartilage formation of composites of synovium-derived mesenchymal stem cells with collagen gel. Cell and tissue research 322(2) (2005) 289-298.

[76] K. Yoneno, S. Ohno, K. Tanimoto, K. Honda, N. Tanaka, T. Doi, T. Kawata, E. Tanaka, S. Kapila, K. Tanne, Multidifferentiation potential of mesenchymal stem cells in three-dimensional collagen gel cultures. J. Biomed. Mater. Res. Part A 75A(3) (2005) 733-741.

[77] S.R. Frenkel, P.E. Di Cesare, Scaffolds for articular cartilage repair. Annals of Biomedical Engineering 32(1) (2004) 26-34.

[78] S.M. Mueller, S. Shortkroff, T.O. Schneider, H.A. Breinan, I.V. Yannas, M. Spector, Meniscus cells seeded in type I and type II collagen-GAG matrices in vitro. Biomaterials 20(8) (1999) 701-709.

[79] P. Angele, J. Abke, R. Kujat, H. Faltermeier, D. Schumann, M. Nerlich, B. Kinner, C. Englert, Z. Ruszczak, R. Mehrl, R. Mueller, Influence of different collagen species on physico-chemical properties of crosslinked collagen matrices. Biomaterials 25(14) (2004) 2831-2841.

[80] H.A. Awad, M.Q. Wickham, H.A. Leddy, J.M. Gimble, F. Guilak, Chondrogenic differentiation of adipose-derived adult stem cells in agarose, alginate, and gelatin scaffolds. Biomaterials 25(16) (2004) 3211-3222.

[81] M.S. Ponticiello, R.M. Schinagl, S. Kadiyala, F.P. Barry, Gelatin-based resorbable sponge as a carrier matrix for human mesenchymal stem cells in cartilage regeneration therapy. Journal of Biomedical Materials Research 52(2) (2000) 246-255.

[82] D. Pelaez, C.Y.C. Huang, H.S. Cheung, Cyclic compression maintains viability and induces chondrogenesis of human mesenchymal stem cells in fibrin gel scaffolds. Stem Cells and Development 18(1) (2009) 93-102.

[83] R. Frenkel Sally, E. Di Cesare Paul, Scaffolds for articular cartilage repair. Ann Biomed Eng 32(1) (2004) 26-34.

[84] R.P. Silverman, D. Passaretti, W. Huang, M.A. Randolph, M. Yaremchuk, Injectable tissue-engineered cartilage using a fibrin glue polymer. Plastic and Reconstructive Surgery 103(7) (1999) 1809-1818.

[85] R. Andriamanalijaona, E. Duval, M. Raoudi, S. Lecourt, J.T. Vilquin, J.P. Marolleau, J.P. Pujol, P. Galera, K. Boumediene, Differentiation potential of human muscle-derived cells towards chondrogenic phenotype in alginate beads culture. Osteoarthritis and Cartilage 16(12) (2008) 1509-1518.

[86] B.O. Diekman, C.R. Rowland, D.P. Lennon, A.I. Caplan, F. Guilak, Chondrogenesis of adult stem cells from adipose tissue and bone marrow: Induction by growth factors and cartilage-derived matrix. Tissue engineering. Part A 16(2) (2010) 523-533.

[87] K.W. Kavalkovich, R.E. Boynton, J.M. Murphy, F. Barry, Chondrogenic differentiation of human mesenchymal stem cells within an alginate layer culture system. In Vitro Cellular & Developmental Biology-Animal 38(8) (2002) 457-466.

[88] H.L. Ma, S.C. Hung, S.Y. Lin, Y.L. Chen, W.H. Lo, Chondrogenesis of human mesenchymal stem cells encapsulated in alginate beads. Journal of biomedical materials research. Part A 64A(2) (2003) 273-281.

[89] M.K. Majumdar, E. Wang, E.A. Morris, BMP-2 and BMP-9 promote chondrogenic differentiation of human multipotential mesenchymal cells and overcome the inhibitory effect of IL-1. Journal of Cellular Physiology 189(3) (2001) 275-284.

[90] I.H. Yang, S.H. Kim, Y.H. Kim, H.J. Sun, S.J. Kim, J.W. Lee, Comparison of phenotypic characterization between "alginate bead" and "pellet" culture systems as chondrogenic differentiation models for human mesenchymal stem cells. Yonsei Medical Journal 45(5) (2004) 891-900.

[91] A. Alshamkhani, R. Duncan, Radioiodination of alginate via covalently-bound tyrosinamide allows monitoring of its fate *in vivo*. J. Bioact. Compat. Polym. 10(1) (1995) 4-13.

[92] A.R. Finger, C.Y. Sargent, K.O. Dulaney, S.H. Bernacki, E.G. Loboa, Differential effects on messenger ribonucleic acid expression by bone marrow-derived human mesenchymal stem cells seeded in agarose constructs due to ramped and steady applications of cyclic hydrostatic pressure. Tissue Engineering 13(6) (2007) 1151-1158.

[93] C.Y.C. Huang, P.M. Reuben, G. D'Ippolito, P.C. Schiller, H.S. Cheung, Chondrogenesis of human bone marrow-derived mesenchymal stem cells in agarose culture. Anatomical Record Part a-Discoveries in Molecular Cellular and Evolutionary Biology 278A(1) (2004) 428-436.

[94] R. Stern, Hyaluronan catabolism: a new metabolic pathway. European Journal of Cell Biology 83(7) (2004) 317-325.

[95] X.Q. Jia, J.A. Burdick, J. Kobler, R.J. Clifton, J.J. Rosowski, S.M. Zeitels, R. Langer, Synthesis and characterization of in situ cross-linkable hyaluronic acid-based hydrogels with potential application for vocal fold regeneration. Macromolecules 37(9) (2004) 3239-3248.

[96] J.B. Leach, K.A. Bivens, C.W. Patrick, C.E. Schmidt, Photocrosslinked hyaluronic acid hydrogels: Natural, biodegradable tissue engineering scaffolds. Biotechnology and Bioengineering 82(5) (2003) 578-589.

[97] J.B. Leach, C.E. Schmidt, Characterization of protein release from photocrosslinkable hyaluronic acid-polyethylene glycol hydrogel tissue engineering scaffolds. Biomaterials 26(2) (2005) 125-135.

[98] Y.D. Park, N. Tirelli, J.A. Hubbell, Photopolymerized hyaluronic acid-based hydrogels and interpenetrating networks. Biomaterials 24(6) (2003) 893-900.

[99] J.A. Wieland, T.L. Houchin-Ray, L.D. Shea, Non-viral vector delivery from PEG-hyaluronic acid hydrogels. Journal of Controlled Release 120(3) (2007) 233-241.

[100] L. Flynn, G.D. Prestwich, J.L. Semple, K.A. Woodhouse, Adipose tissue engineering with naturally derived scaffolds and adipose-derived stem cells. Biomaterials 28(26) (2007) 3834-3842.

[101] X.Z. Shu, Y.C. Liu, F.S. Palumbo, Y. Lu, G.D. Prestwich, *In situ* crosslinkable hyaluronan hydrogels for tissue engineering. Biomaterials 25(7-8) (2004) 1339-1348.

[102] J.X. Zhang, A. Skardal, G.D. Prestwich, Engineered extracellular matrices with cleavable crosslinkers for cell expansion and easy cell recovery. Biomaterials 29(34) (2008) 4521-4531.

[103] G.D. Prestwich, D.M. Marecak, J.F. Marecek, K.P. Vercruysse, M.R. Ziebell, Controlled chemical modification of hyaluronic acid: synthesis, applications, and biodegradation of hydrazide derivatives. Journal of Controlled Release 53(1-3) (1998) 93-103.

[104] W. Knudson, B. Casey, Y. Nishida, W. Eger, K.E. Kuettner, C.B. Knudson, Hyaluronan oligosaccharides perturb cartilage matrix homeostasis and induce chondrocytic chondrolysis. Arthritis and Rheumatism 43(5) (2000) 1165-1174.

[105] A. Lahiji, A. Sohrabi, D.S. Hungerford, C.G. Frondoza, Chitosan supports the expression of extracellular matrix proteins in human osteoblasts and chondrocytes. Journal of biomedical materials research. Part A 51(4) (2000) 586-595.

[106] V.F. Sechriest, Y.J. Miao, C. Niyibizi, A. Westerhausen-Larson, H.W. Matthew, C.H. Evans, F.H. Fu, J.K. Suh, GAG-augmented polysaccharide hydrogel: A novel biocompatible and biodegradable material to support chondrogenesis. Journal of Biomedical Materials Research 49(4) (2000) 534-541.

[107] A. Di Martino, M. Sittinger, V. Risbud Makarand, Chitosan: a versatile biopolymer for orthopaedic tissue-engineering. Biomaterials 26(30) (2005) 5983-5990.

[108] J.K. Francis Suh, H.W.T. Matthew, Application of chitosan-based polysaccharide biomaterials in cartilage tissue engineering: a review. Biomaterials 21(24) (2000) 2589-2598.

[109] J.H. Cho, S.H. Kim, K.D. Park, M.C. Jung, W.I. Yang, S.W. Han, J.Y. Noh, J.W. Lee, Chondrogenic differentiation of human mesenchymal stem cells using a thermosensitive poly(N-isopropylacrylamide) and water-soluble chitosan copolymer. Biomaterials 25(26) (2004) 5743-5751.

[110] T. Chandy, C.P. Sharma, Chitosan--as a biomaterial. Biomaterials, artificial cells, and artificial organs 18(1) (1990) 1-24.

[111] D.L. Elbert, J.A. Hubbell, Conjugate addition reactions combined with free-radical cross-linking for the design of materials for tissue engineering. Biomacromolecules 2(2) (2001) 430-441.

[112] J. Elisseeff, K. Anseth, D. Sims, W. McIntosh, M. Randolph, R. Langer, Transdermal photopolymerization for minimally invasive implantation. Proceedings of the National Academy of Sciences of the United States of America 96(6) (1999) 3104-3107.

[113] J. Elisseeff, K. Anseth, D. Sims, W. McIntosh, M. Randolph, M. Yaremchuk, R. Langer, Transdermal photopolymerization of poly(ethylene oxide)-based injectable hydrogels for tissue-engineered cartilage. Plastic and Reconstructive Surgery 104(4) (1999) 1014-1022.

[114] C.D. Pritchard, T.M. O'Shea, D.J. Siegwart, E. Calo, D.G. Anderson, F.M. Reynolds, J.A. Thomas, J.R. Slotkin, E.J. Woodard, R. Langer, An injectable thiol-acrylate poly(ethylene glycol) hydrogel for sustained release of methylprednisolone sodium succinate. Biomaterials 32(2) 587-597.

[115] S.P. Zustiak, J.B. Leach, Characterization of protein release from hydrolytically degradable poly(ethylene glycol) hydrogels. Biotechnology and Bioengineering 108(1) (2011) 197-206.

[116] A.N. Buxton, J. Zhu, R. Marchant, J.L. West, J.U. Yoo, B. Johnstone, Design and characterization of poly(ethylene glycol) photopolymerizable semi-interpenetrating networks for chondrogenesis of human mesenchymal stem cells. Tissue Engineering 13(10) (2007) 2549-2560.

[117] S.Q. Liu, Q.A. Tian, J.L. Hedrick, J.H.P. Hui, P.L.R. Ee, Y.Y. Yang, Biomimetic hydrogels for chondrogenic differentiation of human mesenchymal stem cells to neocartilage. Biomaterials 31(28) 7298-7307.

[118] S.Q. Liu, Q.A. Tian, L. Wang, J.L. Hedrick, J.H.P. Hui, Y.Y. Yang, P.L.R. Ee, Injectable Biodegradable Poly(ethylene glycol)/RGD Peptide Hybrid Hydrogels for in vitro

Chondrogenesis of Human Mesenchymal Stem Cells. Macromolecular Rapid Communications 31(13) 1148-1154.

[119] C.N. Salinas, K.S. Anseth, The enhancement of chondrogenic differentiation of human mesenchymal stem cells by enzymatically regulated RGD functionalities. Biomaterials 29(15) (2008) 2370-2377.

[120] C.N. Salinas, B.B. Cole, A.M. Kasko, K.S. Anseth, Chondrogenic differentiation potential of human mesenchymal stem cells photoencapsulated within poly(ethylene glycol)-arginine-glycine-aspartic acid-serine thiol-methacrylate mixed-mode networks. Tissue Engineering 13(5) (2007) 1025-1034.

[121] A. Alhadlaq, J. Mao Jeremy, Tissue-engineered osteochondral constructs in the shape of an articular condyle. Journal of Bone and Joint Surgery-American Volume 87(5) (2005) 936-944.

[122] P. Banerjee, D.J. Irvine, A.M. Mayes, L.G. Griffith, Polymer latexes for cell-resistant and cell-interactive surfaces. Journal of Biomedical Materials Research 50(3) (2000) 331-339.

[123] S. VandeVondele, J. Voros, J.A. Hubbell, RGD-grafted poly-L-lysine-graft-(polyethylene glycol) copolymers block non-specific protein adsorption while promoting cell adhesion. Biotechnology and Bioengineering 82(7) (2003) 784-790.

[124] J.D. Kretlow, A.G. Mikos, From material to tissue: biomaterial development, scaffold fabrication, and tissue engineering. AICHE Journal 54(12) (2008) 3048-3067.

[125] E.S. Place, J.H. George, C.K. Williams, M.M. Stevens, Synthetic polymer scaffolds for tissue engineering. Chemical Society Reviews 38(4) (2009) 1139-1151.

[126] D. Puppi, F. Chiellini, A.M. Piras, E. Chiellini, Polymeric materials for bone and cartilage repair. Progress in Polymer Science 35(4) (2010) 403-440.

[127] D.W. Hutmacher, Scaffold design and fabrication technologies for engineering tissues--state of the art and future perspectives. Journal of Biomaterials Science, Polymer Edition 12(1) (2001) 107-124.

[128] E.J. Bergsma, F.R. Rozema, R.R.M. Bos, W.C. Debruijn, Foreign-body reactions to resorbable poly(L-lactidee) bone plates and screws used for the fixation of unstable zygomatic fractures. Journal of Oral Maxillofacial Surgery 51(6) (1993) 666-670.

[129] C. Martin, H. Winet, J.Y. Bao, Acidity near eroding polylactide-polyglycolide in vitro and in vivo in rabbit tibial bone chambers. Biomaterials 17(24) (1996) 2373-2380.

[130] W.-J. Li, R.S. Tuan, Polymeric scaffolds for cartilage tissue engineering. Macromolecular Symposia 227(Biological and Synthetic Polymer Networks and Gels) (2005) 65-75.

[131] J. Yang, A.R. Webb, G.A. Ameer, Novel citric acid-based biodegradable elastomers for tissue engineering. Advanced Materials 16(6) (2004) 511-516.

[132] Y. Kang, J. Yang, S. Khan, L. Anissian, G.A. Ameer, A new biodegradable polyester elastomer for cartilage tissue engineering. Journal of biomedical materials research. Part A 77A(2) (2006) 331-339.

[133] J. Butterworth, T.K. Walker, A study of the mechanism of the degradation of citric acid by *B. pyocyaneus*. Part I. Biochemical Journal 23(5) (1929) 926-935.

[134] K. Gorna, S. Gogolewski, Preparation, degradation, and calcification of biodegradable polyurethane foams for bone graft substitutes. Journal of biomedical materials research. Part A 67A(3) (2003) 813-827.

[135] Z. Li, L. Kupcsik, S.J. Yao, M. Alini, M.J. Stoddart, Chondrogenesis of human bone marrow mesenchymal stem cells in fibrin-polyurethane composites. Tissue engineering. Part A 15(7) (2009) 1729-1737.

[136] P. Bruin, G.J. Veenstra, A.J. Nijenhuis, A.J. Pennings, Design and synthesis of biodegradable poly(ester-urethane) elastomer networks composed of non-toxic building-blocks. Makromolekulare Chemie-Rapid Communications 9(8) (1988) 589-594.

[137] S. Grad, L. Kupcsik, K. Gorna, S. Gogolewski, M. Alini, The use of biodegradable polyurethane scaffolds for cartilage tissue engineering: potential and limitations. Biomaterials 24(28) (2003) 5163-5171.

[138] P.M. van der Kraan, P. Buma, T. van Kuppevelt, W.B. van den Berg, Interaction of chondrocytes, extracellular matrix and growth factors: relevance for articular cartilage tissue engineering. Osteoarthritis Cartilage 10(8) (2002) 631-637.

[139] H.L. Glansbeek, H.M. van Beuningen, E.L. Vitters, P.M. van der Kraan, W.B. van den Berg, Stimulation of articular cartilage repair in established arthritis by local administration of transforming growth factor-beta into murine knee joints. Lab Invest 78(2) (1998) 133-142.

[140] W.-N. Qi, S.P. Scully, Effect of type II collagen in chondrocyte response to TGF-b1 regulation. Experimental Cell Research 241(1) (1998) 142-150.

[141] Y. Zhu, A. Oganesian, D.R. Keene, L.J. Sandell, Type IIA procollagen containing the cysteine-rich amino propeptide is deposited in the extracellular matrix of prechondrogenic tissue and binds to TGF-b1 and BMP-2. Journal of Cell Biology 144(5) (1999) 1069-1080.

[142] R. Vasita, D.S. Katti, Growth factor-delivery systems for tissue engineering: a materials perspective. Expert Review of Medical Devices 3(1) (2006) 29-47.

[143] S.P. Baldwin, W.M. Saltzman, Materials for protein delivery in tissue engineering. Advanced Drug Delivery Reviews 33(1-2) (1998) 71-86.

[144] M.E. Nimni, Polypeptide growth factors: targeted delivery systems. Biomaterials 18(18) (1997) 1201-1225.

[145] B.T. Estes, A.W. Wu, F. Guilak, Potent induction of chondrocytic differentiation of human adipose-derived adult stem cells by bone morphogenetic protein 6. Arthritis & Rheumatism 54(4) (2006) 1222-1232.

[146] X.-B. Jin, Y.-S. Sun, K. Zhang, J. Wang, X.-D. Ju, S.-Q. Lou, Neocartilage formation from predifferentiated human adipose derived stem cells in vivo. Acta Pharmacologica Sinica 28(5) (2007) 663-671.

[147] Y. Wei, Y. Hu, R. Lv, D. Li, Regulation of adipose-derived adult stem cells differentiating into chondrocytes with the use of rhBMP-2. Cytotherapy 8(6) (2006) 570-579.

[148] D. Chin, G.M. Boyle, P.G. Parsons, W.B. Coman, What is transforming growth factor-beta (TGF-beta)? British Journal of Plastic Surgery 57(3) (2004) 215-221.

[149] A. Roberts, Transforming growth factor beta, Lippincott Williams & Wilkins, Philadelphia, 2000.

[150] J. Massague, B. Like, Cellular receptors for type-beta transforming growth-factor-ligand-binding and affinity labelling in human and rodent cell-lines. Journal of Biological Chemistry 260(5) (1985) 2636-2645.

[151] B. Johnstone, T.M. Hering, A.I. Caplan, V.M. Goldberg, J.U. Yoo, In vitro chondrogenesis of bone marrow-derived mesenchymal progenitor cells. Experimental Cell Research 238(1) (1998) 265-272.

[152] H.A. Awad, Y.D.C. Halvorsen, J.M. Gimble, F. Guilak, Effects of transforming growth factor beta 1 and dexamethasone on the growth and chondrogenic differentiation of adipose-derived stromal cells. Tissue Engineering 9(6) (2003) 1301-1312.

[153] F. Barry, R.E. Boynton, B. Liu, J.M. Murphy, Chondrogenic differentiation of mesenchymal stem cells from bone marrow: Differentiation-dependent gene expression of matrix components. Experimental Cell Research 268(2) (2001) 189-200.

[154] G.R. Erickson, J.M. Gimble, D.M. Franklin, H.E. Rice, H. Awad, F. Guilak, Chondrogenic potential of adipose tissue-derived stromal cells in vitro and in vivo. Biochemical and Biophysical Research Communications 290(2) (2002) 763-769.

[155] I. Huang Jerry, A. Zuk Patricia, F. Jones Neil, M. Zhu, H.P. Lorenz, H. Hedrick Marc, P. Benhaim, Chondrogenic potential of multipotential cells from human adipose tissue. Plast Reconstr Surg 113(2) (2004) 585-594.

[156] J.I. Huang, N. Kazmi, M.M. Durbhakula, T.M. Hering, J.U. Yoo, B. Johnstone, Chondrogenic potential of progenitor cells derived from human bone marrow and adipose tissue: A patient-matched comparison. Journal of Orthopaedic Research 23(6) (2005) 1383-1389.

[157] J.U. Yoo, T.S. Barthel, K. Nishimura, L. Solchaga, A.I. Caplan, V.M. Goldberg, B. Johnstone, The chondrogenic potential of human bone-marrow-derived mesenchymal progenitor cells. Journal of Bone and Joint Surgery-American Volume 80A(12) (1998) 1745-1757.

[158] H.M. van Beuningen, H.L. Glansbeek, P.M. van der Kraan, W.B. van den Berg, Osteoarthritis-like changes in the murine knee joint resulting from intra-articular transforming growth factor-beta injections. Osteoarthritis and Cartilage 8(1) (2000) 25-33.

[159] J. Pfeilschifter, Transforming growth factor beta, Springer-Verlag, Berlin, 1990.

[160] T. Hennig, H. Lorenz, A. Thiel, K. Goetzke, A. Dickhut, F. Geiger, W. Richter, Reduced chondrogenic potential of adipose tissue derived stromal cells correlates with an altered TGFbeta receptor and BMP profile and is overcome by BMP-6. Journal of Cellular Physiology 211(3) (2007) 682-691.

[161] D.R. Clemmons, Insulin-like growth factors: their binding proteins and growth regulation., Lippincott Williams & Wilkins, Philadelphia, 2000.

[162] R.F. Loeser, M.D. Todd, B.L. Seely, Prolonged treatment of human osteoarthritic chondrocytes with insulin-like growth factor-I stimulates proteoglycan synthesis but not proteoglycan matrix accumulation in alginate cultures. Journal of Rheumatology 30(7) (2003) 1565-1570.

[163] T.I. Morales, The role and content of endogenous insulin-like growth factor-binding proteins in bovine articular cartilage. Archives of Biochemistry and Biophysics 343(2) (1997) 164-172.

[164] H.P. Guler, J. Zapf, C. Schmid, E.R. Froesch, Insulin-like growth factor-1 and factor-2 in the in healthy man- estimations of half-lives and production-rates. Acta Endocrinologica 121(6) (1989) 753-758.

[165] A.H. Reddi, Role of morphogenetic proteins in skeletal tissue engineering and regeneration. Nature Biotechnology 16(3) (1998) 247-252.

[166] G.I. Im, Y.W. Shin, K.B. Lee, Do adipose tissue-derived mesenchymal stem cells have the same osteogenic and chondrogenic potential as bone marrow-derived cells? Osteoarthritis and Cartilage 13(10) (2005) 845-853.

[167] H.J. Kim, G.I. Im, Chondrogenic Differentiation of Adipose Tissue-Derived Mesenchymal Stem Cells: Greater Doses of Growth Factor are Necessary. Journal of Orthopaedic Research 27(5) (2009) 612-619.

[168] H.-J. Kim, G.-I. Im, Combination of transforming growth factor-beta2 and bone morphogenetic protein 7 enhances chondrogenesis from adipose tissue-derived mesenchymal stem cells. Tissue Engineering, Part A 15(7) (2009) 1543-1551.

[169] Y.-J. Kim, H.-J. Kim, G.-I. Im, PTHrP promotes chondrogenesis and suppresses hypertrophy from both bone marrow-derived and adipose tissue-derived MSCs. [Erratum to document cited in CA149:144296]. Biochemical and Biophysical Research Communications 376(1) (2008) 241.

[170] S. Koelling, J. Kruegel, M. Irmer, R. Path Jan, B. Sadowski, X. Miro, N. Miosge, Migratory chondrogenic progenitor cells from repair tissue during the later stages of human osteoarthritis. Cell stem cell 4(4) (2009) 324-335.

[171] B.O. Diekman, C.R. Rowland, D.P. Lennon, A.I. Caplan, F. Guilak, Chondrogenesis of Adult Stem Cells from Adipose Tissue and Bone Marrow: Induction by Growth Factors and Cartilage-Derived Matrix. Tissue Eng. Part A 16(2) 523-533.

[172] J. Sohier, L. Moroni, C. van Blitterswijk, K. de Groot, J.M. Bezemer, Critical factors in the design of growth factor releasing scaffolds for cartilage tissue engineering. Expert Opinion on Drug Delivery 5(5) (2008) 543-566.

[173] J. Elisseeff, W. McIntosh, K. Fu, T. Blunk, R. Langer, Controlled-release of IGF-I and TGF-b1 in a photopolymerizing hydrogel for cartilage tissue engineering. Journal of Orthopaedic Research 19(6) (2001) 1098-1104.

[174] H. Fan, H. Liu, R. Zhu, X. Li, Y. Cui, Y. Hu, Y. Yan, Comparison of chondral defects repair with in vitro and in vivo differentiated mesenchymal stem cells. Cell transplantation 16(8) (2007) 823-832.

[175] E.B. Hunziker, I.M.K. Driesang, E.A. Morris, Chondrogenesis in cartilage repair is induced by members of the transforming growth factor-beta superfamily. Clinical Orthopaedics Related Research(391) (2001) S171-S181.

[176] p.J.H. Kim S.E., Cho Y.W., Chung H., Jeong S.Y., Lee E.B., Kwon I.C., Porous chitosan scaffold containing microspheres loaded with transforming growth factor-beta1: implications for cartilage tissue engineering. Journal of controlled release : official journal of the Controlled Release Society 91 (2003) 365-374.

[177] J. Sohier, D. Hamann, M. Koenders, N. Cucchiarini, H. Madry, C. van Blitterswijk, K. de Groot, J.M. Bezemer, Tailored release of TGF-beta(1) from porous scaffolds for cartilage tissue engineering. International Journal of Pharmaceutics 332(1-2) (2007) 80-89.

[178] A. Kanematsu, S. Yamamoto, M. Ozeki, T. Noguchi, I. Kanatani, O. Ogawa, Y. Tabata, Collagenous matrices as release carriers of exogenous growth factors. Biomaterials 25(18) (2004) 4513-4520.

[179] H.D. Kim, R.F. Valentini, Retention and activity of BMP-2 in hyaluronic acid-based scaffolds in vitro. Journal of Biomedical Materials Research 59(3) (2002) 573-584.

[180] M. Yamamoto, Y. Ikada, Y. Tabata, Controlled release of growth factors based on biodegradation of gelatin hydrogel. Journal of Biomaterials Science-Polymer Edition 12(1) (2001) 77-88.

[181] J. Ziegler, U. Mayr-Wohlfart, S. Kessler, D. Breitig, K.P. Gunther, Adsorption and release properties of growth factors from biodegradable implants. Journal of Biomedical Materials Research 59(3) (2002) 422-428.

[182] H. Park, J.S. Temenoff, T.A. Holland, Y. Tabata, A.G. Mikos, Delivery of TGF-beta 1 and chondrocytes via injectable, biodegradable hydrogels for cartilage tissue engineering applications. Biomaterials 26(34) (2005) 7095-7103.

[183] O. Jeon, S.W. Kang, H.W. Lim, J.H. Chung, B.S. Kim, Long-term and zero-order release of basic fibroblast growth factor from heparin-conjugated poly(L-lactide-co-glycolide) nanospheres and fibrin gel. Biomaterials 27(8) (2006) 1598-1607.

[184] J.S. Park, D.G. Woo, H.N. Yang, H.J. Lim, H.-M. Chung, K.-H. Park, Heparin-bound transforming growth factor-beta 3 enhances neocartilage formation by rabbit mesenchymal stem cells. Transplantation 85(4) (2008) 589-596.

[185] J.E. Lee, K.E. Kim, I.C. Kwon, H.J. Ahn, S.-H. Lee, H. Cho, H.J. Kim, S.C. Seong, M.C. Lee, Effects of the controlled-released TGF-b1 from chitosan microspheres on chondrocytes cultured in a collagen/chitosan/glycosaminoglycan scaffold. Biomaterials 25(18) (2004) 4163-4173.

[186] T.A. Holland, Y. Tabata, A.G. Mikos, Dual growth factor delivery from degradable oligo(poly(ethylene glycol) fumarate) hydrogel scaffolds for cartilage tissue engineering. Journal of Controlled Release 101(1-3) (2005) 111-125.

[187] A. Jaklenec, A. Hinckfuss, B. Bilgen, M. Ciombor Deborah, R. Aaron, E. Mathiowitz, Sequential release of bioactive IGF-I and TGF-beta 1 from PLGA microsphere-based scaffolds. Biomaterials 29(10) (2008) 1518-1525.

[188] A.T. Raiche, D.A. Puleo, Cell responses to BMP-2 and IGF-I released with different time-dependent profiles. Journal of biomedical materials research. Part A 69A(2) (2004) 342-350.

[189] A.T. Raiche, D.A. Puleo, In vitro effects of combined and sequential delivery of two bone growth factors. Biomaterials 25(4) (2004) 677-685.

[190] W.M. Saltzman, R. Langer, Transport rates of proteins in porous materials with known microgeometry. Biophysical Journal 55(1) (1989) 163-171.

[191] R.A. Siegel, J. Kost, R. Langer, Mechanistic studies of macromolecular drug release from macroporous polymers. 1. Experiemnts and preliminary theory concerning completeness of drug release. Journal of Controlled Release 8(3) (1989) 223-236.

[192] O.L. Johnson, M.A. Tracy, Peptide and protein drug delivery. in: E. Mathiowitz (Ed.), Encyclopedia of Controlled Drug Delivery, Wiley, Toronto, 1999.

[193] B. Amsden, A model for osmotic pressure driven release from cylindrical rubbery polymer matrices. Journal of Controlled Release 93(3) (2003) 249-258.

[194] R. Schirrer, P. Thepin, G. Torres, Water-absorption, swelling, rupture and salt release in salt silicone-rubber compounds. Journal of Materials Science 27(13) (1992) 3424-3434.

[195] J. Wright, S.K. Chandrasekaran, R. Gale, D. Sawanson, Model for the release of osmotically active agents from monolithic polymeric matrices. AIChE Symposium Series 77(206) (1981).

[196] B.G. Amsden, Y.L. Cheng, Enhanced fraction releasable above percolation-threshold from monoliths containing osmotic excipients Journal of Controlled Release 31(1) (1994) 21-32.

[197] B.G. Amsden, Y.L. Cheng, M.F.A. Goosen, A mechanistic study of the release of osmotic agents from polymeric monoliths. Journal of Controlled Release 30(1) (1994) 45-56.

[198] C. Bouffi, O. Thomas, C. Bony, A. Giteau, M.-C. Venier-Julienne, C. Jorgensen, C. Montero-Menei, D. Noel, The role of pharmacologically active microcarriers releasing TGF-beta3 in cartilage formation in vivo by mesenchymal stem cells. Biomaterials 31(25) (2010) 6485-6493.

[199] A.J. DeFail, C.R. Chu, N. Izzo, K.G. Marra, Controlled release of bioactive TGF-beta(1) from microspheres embedded within biodegradable hydrogels. Biomaterials 27(8) (2006) 1579-1585.

[200] J. Jiang, A. Tang, G.A. Ateshian, X.E. Guo, C.T. Hung, H.H. Lu, Bioactive stratified polymer ceramic-hydrogel scaffold for integrative osteochondral repair. Annals of Biomedical Engineering 38(6) (2010) 2183-2196.

[201] J.S. Park, K. Na, D.G. Woo, H.N. Yang, K.-H. Park, Determination of dual delivery for stem cell differentiation using dexamethasone and TGF-beta 3 in/on polymeric microspheres. Biomaterials 30(27) (2009) 4796-4805.

[202] J.S. Park, K. Park, D.G. Woo, H.N. Yang, H.-M. Chung, K.-H. Park, Lactide-glycolide copolymer microsphere construct coated with TGF-beta 3 loaded nanoparticles for neocartilage formation. Biomacromolecules 9(8) (2008) 2162-2169.

[203] L.D. Solorio, A.S. Fu, R. Hernandez-Irizarry, E. Alsberg, Chondrogenic differentiation of human mesenchymal stem cell aggregates via controlled release of TGF-beta 1 from incorporated polymer microspheres. Journal of Biomedical Materials Research, Part A 92A(3) (2010) 1139-1144.

[204] X. Wang, E. Wenk, X. Zhang, L. Meinel, G. Vunjak-Novakovic, L. Kaplan David, Growth factor gradients via microsphere delivery in biopolymer scaffolds for osteochondral tissue engineering. Journal of Controlled Release 134(2) (2009) 81-90.

[205] C.M. Agrawal, K.A. Athanasiou, Technique to control pH in vicinity of biodegrading PLA-PGA implants. Journal of Biomedical Materials Research 38(2) (1997) 105-114.

[206] M. Ara, M. Watanabe, Y. Imai, Effect of blending calcium compounds on hydrolytic degradation of poly(DL-lactic acid-co-glycolic acid). Biomaterials 23(12) (2002) 2479-2483.

[207] W. Linhart, F. Peters, W. Lehmann, K. Schwarz, A.F. Schilling, M. Amling, J.M. Rueger, M. Epple, Biologically and chemically optimized composites of carbonated apatite and polyglycolide as bone substitution materials. Journal of Biomedical Materials Research 54(2) (2001) 162-171.

[208] W. Heidemann, S. Jeschkeit-Schubbert, K. Ruffieux, J.H. Fischer, H. Jung, G. Krueger, E. Wintermantel, K.L. Gerlach, pH-stabilization of predegraded PDLLA by an admixture of water-soluble sodium hydrogenphosphate-results of an in vitro- and in vivo-study. Biomaterials 23(17) (2002) 3567-3574.

[209] L. Lu, S.J. Peter, M.D. Lyman, H.L. Lai, S.M. Leite, J.A. Tamada, S. Uyama, J.P. Vacanti, R. Langer, A.G. Mikos, *In vitro* and *in vivo* degradation of porous poly(DL-lactic-co-glycolic acid) foams. Biomaterials 21(18) (2000) 1837-1845.

[210] J. Suganuma, H. Alexander, Biological response of intramedullary bone to poly-L-lactic acid. J Appl Biomater 4(1) (1993) 13-27.

[211] O. Bostman, E. Hirvensalo, J. Makinen, P. Rokkanen, Foreign-body reactions to fracture fixation implants of biodegradable synthetic-polymers. Journal of Bone and Joint Surgery-British Volume 72(4) (1990) 592-596.

[212] K. Fu, D.W. Pack, A.M. Klibanov, R. Langer, Visual evidence of acidic environment within degrading poly(lactic-co-glycolic acid) (PLGA) microspheres. Pharmaceutical Research 17(1) (2000) 100-106.

[213] T. Uchida, A. Yagi, Y. Oda, Y. Nakada, S. Goto, Instability of bovine insulin in poly(lactide-co-glycolide) (PLGA) microspheres. Chemical & Pharmaceutical Bulletin 44(1) (1996) 235-236.

[214] M. van de Weert, W.E. Hennink, W. Jiskoot, Protein instability in poly(lactic-co-glycolic acid) microparticles. Pharmaceutical Research 17(10) (2000) 1159-1167.

[215] M. Sittinger, D. Reitzel, M. Dauner, H. Hierlemann, C. Hammer, E. Kastenbauer, H. Planck, G.R. Burmester, J. Bujia, Resorbable polyesters in cartilage engineering: Affinity and biocompatibility of polymer fiber structures to chondrocytes. Journal of Biomedical Materials Research 33(2) (1996) 57-63.

[216] A.T. Mehlhorn, P. Niemeyer, K. Kaschte, L. Muller, G. Finkenzeller, D. Hartl, N.P. Sudkamp, H. Schmal, Differential effects of BMP-2 and TGF-beta 1 on chondrogenic differentiation of adipose derived stem cells. Cell Proliferation 40(6) (2007) 809-823.

[217] Y. Han, Y. Wei, S. Wang, Y. Song, Cartilage regeneration using adipose-derived stem cells and the controlled-released hybrid microspheres. Joint, bone, spine : revue du rhumatisme 77(1) (2010) 27-31.

[218] Y. Jung, Y.I. Chung, S.H. Kim, G. Tae, Y.H. Kim, J.W. Rhie, In situ chondrogenic differentiation of human adipose tissue-derived stem cells in a TGF-beta(1) loaded fibrin-poly(lactide-caprolactone) nanoparticulate complex. Biomaterials 30(27) (2009) 4657-4664.

[219] J.S. Park, H.N. Yang, D.G. Woo, S.Y. Jeon, K.-H. Park, The promotion of chondrogenesis, osteogenesis, and adipogenesis of human mesenchymal stem cells by multiple growth factors incorporated into nanosphere-coated microspheres. Biomaterials 32(1) (2011) 28-38.

[220] K.J. Brown, C.R. Parish, Histidine-rich glycoprotein and platelet factor-4 mask heparan-sulfate proteoglycans recognized by acidic and basic fibroblast growth-factor. Biochemistry 33(46) (1994) 13918-13927.

[221] T. Nagayasu, S. Miyata, N. Hayashi, R. Takano, Y. Kariya, K. Kamei, Heparin structures in FGF-2-dependent morphological transformation of astrocytes. Journal of biomedical materials research. Part A 74A(3) (2005) 374-380.

[222] S. Ricard-Blum, O. Feraud, H. Lortat-Jacob, A. Rencurosi, N. Fukai, F. Dkhissi, D. Vittet, A. Imberty, B.R. Olsen, M. van der Rest, Characterization of endostatin binding to heparin

and heparan sulfate by surface plasmon resonance and molecular modeling - Role of divalent cations. Journal of Biological Chemistry 279(4) (2004) 2927-2936.

[223] B. Zhao, Y.F. Li, C. Buono, S.W. Waldo, N.L. Jones, M. Mori, H.S. Kruth, Constitutive receptor-independent low density lipoprotein uptake and cholesterol accumulation by macrophages differentiated from human monocytes with macrophage-colony-stimulating factor (M-CSF). Journal of Biological Chemistry 281(23) (2006) 15757-15762.

[224] P.A. Zuk, M. Zhu, P. Ashjian, D.A. De Ugarte, J.I. Huang, H. Mizuno, Z.C. Alfonso, J.K. Fraser, P. Benhaim, M.H. Hedrick, Human adipose tissue is a source of multipotent stem cells. Mol. Biol. Cell 13(12) (2002) 4279-4295.

[225] K.Y. Lee, W.S. Ha, W.H. Park, Blood compatibility and biodegradability of partially N-acylated chitosan derivatives. Biomaterials 16(16) (1995) 1211-1216.

[226] S.B. Rao, C.P. Sharma, Use of chitosan as a biomaterial: Studies on its safety and hemostatic potential. Journal of Biomedical Materials Research 34(1) (1997) 21-28.

[227] Y.W. Cho, Y.N. Cho, S.H. Chung, G. Yoo, S.W. Ko, Water-soluble chitin as a wound healing accelerator. Biomaterials 20(22) (1999) 2139-2145.

[228] H. Ueno, H. Yamada, I. Tanaka, N. Kaba, M. Matsuura, M. Okumura, T. Kadosawa, T. Fujinaga, Accelerating effects of chitosan for healing at early phase of experimental open wound in dogs. Biomaterials 20(15) (1999) 1407-1414.

[229] K. Bae, E.J. Jun, S.M. Lee, D.I. Paik, J.B. Kim, Effect of water-soluble reduced chitosan on Streptococcus mutans, plaque regrowth and biofilm vitality. Clinical oral investigations 10(2) (2006) 102-107.

[230] N. Liu, X.G. Chen, H.J. Park, C.G. Liu, C.S. Liu, X.H. Meng, L.J. Yu, Effect of MW and concentration of chitosan on antibacterial activity of *Escherichia coli*. Carbohydrate Polymers 64(1) (2006) 60-65.

[231] F.-L. Mi, S.-H. Yu, C.-K. Peng, H.-W. Sung, S.-S. Shyu, H.-F. Liang, M.-F. Huang, C.-C. Wang, Synthesis and characterization of a novel glycoconjugated macromolecule. Polymer 47(12) (2006) 4348-4358.

[232] Z. Shi, K.G. Neoh, E.T. Kang, W. Wang, Antibacterial and mechanical properties of bone cement impregnated with chitosan nanoparticles. Biomaterials 27(11) (2006) 2440-2449.

[233] V.F. Sechriest, Y.J. Miao, C. Niyibizi, A. Westerhausen-Larson, H.W. Matthew, C.H. Evans, F.H. Fu, J.-K. Suh, GAG-augmented polysaccharide hydrogel: a novel biocompatible and biodegradable material to support chondrogenesis. Journal of Biomedical Materials Research 49(4) (2000) 534-541.

[234] B.G. Amsden, A. Sukarto, D.K. Knight, S.N. Shapka, Methacrylated glycol chitosan as a photopolymerizable biomaterial. Biomacromolecules 8(12) (2007) 3758-3766.

[235] D. Le Roith, V.A. Blakesley, in: E. Canalis (Ed.), Skeletal growth factors., Lippincott Williams & Wilkins, Philadelphia, 2000, pp. 31-50.

[236] M. Acemoglu, Chemistry of polymer biodegradation and implications on parenteral drug delivery. International Journal of Pharmaceutics 277(1-2) (2004) 133-139.

[237] A.P. Pego, M.J.A. Van Luyn, L.A. Brouwer, P.B. van Wachem, A.A. Poot, D.W. Grijpma, J. Feijen, In vivo behavior of poly(1,3-trimethylene carbonate) and copolymers of 1,3-trimethylene carbonate with d,l-lactide or e-caprolactone: Degradation and tissue response. Journal of Biomedical Materials Research, Part A 67A(3) (2003) 1044-1054.

[238] C.G. Pitt, Poly-e-caprolactone and its copolymers. Drugs and the Pharmaceutical Sciences 45(Biodegradable Polymer Drug Delivery System) (1990) 71-120.

[239] G.L. Brode, J.V. Koleske, Lactone polymerization and polymer properties. Journal of Macromolecular Science, Chemistry 6(6) (1972) 1109-1144.

[240] K.J. Zhu, R.W. Hendren, K. Jensen, C.G. Pitt, Synthesis, properties, and biodegradation of poly(1,3-trimethylene carbonate). Macromolecules 24(8) (1991) 1736-1740.

[241] S. Sharifpoor, B. Amsden, In vitro release of a water-soluble agent from low viscosity biodegradable, injectable oligomers. European Journal of Pharmaceutics and Biopharmaceutics 65(3) (2007) 336-345.

[242] B. Amsden, Review of osmotic pressure driven release of proteins from monolithic devices. Journal of Pharmacy & Pharmaceutical Sciences 10(2) (2007) 129-143.

[243] S. Sharifpoor, B. Amsden, In vitro release of a water-soluble agent from low viscosity biodegradable, injectable oligomers. European Journal of Pharmaceutics and Biopharmaceutics 65(3) (2007) 336-345.

[244] B.G. Amsden, L. Timbart, D. Marecak, R. Chapanian, M.Y. Tse, S.C. Pang, VEGF-induced angiogenesis following localized delivery via injectable, low viscosity poly(trimethylene carbonate). Journal of Controlled Release 145(2) (2010) 109-115.

[245] C.G. Williams, A.N. Malik, T.K. Kim, P.N. Manson, J.H. Elisseeff, Variable cytocompatibility of six cell lines with photoinitiators used for polymerizing hydrogels and cell encapsulation. Biomaterials 26(11) (2005) 1211-1218.

[246] H. Jin, J.L. Lewis, Determination of Poisson's ratio of articular cartilage by indentation using different-sized indenters. Journal of Biomechanical Engeineering-Transactions. ASME 126(2) (2004) 138-145.

[247] W.C. Hayes, L.M. Keer, G. Herrmann, L.F. Mockros, A mathematical analysis for indentation tests of articular cartilage. J. Biomech. 5(5) (1972) 541-551.

[248] L. Flynn, J.L. Semple, K.A. Woodhouse, Decellularized placental matrices for adipose tissue engineering. Journal of Biomedical Materials Research, Part A 79A(2) (2006) 359-369.

[249] B. Amsden, A. Hatefi, D. Knight, E. Bravo-Grimaldo, Development of biodegradable injectable thermoplastic oligomers. Biomacromolecules 5(2) (2004) 637-642.

[250] K. Hiltunen, J.V. Seppaelae, M. Haerkoenen, Effect of catalyst and polymerization conditions on the preparation of low molecular weight lactic acid polymers. Macromolecules 30(3) (1997) 373-379.

[251] V. Crescenzi, G. Manzini, G. Calzolari, C. Borri, Thermodynamics of fusion of poly-beta -propiolactone and poly-ε-caprolactone. Comparative analysis of the melting of aliphatic polylactone and polyester chains. European Polymer Journal 8(3) (1972) 449-463.

[252] B.G. Amsden, M.F.A. Goosen, An examination of factors affecting the size, distribution and release characteristics of polymer microbeads made using electrostatics. Journal of Controlled Release 43(2-3) (1997) 183-196.

[253] M.L.-S. Tsang, L. Zhou, B.-L. Zheng, J. Wenker, G. Fransen, J. Humphrey, J.M. Smith, M. O'Connor-McCourt, R. Lucas, J.A. Weatherbee, Characterization of recombinant soluble human transforming growth factor-beta receptor type II (rhTGF-beta sRII). Cytokine 7(5) (1995) 389-397.

[254] J.-D. Yan, S. Yang, S.-J. LÜ, R.-Y. Lei, T.-H. Zhu, Expression of Recombinant Human BMP-6 in CHO Cell by Fusion of a BMP-6 Mature Peptide to the Signal Peptide and Propeptide of Another Homologue Protein. Chinese Journal of Biotechnology 23(3) (2007) 414-418.

[255] Y.J. Kim, R.L.Y. Sah, J.Y.H. Doong, A.J. Grodzinsky, Fluorometric assay of DNA in cartilage explants using Hoechst-33258. Analytical Biochemistry 174(1) (1988) 168-176.

[256] R.W. Farndale, D.J. Buttle, A.J. Barrett, Improved quantitation and discrimination of sulfated glycosaminoglycans by use of dimethylmethylene blue. Biochimica Et Biophysica Acta 883(2) (1986) 173-177.

[257] R.L. Goldberg, L.M. Kolibas, An improved method for determining proteoglycans synthesized by chondrocytes in culture. Connective Tissue Research 24(3-4) (1990) 265-275.

[258] S.J. Bryant, K.A. Davis-Arehart, N. Luo, R.K. Shoemaker, J.A. Arthur, K.S. Anseth, Synthesis and characterization of photopolymerized multifunctional hydrogels: Water-

soluble poly(vinyl alcohol) and chondroitin sulfate macromers for chondrocyte encapsulation. Macromolecules 37(18) (2004) 6726-6733.

[259] K.A. Davis, J.A. Burdick, K.S. Anseth, Photoinitiated crosslinked degradable copolymer networks for tissue engineering applications. Biomaterials 24(14) (2003) 2485-2495.

[260] Q. Li, C.G. Williams, D.D.N. Sun, J. Wang, K. Leong, J.H. Elisseeff, Photocrosslinkable polysaccharides based on chondroitin sulfate. Journal of biomedical materials research. Part A 68A(1) (2004) 28-33.

[261] J.L. West, J.A. Hubbell, Photopolymerized hydrogel materials for drug-delivery applications. React. Polym. 25(2-3) (1995) 139-147.

[262] J.A. Burdick, M.N. Mason, A.D. Hinman, K. Thorne, K.S. Anseth, Delivery of osteoinductive growth factors from degradable PEG hydrogels influences osteoblast differentiation and mineralization. Journal of Controlled Release 83(1) (2002) 53-63.

[263] B. Baroli, V.P. Shastri, R. Langer, A method to protect sensitive molecules from a light-induced polymerizing environment. Journal of Pharmaceutical Sciences 92(6) (2003) 1186-1195.

[264] B. Kim, N.A. Peppas, Poly(ethylene glycol)-containing hydrogels for oral protein delivery applications. Biomedical Microdevices 5(4) (2003) 333-341.

[265] M.B. Mellott, K. Searcy, M.V. Pishko, Release of protein from highly cross-linked hydrogels of poly(ethylene glycol) diacrylate fabricated by UV polymerization. Biomaterials 22(9) (2001) 929-941.

[266] S.L. Bourke, M. Al-Khalili, T. Briggs, B.B. Michniak, J. Kohn, L.A. Poole-Warren, A photo-crosslinked poly(vinyl alcohol) hydrogel growth factor release vehicle for wound healing applications. AAPS Pharmsci 5(4) (2003).

[267] F. Gu, R. Neufeld, B. Amsden, Osmotic-driven release kinetics of bioactive therapeutic proteins from a biodegradable elastomer are linear, constant, similar, and adjustable. Pharmaceutical Research 23(4) (2006) 782-789.

[268] F. Gu, H.M. Younes, A.O.S. El-Kadi, R.J. Neufeld, B.G. Amsden, Sustained interferon-gamma delivery from a photocrosslinked biodegradable elastomer. Journal of Controlled Release 102(3) (2005) 607-617.

[269] T. Matsuda, M.J. Moghaddam, K. Sakurai, Photocurable glycosaminoglycan derivatives, crosslinked glycosaminoglycan and method of production thereof, USA Patent 1995.

[270] T. Matsuda, T. Magoshi, Preparation of vinylated polysaccharides and photofabrication of tubular scaffolds as potential use in tissue engineering. Biomacromolecules 3(5) (2002) 942-950.

[271] T. Chandy, C.P. Sharma, Chitosan-as biomaterial. Biomaterials Artificial Cells and Artificial Organs 18(1) (1990) 1-24.

[272] E. Renbutsu, M. Hirose, Y. Omura, F. Nakatsubo, Y. Okamura, Y. Okamoto, H. Saimoto, Y. Shigemasa, S. Minami, Preparation and biocompatibility of novel UV-curable chitosan derivatives. Biomacromolecules 6(5) (2005) 2385-2388.

[273] P.J. VandeVord, H.W.T. Matthew, S.P. DeSilva, L. Mayton, B. Wu, P.H. Wooley, Evaluation of the biocompatibility of a chitosan scaffold in mice. Journal of Biomedical Materials Research 59(3) (2002) 585-590.

[274] Y. Wan, A.X. Yu, H. Wu, Z.X. Wang, D.J. Wen, Porous-conductive chitosan scaffolds for tissue engineering II. *in vitro* and *in vivo* degradation. Journal of Materials Science-Materials in Medicine 16(11) (2005) 1017-1028.

[275] K. Ono, Y. Saito, H. Yura, K. Ishikawa, A. Kurita, T. Akaike, M. Ishihara, Photocrosslinkable chitosan as a biological adhesive. Journal of Biomedical Materials Research 49(2) (2000) 289-295.

[276] M. Ishihara, K. Obara, T. Ishizuka, M. Fujita, M. Sato, K. Masuoka, Y. Saito, H. Yura, T. Matsui, H. Hattori, M. Kikuchi, A. Kurita, Controlled release of fibroblast growth factors and heparin from photocrosslinked chitosan hydrogels and subsequent effect on in vivo vascularization. Journal of biomedical materials research. Part A 64A(3) (2003) 551-559.

[277] B. CarrenoGomez, R. Duncan, Evaluation of the biological properties of soluble chitosan and chitosan microspheres. International Journal of Pharmaceutics 148(2) (1997) 231-240.

[278] D.K. Knight, S.N. Shapka, B.G. Amsden, Structure, depolymerization, and cytocompatibility evaluation of glycol chitosan. Journal of Biomedical Materials Research, Part A 83A(3) (2007) 787-798.

[279] N. Flores-Ramirez, E.A. Elizalde-Pena, S.R. Vasquez-Garcia, J. Gonzalez-Hernandez, A. Martinez-Ruvalcaba, I.C. Sanchez, G. Luna-Barcenas, R.B. Gupta, Characterization and degradation of functionalized chitosan with glycidyl methacrylate. Journal of Biomaterials Science-Polymer Edition 16(4) (2005) 473-488.

[280] S.Y. Cha, J.K. Lee, B.S. Lim, T.S. Lee, W.H. Park, Conjugated vinyl derivatives of chitooligosaccharide: Synthesis and characterization. Journal of Polymer Science Part a-Polymer Chemistry 39(6) (2001) 880-887.

[281] G.T. Hermanson, Editor, Bioconjugate Techniques, 1995.

[282] P. Edman, B. Ekman, I. Sjoholm, Immobilization of proteins in microspheres of biodegradable polyacryldextran. Journal of Pharmaceutical Sciences 69(7) (1980) 838-842.

[283] M.H.H. Aboshosha, N.A.E. Ibrahim, Reaction of cellulose-poly(glycidyl methacrylate) with methylamine. Angew. Makromol. Chem. 152 (1987) 93-106.

[284] H. Sashiwa, N. Yamamori, Y. Ichinose, J. Sunamoto, S. Aiba, Chemical modification of chitosan, 17 - Michael reaction of chitosan with acrylic acid in water. Macromolecular Bioscience 3(5) (2003) 231-233.

[285] S.C. Hsu, T.M. Don, W.Y. Chiu, Free radical degradation of chitosan with potassium persulfate. Polym. Degrad. Stabil. 75(1) (2002) 73-83.

[286] A.A.J. Goldsmith, S.E. Clift, Investigation into the biphasic properties of a hydrogel for use in a cushion form replacement joint. Journal of Biomechanical Engineering-Transactions of ASME 120(3) (1998) 362-369.

[287] R.Y. Hori, L.F. Mockros, Indentation tests of human articular-cartilage. J. Biomech. 9(4) (1976) 259-268.

[288] R.A.A. Muzzarelli, Human enzymatic activities related to the therapeutic administration of chitin derivatives. Cellular and Molecular Life Sciences 53(2) (1997) 131-140.

[289] K. Tomihata, Y. Ikada, In vitro and in vivo degradation of films of chitin and its deacetylated derivatives. Biomaterials 18(7) (1997) 567-575.

[290] R.J. Nordtveit, K.M. Varum, O. Smidsrod, Degradation of fully water-soluble, partially *N*-acetylated chitosan with lysozyme. Carbohydrate Polymers 23(4) (1994) 253-260.

[291] N.E. Fedorovich, J. Alblas, J.R. de Wijn, W.E. Hennink, A.J. Verbout, W.J.A. Dhert, Hydrogels as extracellular matrices for skeletal tissue engineering: State-of-the-art and novel application in organ printing. Tissue Engineering 13(8) (2007) 1905-1925.

[292] A.S. Hoffman, Hydrogels for biomedical applications. Annals of the New York Academy of Sciences 944(Bioartificial Organs III) (2001) 62-73.

[293] K.Y. Lee, D.J. Mooney, Hydrogels for Tissue Engineering. Chemical Reviews (Washington, D. C.) 101(7) (2001) 1869-1879.

[294] N.B. Graham, Hydrogels: their future, Part II. Medical device technology 9(3) (1998) 22-25.

[295] N.B. Graham, Hydrogels: their future, Part I. Medical device technology 9(1) (1998) 18-22.

[296] J.L. Drury, D.J. Mooney, Hydrogels for tissue engineering: scaffold design variables and applications. Biomaterials 24(24) (2003) 4337-4351.

[297] M.P. Lutolf, J.A. Hubbell, Synthetic biomaterials as instructive extracellular microenvironments for morphogenesis in tissue engineering. Nature Biotechnology 23(1) (2005) 47-55.

[298] N.A. Peppas, J.Z. Hilt, A. Khademhosseini, R. Langer, Hydrogels in biology and medicine: from molecular principles to bionanotechnology. Advanced Materials (Weinheim, Germany) 18(11) (2006) 1345-1360.

[299] W.E. Hennink, C.F. van Nostrum, Novel crosslinking methods to design hydrogels. Advanced Drug Delivery Reviews 54(1) (2002) 13-36.

[300] K.T. Nguyen, J.L. West, Photopolymerizable hydrogels for tissue engineering applications. Biomaterials 23(22) (2002) 4307-4314.

[301] T. Vermonden, N.E. Fedorovich, D. van Geemen, J. Alblas, C.F. van Nostrum, W.J.A. Dhert, W.E. Hennink, Photopolymerized thermosensitive hydrogels: synthesis, degradation, and cytocompatibility. Biomacromolecules 9(3) (2008) 919-926.

[302] C. Decker, UV-curing chemistry: past, present, and future. Journal of Coatings Technology 59(751) (1987) 97-106.

[303] K.S. Anseth, A.T. Metters, S.J. Bryant, P.J. Martens, J.H. Elisseeff, C.N. Bowman, In situ forming degradable networks and their application in tissue engineering and drug delivery. Journal of Controlled Release 78(1-3) (2002) 199-209.

[304] K.W. Chun, J.B. Lee, S.H. Kim, T.G. Park, Controlled release of plasmid DNA from photo-cross-linked pluronic hydrogels. Biomaterials 26(16) (2005) 3319-3326.

[305] B.K. Mann, A.S. Gobin, A.T. Tsai, R.H. Schmedlen, J.L. West, Smooth muscle cell growth in photopolymerized hydrogels with cell adhesive and proteolytically degradable domains: synthetic ECM analogs for tissue engineering. Biomaterials 22(22) (2001) 3045-3051.

[306] D.J. Quick, K.S. Anseth, Gene delivery in tissue engineering: A photopolymer platform to coencapsulate cells and plasmid DNA. Pharmaceutical Research 20(11) (2003) 1730-1737.

[307] B. Sharma, G. Williams Christopher, M. Khan, P. Manson, H. Elisseeff Jennifer, *In vivo* chondrogenesis of mesenchymal stem cells in a photopolymerized hydrogel. Plastic and Reconstructive Surgery 119(1) (2007) 112-120.

[308] S.J. Bryant, C.R. Nuttelman, K.S. Anseth, Cytocompatibility of UV and visible light photoinitiating systems on cultured NIH/3T3 fibroblasts in vitro. Journal of Biomaterials Science-Polymer Edition 11(5) (2000) 439-457.

[309] G.M. Cruise, O.D. Hegre, D.S. Scharp, J.A. Hubbell, A sensitivity study of the key parameters in the interfacial photopolymerization of poly(ethylene glycol) diacrylate upon porcine islets. Biotechnology and Bioengineering 57(6) (1998) 655-665.

[310] C.T. Hanks, S.E. Strawn, J.C. Wataha, R.G. Craig, Cytotoxic effects of resin components on cultured mammalian fibroblasts. Journal of Dental Research 70(11) (1991) 1450-1455.

[311] E. Fedorovich Natalja, H. Oudshoorn Marion, D. van Geemen, E. Hennink Wim, J. Alblas, J.A. Dhert Wouter, The effect of photopolymerization on stem cells embedded in hydrogels. Biomaterials 30(3) (2009) 344-353.

[312] S.Y. Lee, G. Tae, Formulation and in vitro characterization of an in situ gelable, photo-polymerizable Pluronic hydrogel suitable for injection. Journal of Controlled Release 119(3) (2007) 313-319.

[313] S.W. Benoit Danielle, R. Durney Andrew, S. Anseth Kristi, The effect of heparin-functionalized PEG hydrogels on three-dimensional human mesenchymal stem cell osteogenic differentiation. Biomaterials 28(1) (2007) 66-77.

[314] C.R. Nuttelman, M.C. Tripodi, K.S. Anseth, Synthetic hydrogel niches that promote hMSC viability. Matrix Biology 24(3) (2005) 208-218.

[315] P.A. Cerutti, Prooxidant states and tumor promotion. Science (Washington, DC, United States) 227(4685) (1985) 375-381.

[316] M. Terakado, M. Yamazaki, Y. Tsujimoto, T. Kawashima, K. Nagashima, J. Ogawa, Y. Fujita, H. Sugiya, T. Sakai, S. Furuyama, Lipid peroxidation as a possible cause of benzoyl peroxide toxicity in rabbit dental pulp. A microsomal lipid peroxidation in vitro. Journal of Dental Research 63(6) (1984) 901-905.

[317] A.J. Engler, L. Richert, J.Y. Wong, C. Picart, D.E. Discher, Surface probe measurements of the elasticity of sectioned tissue, thin gels and polyelectrolyte multilayer films: Correlations between substrate stiffness and cell adhesion. Surface Science 570(1-2) (2004) 142-154.

[318] R.L. Saunders, D.A. Hammer, Assembly of human umbilical vein endothelial cells on compliant hydrogels. Cellular and Molecular Bioengineering 3(1) (2010) 60-67.

[319] A.L. Sieminski, R.P. Hebbel, K.J. Gooch, The relative magnitudes of endothelial force generation and matrix stiffness modulate capillary morphogenesis in vitro. Experimental Cell Research 297(2) (2004) 574-584.

[320] B.D. Mather, K. Viswanathan, K.M. Miller, T.E. Long, Michael addition reactions in macromolecular design for emerging technologies. Progress in Polymer Science 31(5) (2006) 487-531.

[321] H.D. Han, L.S. Mangala, J.W. Lee, M.M.K. Shahzad, H.S. Kim, D.Y. Shen, E.J. Nam, E.M. Mora, R.L. Stone, C.H. Lu, S.J. Lee, J.W. Roh, A.M. Nick, G. Lopez-Berestein, A.K. Sood, Targeted gene silencing using RGD-labeled chitosan nanoparticles. Clin. Cancer Res. 16(15) (2010) 3910-3922.

[322] F. Wang, X.R. Li, Y.X. Zhou, Y.H. Zhang, X.W. Chen, J.X. Yang, Y.Q. Huang, Y. Liu, Nanoscaled polyion complex micelles for targeted delivery of recombinant hirudin to platelets based on cationic copolymer. Mol. Pharm. 7(3) (2010) 718-726.

[323] Y. Yang, X.D. Liu, W.T. Yu, H.J. Zhou, X.X. Li, X.J. Ma, Homogeneous synthesis of GRGDY grafted chitosan on hydroxyl groups by photochemical reaction for improved cell adhesion. Carbohydrate Polymers 80(3) (2010) 733-739.

[324] T. Masuko, N. Iwasaki, S. Yamane, T. Funakoshi, T. Majima, A. Minami, N. Ohsuga, T. Ohta, S.I. Nishimura, Chitosan-RGDSGGC conjugate as a scaffold material for musculoskeletal tissue engineering. Biomaterials 26(26) (2005) 5339-5347.

[325] G.B. Schneider, A. English, M. Abraham, R. Zaharias, C. Stanford, J. Keller, The effect of hydrogel charge density on cell attachment. Biomaterials 25(15) (2004) 3023-3028.

[326] S. Duggal, K.B. Froensdal, K. Szoeke, A. Shahdadfar, J.E. Melvik, J.E. Brinchmann, Phenotype and gene expression of human mesenchymal stem cells in alginate scaffolds. Tissue Engineering, Part A 15(7) (2009) 1763-1773.

[327] J.A. Kuphal, L.H. Sperling, L.M. Robeson, Miscible blends of styerene acrylic-acid copolymers with alipathic, crystalline polyamides. Journal of Applied Polymer Science 42(6) (1991) 1525-1535.

[328] R.E. Canfield, Amino acid sequence of egg white lysozyme. Journal of Biological Chemistry 238(8) (1963) 2698-&.

[329] A.J. Celeste, J.A. Iannazzi, R.C. Taylor, R.M. Hewick, V. Rosen, E.A. Wang, J.M. Wozney, Identification of transforming growth-factor-beta family members present in bone-inductive protein purified from bovine bone. Proceedings of the National Academy of Sciences of the United States of America 87(24) (1990) 9843-9847.

[330] M.B. Sporn, A.B. Roberts, L.M. Wakefield, R.K. Assoian, Transforming growth-factor-beta- biological function and chemical structure. Science 233(4763) (1986) 532-534.

[331] R.A. Siegel, R. Langer, Controlled release of polypeptides and other macromolecules. Pharmaceutical Research(1) (1984) 2-10.

[332] A.P. Pego, A.A. Poot, D.W. Grijpma, J. Feijen, *In vitro* degradation of trimethylene carbonate based (co)polymers. Macromolecular Bioscience 2(9) (2002) 411-419.

[333] L.R. Wetter, H.F. Deutsch, Immunological studies on egg white proteins. 4. Immunochemical and physical studies of lysozyme. Journal of Biological Chemistry 192(1) (1951) 237-242.

[334] P.G. Righetti, T. Caravaggio, Isoelectric points and molecular-weights of proteins-Table. Journal of Chromatography 127(1) (1976) 1-28.

[335] K. Hirayama, S. Akashi, M. Furuya, K. Fukuhara, Rapid confirmation and revision of the primary structure of bovine serum-albumin by ESIMS and frit-FAB LC MS Biochemical and Biophysical Research Communications 173(2) (1990) 639-646.

[336] J.T. Connelly, A.J. Garcia, M.E. Levenston, Inhibition of in vitro chondrogenesis in RGD-modified three-dimensional alginate gels. Biomaterials 28(6) (2007) 1071-1083.

[337] T. Re'em, O. Tsur-Gang, S. Cohen, The effect of immobilized RGD peptide in macroporous alginate scaffolds on TGF beta 1-induced chondrogenesis of human mesenchymal stem cells. Biomaterials 31(26) (2010) 6746-6755.

[338] J.C. Chang, S.H. Hsu, D.C. Chen, The promotion of chondrogenesis in adipose-derived adult stem cells by an RGD-chimeric protein in 3D alginate culture. Biomaterials 30(31) (2009) 6265-6275.

[339] B.T. Estes, A.W. Wu, F. Guilak, Potent induction of chondrocytic differentiation of human adipose-derived adult stem cells by bone morphogenetic protein 6. Arthritis and Rheumatism 54(4) (2006) 1222-1232.

[340] C.M. Wang, R.R. Varshney, D.A. Wang, Therapeutic cell delivery and fate control in hydrogels and hydrogel hybrids. Advanced Drug Delivery Reviews 62(7-8) 699-710.

[341] D.A. Wang, Y.H. Gong, K. Su, Method of phase transfer cell culture for self-forming tissue regeneration, USA Patent.

[342] C. Chu, J.J. Schmidt, K. Carnes, Z. Zhang, H.J. Kong, M.-C. Hofmann, Three-dimensional synthetic niche components to control germ cell proliferation. Tissue Engineering, Part A 15(2) (2009) 255-262.

[343] S.Q. Liu, Q. Tian, L. Wang, J.L. Hedrick, J.H.P. Hui, Y.Y. Yang, P.L.R. Ee, Injectable biodegradable poly(ethylene glycol)/RGD peptide hybrid hydrogels for *in vitro* chondrogenesis of human mesenchymal stem cells. Macromolecular Rapid Communications 31(13) (2010) 1148-1154.